Coastal climate change and Variability in the Benguela Current System

Folly Serge Tomety

A thesis presented for the degree of

Doctor of Philosophy

Department of Oceanography

Faculty of Science

UNIVERSITY OF CAPE TOWN

November 2021

I dedicate this thesis to my parents Ekoue Philbert Tomety and Akofa Gnonhale Honorine Sossah, to my sweetheart Ayele Mawussi Aziadapou and my champion Ekoue Michel-Egino Tomety

Plagiarism declaration.

I, **Folly Serge Tomety**, hereby declare that except where specific reference is made to the work of others, the content of this thesis is my own work and have not been submitted in whole or nor in part for consideration for any other degree or qualification in this, or any other University. I therefore authorise the University to reproduce for the purpose of research the content of this thesis.

Signature: Signed by candidate Date: 30/11/2021

ACKNOWLEDGEMENTS

Firstly, I would like to express my immense gratitude to my supervisors Prof. Mathieu Rouault and Dr. Serena Illig for their useful advice, guidance throughout this thesis and for their constructive feedback that helped to improve the writing of this thesis. Mathieu thank you for having trust in me and for giving me the opportunity to do this PhD. Thank you, Serena, for your expertise and sense of explanation. I would like to acknowledge the funding by the Nansen Tutu Centre (NTC), the Sarchi-NRF for this thesis. This work was also supported by the TRIATLAS, the European Union's funded project.

I am extremely grateful to Prof. John Field for his time and help in reviewing the English of this thesis. I would like also to extend my deepest gratitude to prof Noel Keenlyside, from the University of Bergen, who was more than indispensable in this work, especially during the last year of my thesis. His experience and immense knowledge have been invaluable in my thesis. I am also grateful to Dr. Annette Samuelsen for the opportunity she gave to spend time in Norway for my PhD purpose. To Dr. Yanchen Hu from Nansen Environmental and Remote sensing Center (NERSC) Bergen, Norway, thank you to provide me the model NorESM data output and help me with the extraction. I would like to thank Dr. Francois Counillons as well and Dr. Julien Jouanno for Providing HadISST2 data and NEMO model output data, respectively.

I am grateful to all members and academic staff from the Department of Oceanography at the University of Cape Town. Many thanks to Cashifa Karriem for her helpful administrative work done during my PhD studies at University of Cape Town. Special thanks to Dr. Marie-Lou Bachèlery, who provided stimulating discussions as well as happy distractions to rest my mind outside of my research, especially, when we were in Norway.

I would like to thank my family specially my Dad and Mum, two sisters and my champion for their support and motivation throughout this journey. Thank you for believing in me.

I cannot end this acknowledgement without mentioning my friends Mesmin AWO, Dodzi Motchon, and Rodrigue Anicet Imbol for their support and motivation throughout this journey. Special thanks to you Mesmin, you are a wonderful person, you were here at the right moment when everything seemed to be dark in my PhD journey. You were not only a friend but also my advisor. I am forever grateful for your motivation when I was down, and your honest feedback have been invaluable.

ABSTRACT

The thesis aims to seek to document the long-term change and decadal variability in the Benguela Upwelling System and study the possible mechanisms behind these changes. The Benguela Upwelling System is one of the four most productive fisheries areas in the world, and it is therefore important to understand the mechanisms leading to changes at different time and space scales before developing scenarios or forecasts for the future of the region. The first part of the thesis (**chapter 3**) uses four satellite-derived Sea Surface Temperature (SST) datasets combined with various climate reanalysis data to investigate the long-term SST trends in the Benguela Upwelling System over the period 1982-2017. The use of different datasets shows different trends depending on the dataset, which is a concern. However, after a thorough examination, there is some consensus. Results show that the Angola-Benguela Upwelling System has significantly changed during the last three decades. The changes vary in space and depend on season. Cooling trends are observed in the southern part of the Benguela Upwelling System in the austral summer and autumn. The cooling trend is consistent with a positive trend in upwelling-favourable equatorward winds due to the intensification and poleward expansion of the South Atlantic Subtropical high-pressure atmospheric system. A warming trend is observed in Southern Angola and Northern Benguela in late spring and summer. Results also show that the warming or cooling trends in the Benguela Upwelling System are not as linear as the trend in global air temperature. Indeed, when studying trends for the 1982-2017 period, trends tend to slow down and can reverse sign in some regions and recent time, suggesting decadal variability. Most discrepancy between SST datasets occurs from 1982 to 1985, the start of the satellite era. The second part of the thesis (**chapter 4**) focuses on understanding the mechanisms leading to the warming trends along the Angolan and Northern Benguela coast. To do so, the Ocean General Circulation Model NEMO (OGCM NEMO) is used. The model produces an unrealistic cooling trend in the Northern Benguela due to a positive trend in upwelling-favourable wind model forcing. The modelled warming trend in Southern Angola is properly simulated which allows me to use the model to study the mechanisms leading to the warming trend in Angola. Analysis of the model net heat budget components and their contribution to the overall SST trend suggests that the

warming trend observed along the Angolan and Namibian coasts through the austral summer is primarily associated with the intensification of the poleward flow along the coast, bringing more warm water from the tropics to the region and also due to weakening of the vertical flow of cold water to the surface. Locally, the net surface heat flux has decreased and tends to create a negative SST trend but does not offset the warming trend created by the intensification of the flow. The poleward intensification of the Angola Current is attributed to the intensification of the cyclonic circulation around the Angola Dome. Lastly, in **chapter 5**, the decadal variability in the Benguela upwelling system, identified in Chapter 3, is investigated using a long-term ocean model simulation of 110 years (1900 - 2010) of the global ocean-ice components of the Norwegian Earth System Model (NorESM). The results reveal the presence of three dominant scales of variability: the interannual (2-8 years), quasi-decadal (9-14 years) and interdecadal (19-26 years) variability in the Southern Benguela upwelling system. The Southern Benguela SST correlations with the global SST reveal that at quasi-decadal scale the Southern Benguela SST is linked to the south Atlantic SST and the north-east Pacific SST fluctuations, while at the interdecadal scale the Southern Benguela SST modulation is linked to the equatorial and northern Pacific SST, Indian SST and Atlantic SST fluctuations except the equatorial Atlantic SST.

TABLE OF CONTENTS

LIST OF FIGURES

LIST OF TABLES

LIST OF ACRONYMS

ABF: Angola Benguela Front

ABFZ: Angola Benguela Frontal Zone

AMM: Atlantic Meridional Mode

ATSR: Along-Track Scanning Radiometer

AVHRR: Advanced Very High-Resolution Radiometer

BC: Benguela Current

BLLCJ: Benguela Low-Level Coastal Jet

CB: Central Benguela

ICOADS: International Comprehensive Ocean Atmosphere Data Set

DFS5.2: DRAKKAR Forcing Set version 5.2

EBUS: Eastern Boundary Upwelling System

ECMWF: European Centre for Medium-Range Weather Forecasts

ENSO: El Niño Southern Oscillation

EUC: Equatorial Under Current

EXEBUS: Extreme Events in the Benguela Upwelling system

GEOS-5: Goddard Earth Observation System version 5

GMAO: Global Modelling Assimilation Office

HadISST: Hadley Centre Sea Ice and Surface Temperature

IPO: Interdecadal Pacific Oscillation

JMA: Japan Meteorological Agency

JRA-55: Japanese 55-year reanalysis

MERRA2: The Modern-Era Retrospective Analysis for Research and Application, Version 2

MICOM: Miami Isopycnic Coordinate Model

MLD: Mixed layer Depth

NB: Northern Benguela

NCEP1: National Centers for Environmental Prediction version 1

NCEP2: National Centers for Environmental Prediction version 2

NCEP-GTS: National Centers for Environmental Prediction Global Telecommunication System

NEMO: Nucleus for European Modelling of the Ocean

NOAA: National Oceanic and Atmospheric Administration

NorESM: Norwegian Earth System Model

OGCM: Ocean General Circulation Model

OISST: Optimum Interpolation Sea Surface Temperature

PDO: Pacific Oscillation

Qnet: Net surface heat fluxes

SAM: Southern Annular Mode

SASD: South Atlantic Subtropical Dipole

SASH: South Atlantic Subtropical High

SB: Southern Benguela

SD: Standard Deviation

SECC: South Equatorial Counter Current

SEUC: South Equatorial Under Current

SLP: Sea Level Pressure

SSH: Sea Surface Height

SST: Sea Surface Temperature

TPI: Tripole Index

CHAPTER 1

1 INTRODUCTION

Upwelling is a process that involves wind-driven motion of dense, cooler, and nutrient-rich water from below the ocean to the surface. The increased availability of nutrients in the sunlight layer of the upwelling regions results in high levels of phytoplankton, zooplankton, and fish production. Additionally, upwelling regions play an important role in the modulation of climate. The cold water at the surface cools down the air temperature and decreases the water vapour saturation point leading to fog and stratocumulus clouds that have an important role in the net heat budget at the surface of the ocean. There are at least five different types of upwelling: open ocean upwelling, coastal upwelling, upwelling associated with eddies, upwelling associated with topography, and broad-diffusive upwelling in the ocean interior. Open ocean upwelling refers to the upwelling that takes place along the equator and is associated with wind divergence. Coastal upwelling refers to the upwelling that takes place along the coasts of the continents. Upwelling associated with eddies refers to the submesoscale upwelling that takes place in eddies. The topographically associated upwelling is upwelling that occurs when topography causes a deflection of deep currents. The broad-diffusive upwelling is the upwelling that takes place in the ocean interior.

Along continents, there are four major coastal upwellings regions located along the subtropical eastern boundaries of the world's major ocean basins (Pacific and Atlantic Oceans). They are called the Eastern Boundary Upwelling Systems (EBUS). These four major upwellings regions represented in **Figure 1.1,** are the California Upwelling System off California and Oregon, the Humboldt Upwelling System off Peru and Chile, the Canary Upwelling System off Northwest Africa, and the Benguela Upwelling System off Angola, Namibia and South Africa (Chavez and Messié, 2009). In these systems, coastal upwelling is forced by a combination of alongshore wind, triggered by the cross-shore gradient of sea level pressure, the friction generated by the coast affecting wind speed, and the Coriolis effect. Alongshore wind stress and the Coriolis effect

induce offshore surface water transport. This creates a transport divergence leading to upwelling at the coast (**Figure 1.2**). In addition, a divergent oceanic circulation created by the cyclonic wind stress curl can contribute to the coastal upwelling. These coastal upwellings leave a strong imprint on the sea surface temperature (SST) and Chlorophyll-*a* concentration (Chavez and Messié, 2009). Coastal upwellings support vast and diversified marine resources and therefore represent an important source of food security and economics for the populations of the neighbouring coastal countries. These four major coastal upwellings combined, represent less than 1% of the ocean surface but are among the most productive marine ecosystems in the world, providing around 20% of global fish catches (Fréon et al., 2009; Sydeman et al., 2014). Concern for the future of coastal upwelling regions under global warming scenarios motivated me to study the long-term change and variability in the Benguela Upwelling System.

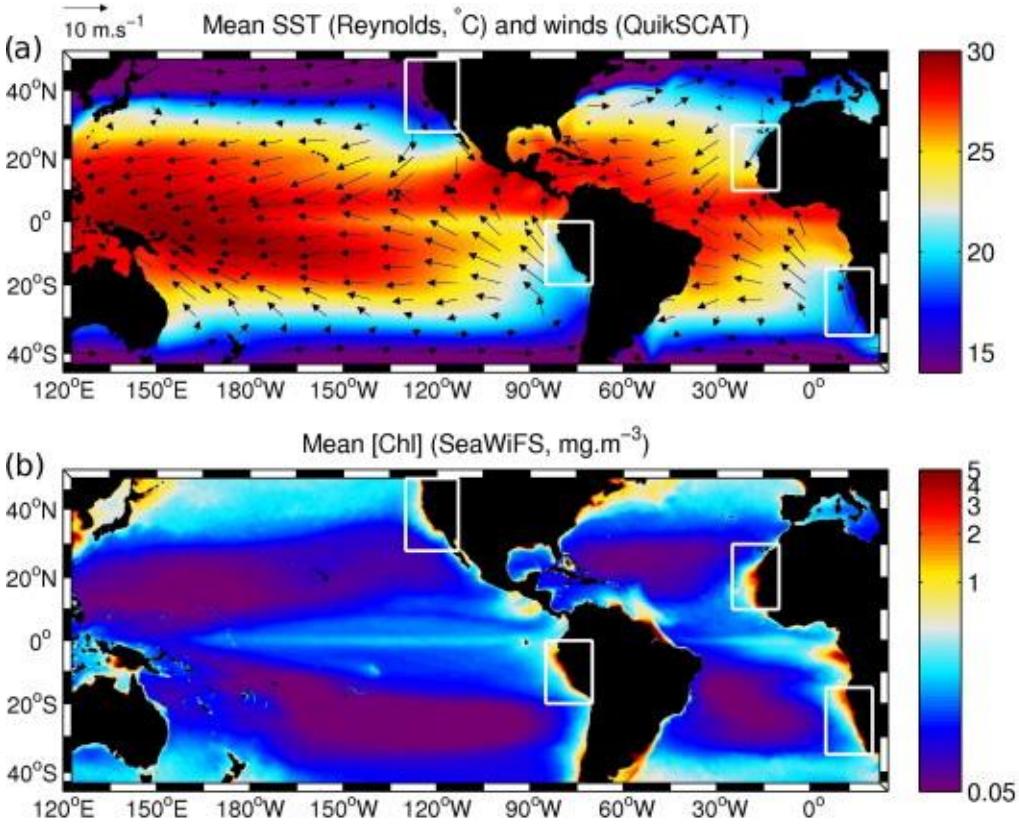

Figure 1.1: Basin-scale maps of mean sea surface temperature (SST), wind and Chlorophyll-*a* concentration, showing the location of the four major EBUS (white boxes). SST (colour shading in (a)) is daily Optimum Interpolation SST (Reynolds et al., 2007) averaged from October 1981 to

February 2007; surface wind (arrows in (a)) are estimated from QuikSCAT (Liu et al., 1998) and averaged from July 1999 to April 2008; Chlorophyll data are from SeaWiFS monthly climatology averaged over the year. Figure from (Chavez and Messié, 2009).

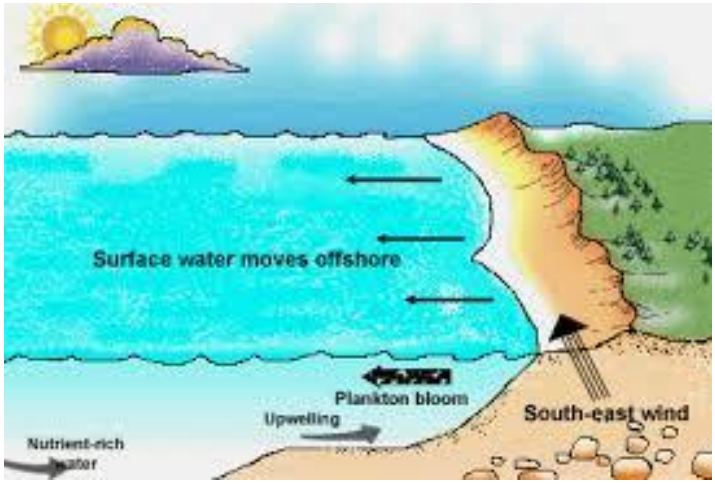

Figure 1.2: Schematic picture of upwelling in the southern hemisphere. The big dotted arrow represents the alongshore wind the thin arrows represent the associated Ekman transport and the grey arrows represent the upwelling. Source https://ediss.sub.uni-hamburg.de/volltexte/2016/7688/pdf/Dissertation.pdf.

1.1 LITERATURE REVIEW

1.1.1 Study area

Like the regions of North-West Africa, Peru, and California, the western coast of Southern Africa is dominated by a coastal upwelling system. The Southern African upwelling is often referred to as the Benguela Upwelling System or Benguela Current System (BCS). It extends from the tip of Africa from 35°S to about 14°S off Angola (Field and Shillington, 2006), and is one of the most productive coastal regions in the world (Carr, 2001; Carr and Kearns, 2003; Chavez and Messié, 2009). In contrast to the other EBUS, the Benguela Upwelling System is embedded between two warm water regions (Boyd and Agenbag, 1985; Hutchings et al., 2009): the warm Indian water of the Agulhas Current in the south and the warm tropical water coming from the equatorial Atlantic in the north (**Figure 1.3b**). The Benguela Upwelling System is mainly driven by

the wind. Furthermore, the intensity, the extension, and the variability of the Benguela Upwelling System are determined by the atmospheric features (atmospheric circulation, orography effect, and its variability), the oceanic features (bathymetry, oceanic circulation, and its variability), and the coastline orientation.

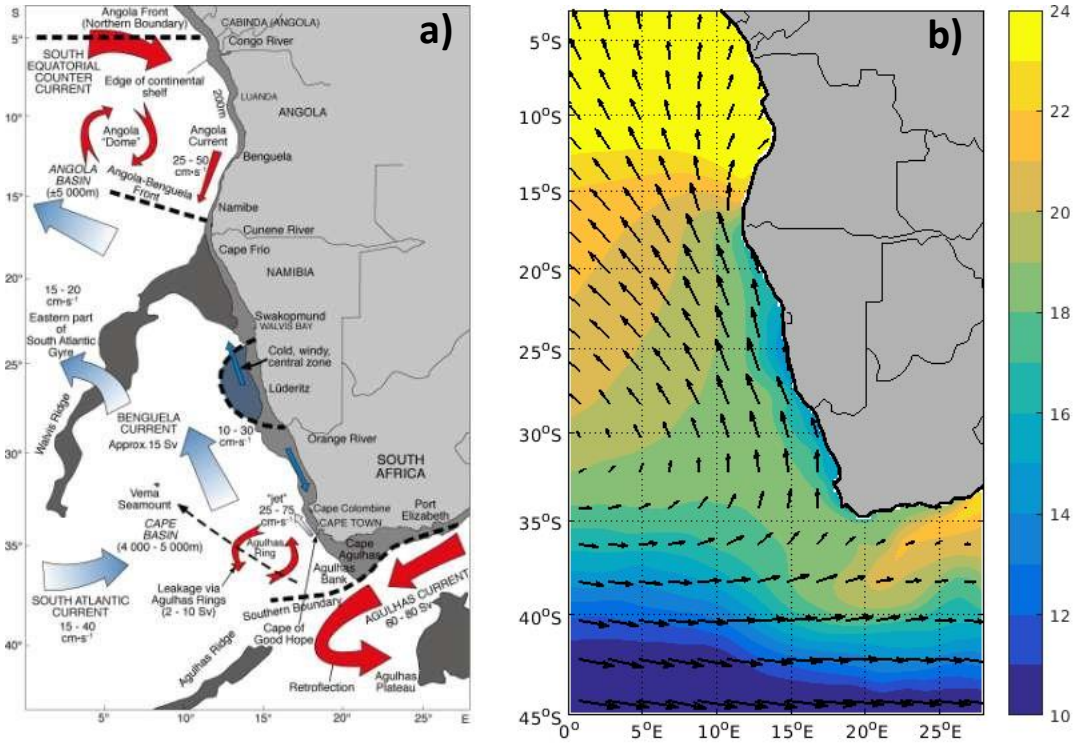

Figure 1.3: a) Main features of the Benguela upwelling, showing prevailing currents and interaction with the warmer water off Angola and the Agulhas current. Red arrows represent the warm currents and blue arrows the cold current. Figure from (Shannon, 2006). b) SST annual mean of OISST (¼°× ¼°) from 1982-2017 and annual mean wind speed and direction at 10m of ERA5 from 1982-2017

1.1.2 Mean atmospheric circulation

The upwelling in the Benguela Upwelling System results from the interaction of basin-scale atmospheric systems such as low and high-pressure systems (**Figure 1.4**) and their associated cyclonic and anticyclonic surface speed circulation respectively, combined with regional and local effects caused by an atmospheric pressure differential across the land and the

open ocean leading to a sea breeze effect and friction at the coast. The most important atmospheric circulation, in the Benguela Upwelling System, is the South Atlantic Subtropical High (SASH). This quasi-permanent high anticyclone is centered around 29°S, 8°W. It moves south in austral summer and north in winter (Shannon, 1985; Preston-Whyte and Tyson, 1988; Sun et al., 2017). The annual meridional migration of the SASH is estimated to be about 5-6°. This migration impacts the meridional wind speed along the coast and the associated upwelling rate.

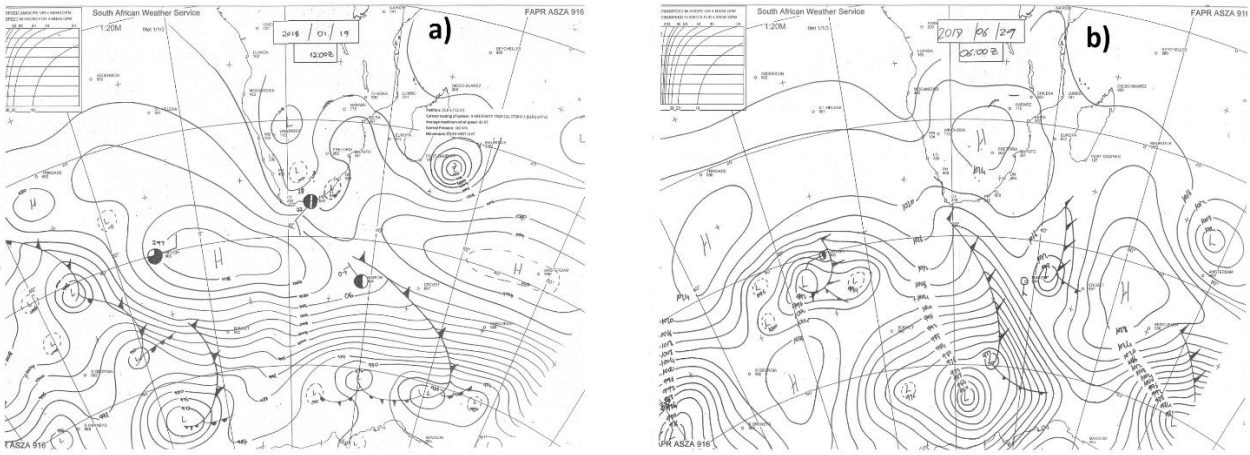

Figure 1.4: A typical scenario of atmospheric circulation in south Atlantic in austral **a)** summer and **b)** winter. H- means high-pressure system; L- means low-pressure system. Source South Africa Weather Service.

The continental low pressure, active in austral summer (**Figure 1.4**), will enhance the gradient of pressure between land and the SASH and increase the meridional wind speed (Bakun, 1990) at the coast of Angola, Namibia, and South Africa. Low-pressure systems such as coastal lows or cold fronts generate cyclonic motion which creates Northwesterly winds (Preston-Whyte and Tyson, 1988), suppresses upwelling, and can lead to downwelling at the coast. The role of low-pressure systems is especially important at the seasonal scale in the Southern Benguela in austral winter and less important in the Central Benguela and Northern Benguela.

Orography and orientation of the coast have an impact on coastal surface wind and associated wind stress curl and Ekman pumping and can create intense upwelling cells or retention areas. Seven upwelling cells have been identified in the Benguela Upwelling System (Nelson and Hutchings, 1983; Lutjeharms and Meeuwis, 1987; Shannon and Nelson, 1996; Veitch

et al., 2009). These upwelling cells are Cunene (17-18°S) cell, Northern Namibia cell also called Palgrave Point (21°S) cell, Walvis Bay (23-24°S) cell, Lüderitz (25.5-27°S) cell, Namaqua (30°S) cell, Cape Columbine (32-33°S) cell, and Cape Peninsula (34-34.5°S) cell (**Figure 1.5**). The Lüderitz cell is the most vigorous and prominent upwelling cell (Shannon, 1985; Hagen et al., 2001; Hutchings et al., 2009; Veitch et al., 2010) where strong winds throughout the year, high turbulence, and strong offshore transport constitute a barrier to epipelagic fish species (Hutchings et al., 2009).

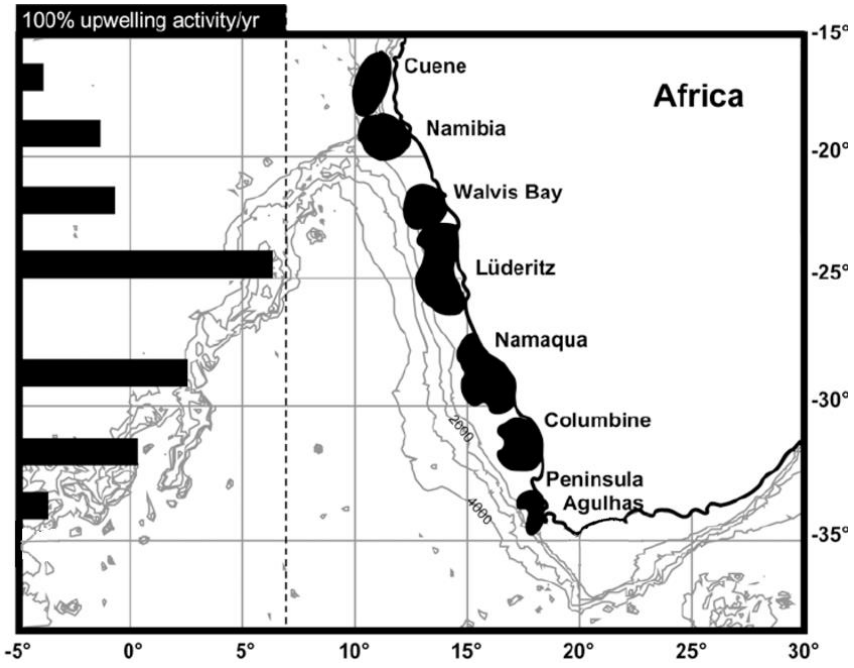

Figure 1.5: Geographic location and annual frequency of occurrence of seven identified upwelling cells in the Benguela System (modified from Volbers et al. (2003)).

North of the Lüderitz cell (Northern Benguela), the upwelling is quasi-permanent with less upwelling in austral summer, while in the south (South Benguela), the upwelling is seasonal with a peak in austral summer where the SASH is farthest poleward (Sun et al., 2017). In austral winter, when the SASH is the furthest north, the Southern Benguela experiences mostly north-westerly wind, which suppresses upwelling and relatively weak south-westerly wind (Hutchings et al., 2009).

1.1.3 Oceanic circulation: Surface and Subsurface currents

Several studies have shown that in addition to the Benguela Current itself, the Benguela Upwelling System is also influenced by the intrusion of tropical water from Angola in the north and of warm water of Agulhas Current in the south.

The oceanic circulation in the Benguela Upwelling System is mostly dominated by the Benguela Current (BC), which is the eastern branch of the South Atlantic subtropical gyre flowing northward from 35°S (**Figure 1.3 a**). This current which extends from the South African and Namibian coast to about ~300 km off the coast (Nelson and Hutchings, 1983), is generated by the large-scale wind pattern related to the SASH and is found in the upper 1000m (Garzoli and Gordon, 1996). The Benguela Upwelling System is influenced by the South Atlantic Current (Veitch et al., 2010) that brings South Atlantic Central Water (SACW) and Eastern Atlantic Central Water (ESACW) toward the BUS. The ESACW is a mixture of Agulhas leakage water and SACW (Mohrholz et al., 2008). Mohrholz et al. (2008) found that the southern Benguela region is dominated by ESACW while the northern Benguela region is dominated by the SACW. Tim et al. (2018) reported that the central water masses that are upwelled in the Benguela Upwelling System are 70.4% and 48.2% fed by the Indian ocean water via Agulhas leakage respectively in South Benguela and North Benguela region. Furthermore, Rouault et al. (2009) and Tim et al. (2019) among others suggested an increase of the Agulhas leakage due to an increase of the Westerlies wind over the Southern Hemisphere. The intensification of the Agulhas leakage will have an impact on Benguela upwelling water masses characteristics.

The North of the Benguela Upwelling System is influenced by a seasonal poleward flow originating from the extension of the Angola Current, a narrow current along the Angolan coast (**Figure 1.3 a**). It forms with the northward Benguela Current a convergence zone called the Angola Benguela Frontal Zone (ABFZ) (Shannon et al., 1987; Stramma and England, 1999; Mohrholz et al., 2001), which is a thermal front with typical temperature gradients of 4°C per 1° of latitude. The Angola Current is the eastern limb of Angola Gyre, a cyclonic motion (Mercier et al., 2003) which is fed by the equatorial current composed by the Equatorial Under Current (EUC), the South Equatorial Under Current (SEUC), and the South Equatorial Counter Current (SECC)

(Peterson and Stramma, 1991; Wacongne and Piton, 1992). The Angola Current is observed between 0 to 300 m depth with mean southward flow observed around 50 m and velocities between 0.4 to 0.5 m/s. The Angola Current transports warm, saline, low oxygen, and rich-nutrient water southward into the Benguela region (Monteiro et al., 2008; Rouault, 2012). The mean southward transport of the Angola Current is estimated to be about 0.45 Sv at 17°S by Rouault (2012) and about 0.32 Sv at 11°S by Kopte et al. (2017). The Angola Current flow has strong seasonal and Inter-annual variability with periodically alternating poleward and equatorward flow (Kopte et al., 2017). The maximum poleward transport is observed in February-March and September-October, corresponding to the period of intrusion of warm tropical water into the Benguela (Rouault, 2012). This impacts the seasonal variability of the ocean surface temperature of the Northern Benguela which has strong seasonality compared to the Central Benguela and Southern Benguela (Demarcq et al., 2003). At the interannual scale, the prolonged strong intrusions of tropical warm water are called Benguela Niños.

1.1.4 Variability in the Benguela upwelling: interannual variability, trends and decadal variability

1.1.4.1 Interannual variability of the Benguela Upwelling System

The Benguela Upwelling System also exhibits strong interannual and decadal variability (Hutchings et al., 2009). Like wind and ocean currents, the ocean temperature in the Benguela Upwelling System is influenced at interannual scale by ocean waves as well as the remote effect of climate modes such as El Niño Southern Oscillation (ENSO) (Rouault et al., 2010; Dufois and Rouault, 2012; Blamey et al., 2015). The Northern Benguela is under the influence of the Benguela Niño, and Benguela Niña phenomena linked to the propagation of coastal trapped waves triggered remotely in the Equatorial region (Shannon et al., 1986; Rouault et al., 2007; Lübbecke et al., 2010; Bachèlery et al., 2016; Rouault et al., 2018; Bachèlery et al., 2020; Illig et al., 2020). Coastal trapped waves induce poleward advection of warm tropical water to the Northern Benguela. These waves are responsible for about 80% of the Sea Surface Height (SSH) anomalies (Bachèlery et al., 2016) off Angola and Northern Namibia. Coastal trapped waves deepen or shallow the thermocline and favour the Benguela Niño warm events and Benguela

Niña cold events, respectively. The interannual variability of Benguela Niños/Niñas has been intensively studied in the region (Florenchie et al., 2003; Florenchie et al., 2004; Rouault et al., 2007; Lübbecke et al., 2010; Bachèlery et al., 2016; Rouault et al., 2018; Imbol Koungue et al., 2019; Bachèlery et al., 2020) and has been found as the main mode of interannual variability of SST (e.g., Florenchie et al., 2003; Rouault et al., 2018) in the Northern Benguela and Southern Angola. The Benguela Niños/Niñas have no impact on the Central and South Benguela. However, some studies that have been done in these regions reveal that the Benguela is impacted by large-scale climate modes such as ENSO (Agenbag, 1996; Rouault et al., 2010; Dufois and Rouault, 2012; Blamey et al., 2015). Rouault et al. (2010) found that the correlation between SST in Southern Benguela and the Southern Annular Mode (SAM) is not coherent. The ENSO impact the Southern Benguela upwelling by modulating the latitudinal variation of SASH (Dufois and Rouault, 2012; Sun et al., 2017).

1.1.4.2 Trends and Decadal Variability

Reduced equatorward coastal wind decreases the upwelling rate and limits nutrient enrichment of the euphotic zone with negative impacts on primary production, while stronger upwelling conditions may increase the nutrient supply and at the same time increase the offshore transport (Bakun et al., 2010; Bakun et al., 2015; García-Reyes et al., 2015). Accordingly, understanding long-term trends in the Benguela Upwelling System, which is part of my thesis objective, is of great importance for the ecological functioning, resources productivity, and environmental health of the Benguela Upwelling System. Under global climate warming, Bakun (1990) proposed that an increase in coastal upwelling-favourable winds would lead to the intensification of the continental-oceanic pressure gradient and increase upwelling rate. Several studies have identified trends in upwelling in the Benguela region (**Table 1.1**). Some support Bakun hypothesis and some contradict it. Most of these studies are focused on wind analysis. Narayan et al. (2010) found a positive trend in meridional wind stress at Luderitz over 1960-2000 using International Comprehensive Ocean-Atmosphere Data Set (ICOADS) wind data. Sydeman et al. (2014) found positive trends in the South of Benguela Upwelling System, over the last 60 years, in several wind data sets. Lamont et al. (2018), using synoptic-scale upwelling indices based

on Ekman transport derived from National Centers for Environmental Prediction version 2 (NCEP2) reanalysis dataset over the period 1979 to 2015, found a weakening of the upwelling in the Northern Benguela and a strengthening in the Southern Benguela. In contrast, Narayan et al. (2010) study found no trend over the period 1960-2000 when using ERA 40 surface wind speed reanalysis dataset. Few studies focus on ocean SST, a good indicator of the upwelling strength. There is also substantial but conflicting evidence of negative trends in SST (García-Reyes et al., 2015). A negative trend in SST was found by Narayan et al. (2010) and Santos et al. (2012) over the period 1960-2009 using HadISST. However, a positive trend in SST was observed with the same datasets over the period 1870-2006. Rouault et al. (2010) updated by Blamey et al. (2015) found that the upwelling in the Northern Benguela shows a positive trend in SST and the upwelling in South Benguela shows a negative trend while the Central Benguela has not significantly changed. Vizy and Cook (2016) found a positive trend along the Namibian coast in several reanalysis datasets. Recently, using a coupled ocean-atmospheric model, Vizy et al. (2018) found a negative trend in mixed layer temperature in the Northern Benguela upwelling. However, caution is required when extracting trends from a climate model (Vizy et al., 2018), particularly in regions like tropical Atlantic, where these models are known to produce a mean warm bias (Richter et al., 2012; Toniazzo and Woolnough, 2014; Exarchou et al., 2018; Koseki et al., 2018). Abrahams et al. (2021) using a series novel of metrics related to SST from OISST (¼°× ¼°) and upwelling index based on ERA5 wind speed and direction found that in Southern Benguela, an increase of the upwelling favorable winds is associated with a decrease of the SST while in the Northern Benguela an increase of upwelling favorable wind shows an increase of SST.

Table 1.1: Upwelling trends in the Benguela upwelling system

Domaine	Author(s)	Data used	Variable	Period of study	Trend results
Northern Benguela	Lamont et al., (2018)	NCEP2	UI based on Ek transport	1979-2015	negative
	Rouault et al. 2010	OISST (1° x 1°)	SST	1982-2009	positive
	Blamey et al.,2015	OISST (1° x 1°)	SST	1982-2012	positive
	Vizy and Cook (2016)	OISST, Era-Int, NCEP2 MERRA	SST	1982-2013	positive
	Vizy et al. (2018)	CRCM model	Mixed layer Temperature	1980-2014	negative
	Abrahams et al., 2021	OISST (¼° x ¼°) and ERA5	Metric based on SST and UI estimated from wind speed and direction	1982-2018	Positive in UI and SST
Central Benguela	Nararyan et al., (2010)	ICOADS	Wind stress	1906-2000	positive
	Nararyan et al., (2010)	ERA-40	Wind speed	1906-2000	No trend
	Nararyan et al., (2010)	HadISST	SST	1970-2006	negative
	Santos et al., (2012)	HadiSST	SST	1960-2009	negative
	Rouault et al. 2010	OISST (1° x 1°)	SST	1982-2009	No trend
	Sideman et al., (2014)	Several datasets	Wind	Up to last 60 years	positive

Southern Benguela	Lamont et al., (2018)	NCEP2	UI based on Ek transport	1979-2015	positive
	Rouault et al. 2010	OISST (1° x 1°)	SST	1982-2009	Negative
	Blamey et al., 205	OISST (1° x 1°)	SST	1982-2012	negative
	Santos et al., (2012)	HadiSST	SST	1960-2009	negative
	Abrahams et al., 2021	OISST (¼° x ¼°) and ERA5	Metric based on SST and UI estimated from wind speed and direction	1982-2018	Positive in UI and Negative in SST

The failure of consensus among studies could be due to varying spatio-temporal resolutions of the datasets (García-Reyes et al., 2015) and the method used to construct the datasets (Blamey et al., 2015). For example, SST data with coarse resolution cannot distinguish nearshore upwelling related temperatures from offshore temperatures. Due to the spatial and temporal availability of data, most of the climate datasets are reconstructed using different types of *in-situ* and satellite data. That could create an artificial trend in datasets. In the Benguela coastal area, Smit et al. (2013) reported large biases of up to 6°C in places between satellite-derived and in-situ climatological temperatures. Moreover, Blamey et al. (2015) indicate serious problems in the validity of the SST datasets for trend studies in the Benguela Upwelling System. Decadal variability could be also another factor explaining the temporal change in the trend. In the Benguela Upwelling System, to our knowledge, there are few or no works on the decadal variability of SST. Only Hutchings et al. (2009) mentioned decadal variability in SST anomalies from a combination of ICOADS and Satellite data in Northern Benguela. However, several studies have identified decadal variability in the southern African climate system, especially in South African rainfall (Dyer and Tyson, 1977; Jury, 2015; Dieppois et al., 2016). In their study, Dieppois et al. (2016), have demonstrated the existence of two significant signals of decadal variability, including an interdecadal and a quasi-decadal period (15-28 years, and 8-13 years respectively)

in southern Africa rainfall linked to Pacific Ocean climate modes such as the Pacific Decadal Oscillation (PDO), the Interdecadal Pacific Oscillation (IPO) and ENSO in both the austral summer rainfall region and the austral winter rainfall region which is where the South Benguela is situated. Furthermore, there are potential links between the region's rainfall and west and south coast of Southern Africa (Wolski et al., 2021).

1.2 THESIS OBJECTIVES

The Benguela Upwelling System is of great importance because it is one of the most productive areas in the world. It is a source of economic for the adjacent countries and plays an important role in the climate of Southern Africa. In the context of global warming, the Benguela upwelling will be impacted, but how? Will it be warm or cool? Understanding the past variability of the Benguela Upwelling System and the mechanisms leading to these changes is the first step before establishing a future scenario for the region. It is also important to find out if the Benguela Upwelling System has already changed in response to global warming and also to understand the natural variability at the interannual scale and decadal scale. For that matter, international collaborative programs (CLIVAR group on EBUS, EU 2020 project TRIATLAS, Belmont Forum EXEBUS) were developed to understand the drivers of the Benguela Upwelling System, its past variability, the impact of these changes on the marine ecosystems and human society, and to predict its future evolution.

My PhD aims at understanding the long-term change and decadal variability in the Benguela Upwelling System. Specifically, my thesis will try to answer the following questions:

- How has the Benguela Upwelling System changed over the last 100 years?
- What is the validity of the data used to study these changes?
- How do the changes vary depending on seasons?
- Is there any decadal variability in the Benguela Upwelling System?
- Are the Benguela Upwelling System changes linked to the major global decadal climate modes?

1.3 THESIS OUTLINE

In the first part of the thesis, I will use satellite-based SST dataset and reanalysis climate datasets to investigate the change in the Benguela Upwelling System over the last 30 years - the satellite era. I will then investigate the decadal variability and change over the last 50 years with a numerical model, ocean component of the Nucleus for European Modelling of the Ocean (NEMO), forced by reanalysis wind speed. Last, I will examine the change over the last 100 years with a numerical model, ocean component of Norwegian Earth System Model (NorESM), mostly forced by 20 Century Reanalysis (20CR) data. For that purpose, my study will be organized as follow:

Chapter 2 provides a description of the different datasets I used, such as satellite-based products, reanalysis datasets, and models. In the second part, I detail the methods used for this study.

Chapter 3 documents the long-term changes in the Benguela Upwelling System during the satellite era (last 35 years) by comparing trends in different SST and wind datasets at the seasonal scale. I will also compare the results obtained using various datasets.

Chapter 4 examines the long-term changes for the last 35 years using numerical model outputs in which a strong warming trend exists in the ABFZ. This chapter investigates the main processes driving the changes and their seasonal dependence. The Ocean General Circulation Model OGCM NEMO 3.6 simulation is used for that purpose.

Chapter 5 focuses on the decadal variability of the Benguela Upwelling System over the last 100 years using the ocean component of the NorSEM forced by 20 Century reanalysed data. It also seeks to link the change in the Benguela Upwelling System to decadal changes in the Atlantic and Pacific climate modes, the main global drivers of decadal change of climate.

Chapter 6 is a conclusion chapter with perspectives for future work.

CHAPTER 2

2 DATA AND METHODS

2.1 DATA

This study uses a variety of climate variables, mainly sea surface temperature and atmospheric variables derived from various reanalyzed climate datasets. I also use ocean model outputs. The datasets are described below, and a summary of their characteristics is presented in **Table 2.1** for observed oceanic data and **Table 2.2** for atmospheric data.

2.1.1 Gridded observational oceanic data.

Table 2.1: SST products, their data sources, their resolution, and the methods used for their reconstruction.

	In situ observation input	Satellite input	Spatial Resolution	Temporal resolution	Ship-Buoys Correction	Method use for reconstruction
OISST1	ICOADS, GTS,	AVHRR	1° x 1°	Monthly	0°C	Optimal interpolation
OISST0.25	ICOADS, GTS,	AVHRR Pathfinder	0.25° x 0.25°	daily	0.14°C subtracted from ship	Optimal interpolation
HadISST1	ICOADS, GTS,	AVHRR, ATSR	1° x 1°	monthly	0°C	2-step reconstruction technique
HadISST2	ICOADS, GTS	AVHRR Pathfinder ATSR	1° x 1°	monthly		2-step reconstruction technique

ERSST5	ICOADS, Argo floats	N/A	2° x 2°	monthly	0.12°C subtracted from ship	Reconstruction techniques (EOT)
AVHRR Pathfinder	N/A	AVHRR Pathfinder	4km x 4km	daily	N/A	N/A

Sea Surface Temperature (SST) is a good indicator of upwelling strength in Eastern Boundary Currents. The colder is the SST, the stronger is the upwelling in the eastern boundary current. However, this statement is not always true in some regions, like regions at higher latitudes where the SST can be colder despite the absence of upwelling. For that reason, most studies use SST based indices to estimate the strength of upwelling. Others use the SST gradient. For instance, Demarcq and Faure (2000); Narayan et al. (2010) estimated the upwelling index based on differences between offshore SST and nearshore location. SST is also a fundamental variable in climate studies. The daily (Reynolds et al., 2007) and the weekly (Reynolds et al., 2002) optimum Interpolation (OI) SST, the Hadley SST (HadISST) (Rayner et al., 2003), and Pathfinder SST, all derived from Advanced Very High-Resolution Radiometer (AVHRR) and the ERSST (Huang et al., 2017), are broadly used for climate monitoring, prediction, and verification. For this study, comparisons between products are conducted to assess and evaluate the long-term change and coastal variability in the Benguela Upwelling System (see **Chapters 3** and **5**).

2.1.1.1 Weekly Optimum Interpolation Sea Surface Temperature (OISST)

Weekly OISST (Reynolds et al., 2002) gridded at 1° × 1° (OISST1) spatial resolution is an earlier generation of OISST. The OISST1 is derived from the AVHRR instruments on board NOAA (National Oceanic and Atmospheric Administration) satellites, *in-situ* data from ship measurements, buoys, from the International Comprehensive Ocean-Atmosphere Data Set (ICOADS) and the National Centre for Environmental Prediction Global Telecommunication System (NCEP GTS) after 1998. Even if OISST1 does not resolve some coastal area features due to its coarse resolution and the interpolation scheme used, it has been used satisfactorily in regions where anomalous events cover a large region (Rouault et al., 2003). It has been

successfully used in many studies in the Angola Benguela current system of Southern Africa (Roy et al., 2001; Rouault et al., 2003; Rouault et al., 2010; Rouault, 2012). The monthly or weekly data can be downloaded from the NOAA website https://www.esrl.noaa.gov/psd/data/gridded/data.noaa.oisst.v2.html.

2.1.1.2 Daily OISST

The daily OISST (Reynolds et al., 2007) gridded at 1/4° × 1/4° resolution (OISST0.25) is a new generation of OISST with daily rather than weekly resolution as in OISST1. As OISST1 the OISST0.25 records are based on *in situ* ship and buoy observations from ICOADS and NCEP GTS data after 2006 (Woodruff et al., 2011), and satellite data from the AVHRR (Pathfinder dataset from September 1981 to December 2005 and operational AVHRR from January 2006). The OISST0.25 makes use of Empirical Orthogonal Teleconnections (EOT) mode for the bias correction scheme rather than the Poisson method used in the OISST1. Moreover, the daily OISST makes use of input datasets reprocessed from the start of satellite AVHRR mission instead of operational data. This improves SST retrievals. The daily OISST is available from 1982 onward and can be downloaded at https://psl.noaa.gov/data/gridded/data.noaa.oisst.v2.highres.html.

2.1.1.3 Hadley SST version 1

The Hadley SST version 1 (HadISST1) is a reconstructed SST dataset from the UK Meteorological Office, Hadley center (Rayner et al., 2003). The HadISST1 data uses *in situ* SST data from ships and buoys and since 1981 it uses the bias-adjusted SSTs from the satellite AVHRR and along-track Scanning Radiometer (ATSR) SST from 1996 to 2010. It is an analyzed product that uses a 2-step reduced space optimal interpolation method based on covariance adjustment to smooth data and fill the data gaps. Note that the level of uncertainty in the HadISST1 is high due to the technique used (Rayner et al., 2003). The data is available from 1900 onwards, gridded at a 1°×1° spatial resolution with monthly resolution and can be downloaded at https://www.metoffice.gov.uk/hadobs/hadisst/data/download.html.

2.1.1.4 Hadley SST version 2 (HadISST2)

The HadISST2 (Kennedy et al., 2020; Rayner et al., 2020) is an improvement of HadISST1 with new data sources, new adjustments, and improvement of the method of estimating ice concentrations where only information about the sea ice edge is known (Titchner and Rayner, 2014). As HadISST1, HadISST2 uses in situ SST data from ships and buoys and satellite SST data such as AVHRR and ATSR. The HadISST2 product is an ensemble of 10 realizations that provides information about the likely spread arising from uncertainty in the measurement and reconstruction. The data was obtained directly from the producers and is available from 1850-2010.

2.1.1.5 Extended Reconstructed Sea Surface Temperature version 5 (ERSST5)

The ERSST5 (Huang et al., 2017) is a global monthly reconstructed product. The ERSST5 uses new datasets from ICOADS release 3.0 SST, Argo floats above 5 meters, Hadley centre Sea Ice and SST version 2 ice concentration. ERSST5 is an analyzed product reconstructed using localized Empirical Orthogonal Teleconnection (EOT) after a bias-corrected first-guess is applied to *in situ* SSTs. The ship SST biases are corrected relative to the buoy observations. The data is available from 1854 onward, gridded at a 2°×2° spatial resolution with monthly resolution and can be downloaded at https://www.ncdc.noaa.gov/data-access/marineocean-data/extended-reconstructed-sea-surface-temperature-ersst-v5.

2.1.1.6 AVHRR Pathfinder version 5.3

The AVHRR Pathfinder Level Collated (L3C) SST dataset (hereafter Pathfinder) is made by reprocessing all AVHRR instrument SST onboard NOAA satellites. It is a collection of global, twice-daily SST data at 4 km spatial resolution from 1981 to the present using the same algorithm (Kilpatrick et al., 2001). In this thesis, I use the latest version (version 5.3), which has improved the warm bias compared to previous versions. Note, that the Pathfinder dataset uses infrared radiation emitted from the ocean to infer SST and the biggest challenge in retrieving SST from an infrared instrument is the notorious cloud detection problem as clouds also emit infrared radiation and sometimes have a similar temperature as the ocean. The cloud-contaminated data

are often difficult to identify. Moreover, the regions of high SST gradient are often falsely flagged as clouds (Stowe et al. 1999). For that matter, the Pathfinder dataset is available at various quality levels (0-7) based on a hierarchical suite of tests, with 0 being the lowest quality and 7 being the highest (Kilpatrick et al., 2001). Quality level 4 is recommended as the lowest quality level for acceptable SST daily data. Therefore, monthly means were calculated using quality level 4 or higher. This reduces the data coverage but improves the quality of the data. **Figure 2.1** summarizes the number of valid daily observations used for the monthly mean calculation. On average, there are about 8 days of good data per month, representing about 25% of valid recorded data per month for each grid point in the Benguela Upwelling System. I select the Pathfinder because first, it uses AVHRR data products so it is useful to compare Pathfinder with OISST which also uses AVHRR and also because it has been used in the EBUS including the Benguela Upwelling System to evaluate high-resolution models (Penven et al., 2001; Penven et al., 2003; Blanke et al., 2005; Penven et al., 2005; Veitch et al., 2009; Albert et al., 2010; Giraud and Paul, 2010; Veitch et al., 2010; Colas et al., 2012; Echevin et al., 2012). The Pathfinder was also used by Blamey et al. (2015) to establish their SST trend in the Benguela Upwelling System. It can be downloaded from https://www.nodc.noaa.gov/satellitedata/pathfinder4km53/.

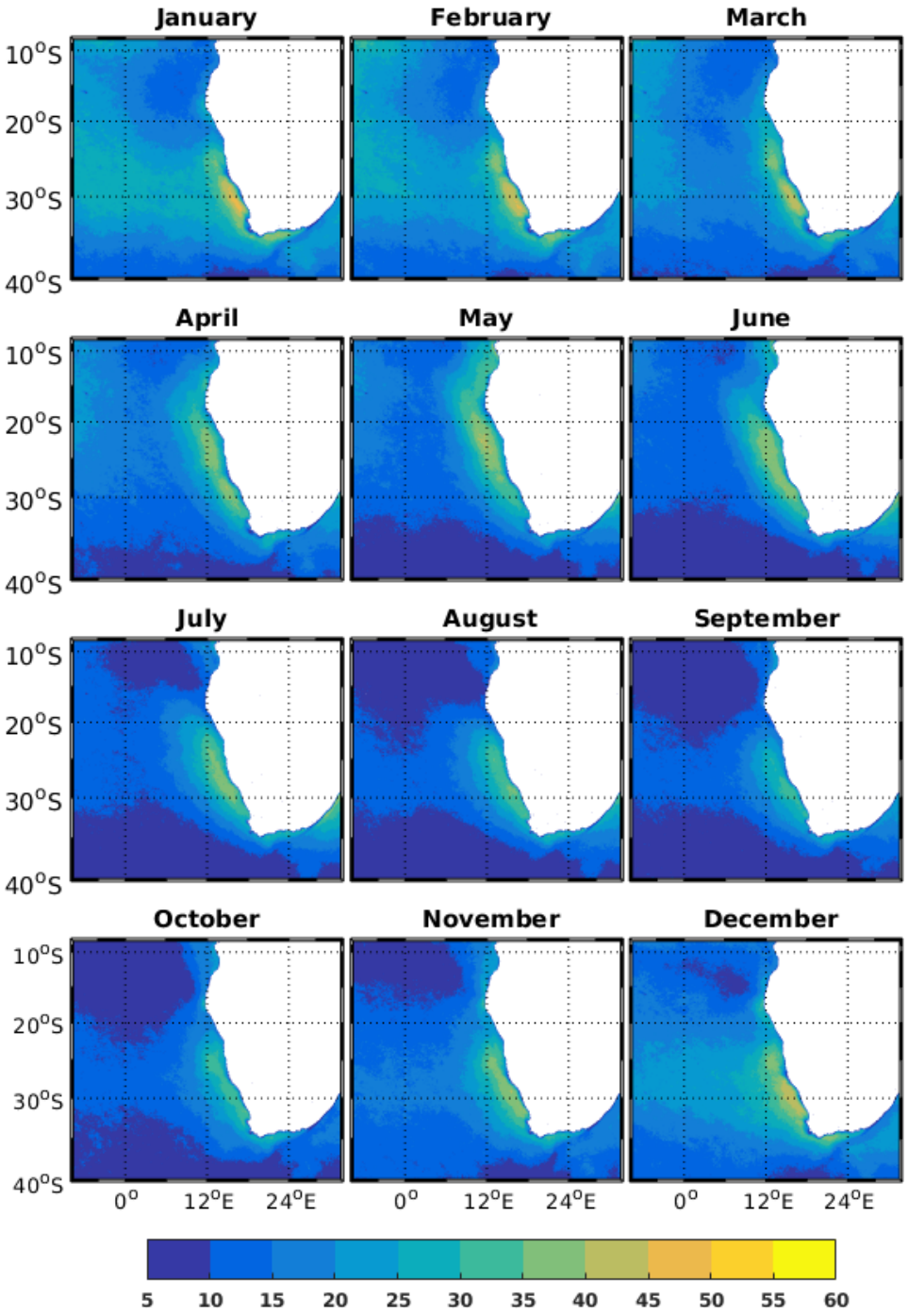

Figure 2.1: Annual cycle of percentage of daily valid data recorded from AVHRR Pathfinder during the period 1982-2017.

2.1.2 Climate indices

Climate indices are also used in this thesis to investigate the connection of the Benguela Upwelling System to climate modes.

- The Pacific Decadal Oscillation (PDO) index: the PDO index is defined as the leading Principal Component (PC) of monthly SST anomalies in the North Pacific Ocean, poleward of 20°N. The monthly mean global average SST anomalies are removed to separate this pattern of variability from any "global warming" signal that may be present in the data. The index is derived using UKMO Historical SST data set for 1900-1981 and weekly OISST from 1982 to the present. This index can be downloaded from http://research.jisao.washington.edu/pdo/PDO.latest. For more detail see (Mantua et al., 1997; Zhang et al., 1997).

- The Interdecadal Pacific Oscillation IPO is based on the Tripole Index (TPI): the TPI IPO index is defined as the difference between the SSTA averaged over the central equatorial Pacific (10°S–10°N, 170°E–90°W) and the average of the SSTA in the Northwest (25°N–45°N, 140°E–145°W) and Southwest Pacific (50°S–15°S, 150°E–160°W). For more details, see Henley et al. (2015). There are two versions of TPI from different sources of datasets: the unfiltered and the filtered one. In this study, I used the filtered one from ERSST5. This index can be downloaded from https://psl.noaa.gov/data/timeseries/IPOTPI/tpi.timeseries.ersstv5.data.

- The Atlantic Multi-decadal Oscillation (AMO) index: the AMO has been identified as a coherent mode of natural variability occurring in the North Atlantic Ocean with an estimated period of 60-80 years. The AMO index is estimated as the average anomalies SST in the North Atlantic basin, typically over 0-80N. The monthly mean global average SST anomalies are removed from spatially averaged timeseries to separate this pattern of variability from any global warming (Trenberth and Shea, 2006). The AMO index is derived using HadiSST1 and can be downloaded from https://climatedataguide.ucar.edu/climate-data/atlantic-multi-decadal-oscillation-amo.

2.1.3 Atmospheric Reanalysis datasets.

Table 2.2: Summary of the main characteristics of the five reanalysis datasets used in the present study.

	Institution	Assimilation scheme	horizontal Resolution	Temporal resolution	Vertical levels	Period of coverage
NCEP-2	NOAA/NCEP DOE	3D-Var	2.5° x 2.5°	6h	17	1979 to present
ERA-Int	ECMWF	4D-Var	0.75° x 0.75°	6h	60	1979 to 2019
ERA5	ECMWF	4D-Var ensemble	0.25° x 0.25°	1h	139	1950 to present
JRA-55	JMA	4D-Var	1.25° x 1.25°	6h	60	1958 to present
MERRA-2	NASA GEOS-5	4D-Var	0.625° x 0.625°	1h	72	1980 to present

Resulting from the assimilation of observations from different sources into global atmospheric models, the climate reanalysis datasets are very popular for a wide range of studies of the atmosphere owing to their homogenous and global nature compared to raw observations. They are useful to understand the interannual and long-term climate variability. They are particularly useful in the Benguela Upwelling System where there is a lack of long and homogenous timeseries of historical wind data from observational measurements. In this thesis, I analyse and compare five global atmospheric reanalysis datasets focusing on wind speed and direction and geopotential height at the 1000 hPa pressure level. This multi-reanalysis approach will help to quantify the uncertainty inherent in the estimation of the long-term change and to identify robust signals across datasets.

2.1.3.1 NCEP-DOE reanalysis II

The National Centre for Environmental Prediction Department of Energy Reanalysis 2 (NCEP-DOE) (Kanamitsu et al., 2002) is a reanalysis developed by the National Oceanic and Atmospheric Administration (NOAA). It covers the satellite period from 1979 to the present. It is an improved version of the NCEP reanalysis (NCEP 1) and fixed some identified problems with an updated parameterization of physical processes. The data assimilation is a three-dimensional variational technique (3D-Var). It has a 2.5° x 2.5° spatial resolution. The data is available 4-times daily, daily and monthly and can be downloaded from https://www.esrl.noaa.gov/psd/data/gridded/data.ncep.reanalysis2.html.

2.1.3.2 Era-Interim

The Era-Interim (ERA-Int), is produced by the European Centre for Medium-Range Weather Forecasts (ECMWF), uses a 4D variational technique to assimilate observational data from many sources to produce a gridded observational data set (Dee et al., 2011). The spatial resolution of the data is approximatively 0.75° x 0.75° on 60 vertical levels from the surface up to 0.1 hpa. The data is available from 1979 to 2019 and can be downloaded from https://apps.ecmwf.int/datasets/.

2.1.3.3 ERA5

The ERA5 (Hersbach et al., 2020), is the fifth generation of ERA and the latest ECMWF atmospheric reanalysis. Replacing the ERA-Int, which stopped in August 2019, ERA5 provides much higher native spatial resolution (0.25° x 0.25°) on 137 vertical levels. ERA5 uses a 4D-Var ensemble scheme. ERA5 covers the period 1950 to the present. The data can be downloaded from https://www.ecmwf.int/en/forecasts/datasets/reanalysis-datasets/era5.

2.1.3.4 Japanese 55-year reanalysis JRA-55

The Japanese 55-year Reanalysis (JRA-55) is the second Japanese global atmospheric reanalysis produced by the Japan Meteorological Agency (JMA) (Kobayashi et al., 2015). It is the first comprehensive reanalysis applying a 4D-Var scheme. It covers the period since 1958. The

main objectives for this new reanalysis were to fix problems found in the previous ones and to produce a suitable comprehensive atmospheric dataset for long term variability and climate change studies. The data can be downloaded from https://rda.ucar.edu/datasets/ds628.0/.

2.1.3.5 MERRA-2

MERRA-2 (Molod et al., 2015) is the most recent reanalysis produced by NASA's Global Modelling and Assimilation Office (GMAO). It uses the Goddard Earth Observing System-5 (GEOS-5) atmospheric general circulation model (AGCM) with a 4D-VAR data assimilation scheme. The data are hourly fields produced with a horizontal resolution of 0.625 × 0.5 and 72 hybrid-eta levels from the surface to 0.01hpa. The data can be downloaded from https://gmao.gsfc.nasa.gov/reanalysis/MERRA-2/.

2.1.4 Ocean model outputs

2.1.4.1 Tropical Atlantic Simulation (TATLT025) using NEMO 3.6

2.1.4.1.1 The model Configuration

The Oceanic model NEMO 3.6 (Nucleus for European Modelling of the Ocean program) is used to produce a multi-decadal (1958-2015) ocean simulation. This model, as detailed by Madec et al. (2017), is a three-dimensional, free surface, hydrostatic, primitive-equation global ocean general circulation model. The regional configuration, with 0.25° horizontal resolution, covers the whole tropical Atlantic. The vertical grid consists of 75 levels, with a vertical resolution of ~1m within the first 20m and 24 levels within the first 100m. At the lateral boundaries, the model is forced with the daily outputs of the Global MERCATOR reanalysis GLORYS2V3 and the surface forcing consists of the 3-h wind field, atmospheric temperature, humidity and daily fields of longwave, shortwave radiation, and precipitation from DFS5.2 (DRAKKAR Forcing Set version 5.2; Dussin et al. (2016) at the surface. The atmospheric fluxes of momentum, heat and freshwater are provided by the bulk formulae (Large and Yeager, 2009). This configuration and model output have already been used by Imbol Koungue et al. (2019) for Benguela Niño and Benguela Niña studies since 1958. Note that there is no restoring of SST. For further details regarding

parameterization and validation, including observation data of SST, SSH, vertical profiles of temperature and currents, one can refer to Hernandez et al. (2017) and Imbol Koungue et al. (2019). The major advantage of that simulation is that along with traditional parameters (such as sea level, temperature, salinity, and currents), the components of the mixed-layer heat budget were saved which allows disentangling and studying in details the processes contributing to the SST trend in the Benguela Upwelling System.

2.1.4.1.2 The model mixed-layer heat balance

The mixed-layer heat content equation can be written as follow:

$$< \partial_t T > = \underbrace{-< u\partial_x T + v\partial_y T >}_{Hor\ ADV} + \underbrace{< D_t(T) >}_{L\ Diff} - \underbrace{< w\partial_z T >}_{Z\ ADV} + \underbrace{\frac{1}{h}\frac{\partial h}{\partial t}(< T > -T_{z=-h})}_{V\ ENT} + \underbrace{\frac{1}{h}(K_z\partial_z T)_{z=-h}}_{Z\ Diff} + \underbrace{\frac{Q_{ns} + Q_s(1 - F_{z=-h})}{\rho_o C_p h}}_{Sforc} \quad \text{Eq. 2.1}$$

With $< \cdot > = \frac{1}{h}\int_{-h}^{0} \cdot \partial_z$ representing depth-averaged integration over the variable mixed layer depth. T is the model potential temperature, (u, v, w) the velocity components, $D_t(T)$ is the lateral diffusion operator, Kz is the vertical diffusion coefficient for tracers, C_p is the specific heat of sea water, ρ_o is the surface density, and h is the mixed-layer depth.

Q_{ns} and Q_s are respectively the non-penetrative (turbulent latent and sensible heat fluxes and total infrared longwave heat flux) and penetrative components of the air-sea heat flux (shortwave radiation). $F_{z=-h}$ is the fraction of the shortwave radiation that reaches the mixed-layer depth (MLD). The MLD is defined as the depth where the density increase compared to density at 10 m equals 0. 03 kg.m^{-3}.

The terms “Hor ADV” represents the horizontal advection. “L Diff” is the lateral diffusion “V ENT” and “Z ADV” are respectively the vertical entrainment and advection and finally “Sforc” is the net heat fluxes storage in the mixed layer.

2.1.4.2 Global ocean simulation using the ocean-ice components of the NorESM

To analyze the decadal variability, it is important to have a long simulation of at least a century. I am using the output of the 110 years (1900-2010) of the global ocean-ice components of the Norwegian Earth System Model (NorESM) (Bentsen et al., 2013). This model originates from the Miami Isopycnic Coordinate Model MICOM (Bleck and Smith, 1990; Bleck et al., 1992), The Ocean-ice components of the NorSEM is a tripolar grid with about 1° horizontal resolution except towards the equator where the meridional resolution is about 0.25°. The ocean model has 52 layers: 51 isopycnals referenced to pressure at 2000 dbar and one surface mixed layer divided into two non-isopycnic layers. The model is forced by the 3h data air temperature, humidity, winds and diagnosed air density of adjusted 20 centuries reanalysis (20CRadj) (He et al., 2016). The turbulent momentum, heat and moisture fluxes are computed by bulk formulae (Large and Yeager, 2009). The model is initialized by the January mean climatology of potential temperature taken from the World Ocean Atlas WOA98 (Antonov et al., 1998; Boyer, 1998). The climatology river runoff (Dai and Trenberth, 2002) is used for the period 1871-1948 and 2008-2009 while the monthly varying river and coastal runoff dataset from the period 1948-2008 (Dai et al., 2009) are used as the continental freshwater input. Further information about the model setup, parametrization and validation for global SST refer to He et al. (2016).

2.2 METHODS

To study the long-term trends in the Benguela Upwelling System in SST and wind speed in **chapter 3**, over the period 1982-2017, I use the satellite-derived OISST1, OISST0.25, HadISST1 and Pathfinder and the reanalysis NCEP2, MERRA-2, ERA-Interim, ERA5 and JRA-55. Note that the geopotential height from the 5 reanalysis datasets previously cited is also used in this chapter. To further investigate trends and variability within the coastal zone, four domains are selected

along the west coast of Africa within the Angola-Benguela Upwelling System. As the main upwelling occurs in a narrow band of 25 to 150km off the coast (Chavez and Messie 2009; Fennel et al., 2012), each domain is within 1° wide off the coast. However, each domain has been extended up to 3° wide for winds because coastal winds belong to large scale features such as the SASH and low-pressure system, and as I will show later, the reanalysed wind data, which are modelled, do have problems close to the coast. The latitudinal extend of each domain is chosen to be the same size. The domains are the Angola Benguela Front (ABF) (15-19°S), which is the transition region between warm tropical water and cold Benguela upwelling water; Northern Benguela (NB) (20-24°S), which is the perennial upwelling region but under the influence of Benguela Niños and Niña, Central Benguela (CB) (25-29°S) which is the most perennial upwelling region and Southern Benguela (SB) (30-34°S) which has a seasonal upwelling. The SB and NB domains are similar to the ones used in Rouault et al. (2010) and Rouault (2012), respectively. The ABF domain is similar to the one used in most Benguela Niños and Niñas studies.

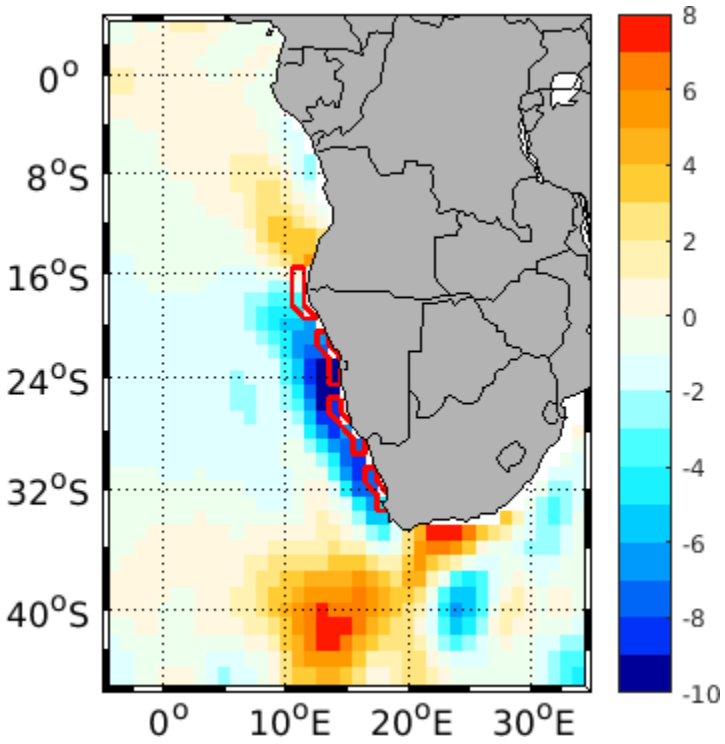

Figure 2.2: Zonal SST gradient (°C/1000km) of long-term mean of OISST from 1982-2017. The red lines delimit the four domains used for analysis: ABF, NB, CB, and SB.

In **chapter 4**, to investigate the mechanism of long-term changes of the last 35 years in the Angola-Namibia region, I used OISST1, OISST0.25, HadISST1 and the numerical simulation NEMO 3.6. to understand the mechanisms behind the changes. I use the same simulation NEMO 3.6 in **chapter 4,** to investigate the decadal variability of the Benguela Upwelling System over the last 50 years in **chapter 5**. Finally, I use HadISST1, HadISST2, ERSST5, and NorESM to investigate the decadal variability in the Benguela Upwelling System over the last 110 years. Note that to investigate the decadal variability in the whole upwelling, the previous domains have been extended to 4°-width coastal band. The coastal upwelling can extend far offshore up to 300 km (Desbiolles et al., 2014) due to wind stress curl extending far to the west and also eddies and filaments advected to the west. Furthermore, the zonal SST gradient (**Figure 2.2**) delineates the Benguela upwelling zone of influence up to 4° off the coast. All the data and periods used for each chapter of results (3 to 5) are summarized in Table 2.3

Table 2.3: Summary of data/model outputs and the period of study used for each chapter of results.

Chapter	Data used	Period of study
Chapter 3	**Oceanic observation**: OISST1, OISST0.25, HadISST1 and Pathfinder **Atmospheric Reanalysis**: NCEP2, MERRA-2, ERA-Interim, ERA5 and JRA-55 (1982-2013)	1982-2017
Chapter 4	**Oceanic observation**: OISST, OISST0.25, HadISST1 **Model outputs**: NEMO	1982-2015
Chapter 5	**Oceanic observation**: OISST1 (1982-2009), HadISST1, HadISST2, ERSST5 **Model outputs:** NorESM **Climate Index**: PDO (based on PC UKMO historical SST), IPO (ERSST5 based on tripole Index), AMO (based on HadiSST1)	1910-2009

2.2.1 Linear least square regression fit (linear trend)

2.2.1.1 Linear trend

To calculate the long-term change in the Benguela Upwelling System, I calculate the linear trend of SST and wind speed at each grid point of my larger domain of study and in the four averaged regional domains ABF, NB, CB and SB, from a linear least square regression. This linear least square regression can be expressed as:

$$Y = B_0 + B_1 t \qquad \text{Eq. 2.2}$$

where the dependent variable (Y) is the timeseries of the parameter analysed (wind speed or SST) and the independent one is time (t). The coefficient B_0 is the intercept and the regression coefficient B_1 (the slope) is the linear rate of the parameter. Positive values of B_1 denote an increasing trend which means the parameter analysed increases over time, whereas negative values indicate a decreasing trend. Here I estimate the decadal linear trend, which is the rate of change over a period of ten years (per decade).

2.2.1.2 Statistical significance test for the trend (Student's t-test)

To test the statistical significance of trends, the Student's t-test is applied. The Student's t-test is any statistical hypothesis test in which the test statistic follows the Student's t-distribution with N-2 degree of freedom, when the sample size N is large (N > 20). The t-statistics, tested against the t-distribution values, can be expressed as:

$$T = \frac{B_1}{Se(B_1)} \qquad \text{Eq. 2.3}$$

Where $Se(B_1)$ is the standard error of B_1.

2.2.2 Monthly anomalies and normalization

To investigate the trend and the decadal variability in SST and surface wind speed, monthly anomalies are estimated. First, the data are averaged to produce monthly means. The monthly anomalies are then computed by removing the monthly climatology of each month of the timeseries. The monthly anomalies are normalized by dividing each monthly anomaly by the

standard deviation of that month (eg. Rouault, 2012) to help to compare different variables in terms of abnormal events.

2.2.3 Filtering procedure

To investigate a possible decadal variability in the Benguela Upwelling System over the last 100 years (**chapter 5**), the monthly anomalies or the normalized anomalies data are detrended. These detrended anomalies are filtered using a Hanning filter with 11 years windows to remove frequencies less than 11 years. The band-pass Butterworth filter is also used in chapter 5 to reconstruct the timeseries in different decadal dominant time scales of variability

2.2.4 dSST derived from net surface heat fluxes

To investigate the mechanism accountable for the long-term changes in the Angola-Namibia region in **chapter 4**, trends are also estimated for different parameters (such as currents, mixed layer depth, Qnet etc.) involved in the heat budget and on the monthly rates of change of SST ($dSST$). The $dSST$ is the monthly contribution of heat fluxes estimated from Qnet. The $dSST$ here is assimilated to the ''Sforc'' in the NEMO model equation. Assuming that vertical heat flux through the thermocline is weak and as the thermocline is shallow in our region of study, the influence of surface heat on seasonal variation can be modelled through the following expression:

$$dSST = dt * \frac{Q_{net}}{\rho_o * C_p * h_{mld}} \qquad \text{Eq. 2.4}$$

where $dSST$ is the SST change over a time interval dt (here dt is equal to 1 month); Qnet is the net surface heat flux, h_{mld} is the mixed layer depth, ρ_o (ρ_o = 1027 kg.m-3) is the seawater density, C_p (C_p = 4200 J/(kg.°C)) is the seawater heat capacity. The model was applied by Yu et al. (2006) to quantify the role of local heating in the SST fluctuation in the tropical Atlantic.

2.2.5 Wavelet analysis

Wavelet analysis is a powerful tool for detecting time-frequency variations within time-series data (Torrence and Compo, 1998). In **chapters 3** and **5,** I use wavelet analysis with a

continuous wavelet transform, based on the Morlet wavelet with angular frequency 6, in order to investigate potential changes in the spectral content of monthly SST data.

2.2.5.1 Wavelet power spectrum

By representing the time-series in a time scale domain, we can determine which scales of variability periods are the dominant variability modes affecting the SST data. Such decomposition of the monthly SST or wind signals is conducted to produce the local wavelet spectra (or global wavelet spectra in scale dimension only), which produces a good trade-off between time and frequency resolution (Farge, 1992; Torrence and Compo, 1998). Following Torrence and Compo (1998) the significance levels are determined using Monte Carlo simulation of a first-order autoregressive (AR[1]) process. To minimize edge effects and to avoid wraparound issues, the time series are padded with zeroes. The cone of influence, which delineates the area under which power can be underestimated as a result of edge effects and zero padding, is therefore represented on all spectra as a black or white bold line (Torrence and Compo, 1998). A detailed description of wavelet analysis can be found in Torrence and Compo (1998).

2.2.5.2 Wavelet coherence

The Wavelet coherence, another useful quantity from Fourier analysis, is defined as the square of the cross-spectrum normalized by the individual power spectra (Torrence and Compo, 1998; Grinsted et al., 2004). The Wavelet coherence is a measure of the correlation between two timeseries in a time-frequency plane as in the classical wavelet power spectrum (see 2.2.5.1). As in wavelet power spectrum, the statistically significant coherence at the 95 % level confidence limit is determined based on 1000 Monte Carlo simulations of the red noise background spectrum sharing the same autoregressive coefficients as the original data. The relative phase relationship between the two timeseries is represented by arrows and can be interpreted as a lead or lag relationship. If the arrows are pointing rightwards or leftwards, they represent phase coherence or anti-phase coherence, respectively. When arrow phase is pointing down or upwards, it means that the time series are in quadrature: one timeseries is leading the other by 90 degrees or lagging

by 270 degrees. A detailed description of wavelet analysis can be found in Torrence and Webster (1999) and Grinsted et al. (2004).

2.2.6 Composite and bootstrap

The composite analysis is a process of averaging a particular field over some identified occurrences of particular events or periods. It is a useful technique for exploring the large-scale impacts of climate mode teleconnections. In this study, composite analysis is used to investigate the role of global SST on the Benguela Upwelling System at each dominant decadal time scale of variability (cf. chapter 5). The extreme warm or cold events defined when the reconstructed SST anomalies exceed ±1 standard deviation are selected at each dominant decadal-scale and the composite analysis is performed only on extreme warm or cold reconstructed SST events. Although, the reconstructed SSTs are based on harmonics which by definition are symmetric. It seems that the global symmetry is due to the impact of ENSO like conditions or different phases of the South Atlantic dipole mode that are by essence symmetric.

To test the statistical significance of the composite maps in **chapter 5**, the bootstrap method is used. The bootstrap technique is a non-parametric test that uses only the data distribution itself (Efron and Tibshirani, 1991) to determine various confidence levels. It is based on a resampling method. The basic idea is to generate randomly artificial data having the same size as the target. The target in this study is the SST anomalies greater than +1 Standard Deviation (SD) or smaller than -1 SD. I used 10000 iterations corresponding to 10000 randomly artificial averages generated from the initial dataset. In this study, I apply the Bootstrap method to each spatial point separately. In this case, the original data is resampled 10000 times to form 10000 artificial averages and sorted in ascending order. Each grid point of the composite is statistically significant at 95 % if its value can be classified as an “outlier”, meaning that this value is in the upper 2.5% or lower 2.5% of the artificial group distribution.

CHAPTER 3

3 INTER-COMPARISON OF OBSERVATIONAL SST DATA AND REANALYSIS WIND DATA IN THE BENGUELA UPWELLING SYSTEM: TREND ANALYSIS

3.1 INTRODUCTION

Sea Surface Temperature (SST) is a good indicator of upwelling strength in Eastern Boundary Currents such as in the Benguela Current system. South-easterly winds lead to upwelling of cold deep water along the western coast of Southern Africa. Upwelling in the Benguela system is due to the coastal branch of the anticyclonic wind of the South Atlantic Anticyclone (Veitch et al., 2010). This wind, also modulated by the orography, the orientation of the coast and the thermal contrast with the continent, is mostly alongshore and equatorward along the south-west coast of Africa (Nelson and Hutchings, 1983). Satellite remote sensing provides an estimation of SST since the 1980s and therefore allows us to quantify interannual variability and trend. An apparent paradox associated with global warming is that it might lead to intensified upwelling-favourable winds worldwide (Bakun, 1990; Bakun et al., 2015; Rykaczewski et al., 2015; Wang et al., 2015) leading to cooling of SST in upwelling systems such as the Benguela Upwelling System. Rouault et al. (2010) and Blamey et al. (2015) found that the trends in SST for the period 1982-2009 in the Benguela Upwelling System using the 1°×1° Optimum Interpolation SST (OISST1) vary in space and have a distinct seasonality. They revealed that the Angolan and North Namibian coastline displayed a warming trend in all months of the year from 0.2 to 0.5°C per decade (10 years) depending on the season. They found that the central part of the Benguela Upwelling System had not significantly changed while the Southern Benguela had cooled by up to 0.5°C but only from January to August. Vizy and Cook (2016) explain the warming off Angola and Northern

Benguela by a decrease in wind speed due to a poleward shift of the South Atlantic Subtropical High (SASH) which would decrease the upwelling rate and the turbulent sensible and latent heat flux. Such shift was mentioned by Jarre et al. (2015). Detecting trends in coastal upwelling remains a challenge due to cloud cover, sunlight, proximity of the coast, concentration of aerosols, and the unavailability of long enough, homogenous, and well-calibrated time series of observed *in situ* data. By using OISST1 and Pathfinder, Blamey et al. (2015) found a contradictory trend in Southern Africa, indicating a serious problem in the validity of SST trends around Southern Africa. These problems might arise due to the techniques of SST retrieval, the spatial resolution of data, and/or potentially strong SST biases observed by some satellites in the Benguela Upwelling System. Contradictory results were also found in wind speed trend in the Benguela Upwelling System. Narayan et al. (2010) found no trend for the wind speed in the Benguela Upwelling System, over the period 1960-2000 when using ERA 40 reanalysis surface wind speed. Recently, Lamont et al. (2018), using synoptic-scale upwelling indices based on Ekman transport derived from National Centers for Environmental Prediction version 2 (NCEP2) reanalysis dataset over the period 1979 to 2015, found a weakening of the upwelling in the Northern Benguela and a strengthening in the Southern Benguela. This contradictory results also may arise from the fact that the analysis were not done in the same period and trends are obscured by the interannual to multi-decadal variability that result from regional and local ocean and atmospheric processes (García-Reyes et al., 2015). Most studies in the Benguela Upwelling System used either one SST dataset and or one reanalysis products sometimes with coarse resolution which can have limitation detecting the real trend in the upwelling. In addition, most studies assumed a linear or steady trend. No study has not been done on decadal variability in the BUS to my knowledge. In this study, I use a comprehensive comparison approach based on several SST datasets and reanalysed wind dataset to calculate analyse trend in SST and wind speed in the Benguela upwelling system and test the possible existence of decadal variability. This method is useful to address the uncertainty and limitation in the estimation of long-term trends.

To do so, I first compare SST data and reanalysed wind data in the Benguela Upwelling System by analysing their long-term mean and annual cycles. Then, I investigate trends in the

Benguela Upwelling System using these various SST and wind datasets. Geopotential height, an indicator of high- and low-pressure systems, is also analysed in this chapter to look for shifts or intensification of the SASH. Finally, the dominant time-scale of SST variability at interannual and decadal scales in the Benguela Upwelling System is explored using wavelet analysis and filtering of SST data to distinguish any linear trend from decadal variability. Four domains are selected along the west coast of Africa within the Benguela Upwelling System. Each domain is 4° long in latitude and 1° wide off the coast for SST but 3° wide for winds as mentioned in the method (cf section 2.2). As I will show, the reanalysed wind data, which is modelled, does have problems close to the coast. The domains are the Angola Benguela Front (ABF) (15-19°S), Northern Benguela (NB) (20-24°S), Centre Benguela (CB) (25-29°S) and Southern Benguela (SB) (30-34°S).

3.2 LONG-TERM MEAN AND SEASONALITY IN THE BENGUELA UPWELLING SYSTEM

3.2.1 Long-term means of SST

Figure 3.1 presents the annual climatology of SST (upper panel) and standard deviation of the monthly anomalies of SST (lower panel) using OISST1, HadISST1, OISST0.25, and Pathfinder. Figure 3.1 is used to compare the annual mean and variability pattern of SST among datasets, over the period 1982-2017 in the Benguela Upwelling System. All the climatologies display the same large-scale feature with cool SST observed along the Namibian and South African west coasts albeit with different minima (**Figure 3.1**, upper panels), as well as open ocean south of 35°S. The warm waters transported by the Agulhas Current south of Africa are represented differently among datasets. Warm SST, exceeding 26°C, is observed in the Angolan sector north of the ABF in all datasets. OISST1 and HadISST1 have respectively a minimum SST of 17°C and 18°C in the Benguela Upwelling System close to the coast. The OISST0.25 is slightly cooler in the Benguela Upwelling System with a minimum SST of 16°C close to the coast. The Pathfinder has the coolest SST in the Benguela Upwelling System with a minimum temperature around 15°C close to the coast and has a good representation of the Agulhas Current. Overall, Hadley SST annual mean magnitudes, in the Benguela Upwelling System, are 1-3°C higher than the other products especially in the Centre and Southern Benguela, while Pathfinder exhibits the lowest annual mean SST in the Benguela Upwelling System. Having higher resolution, these

results are expected. However, HadISST1, having the same resolution as OISST1 is conspicuously different.

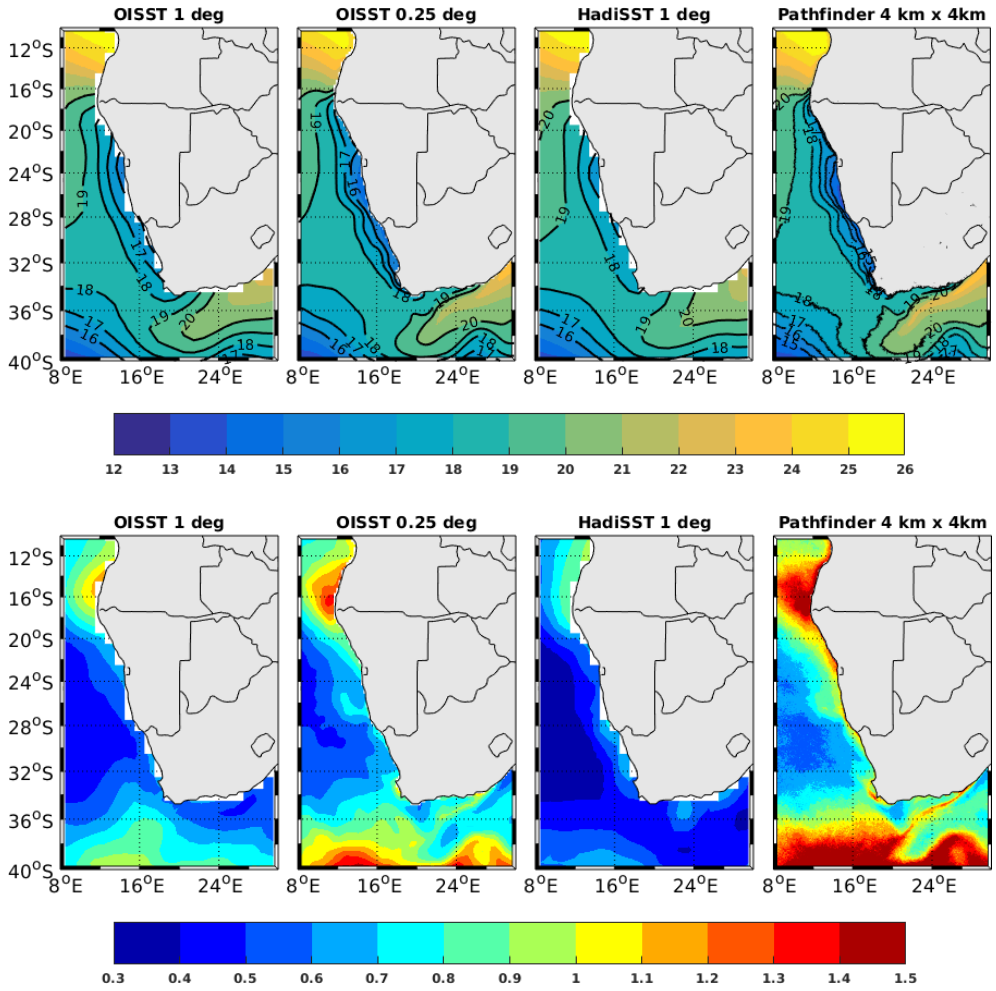

Figure 3.1: Top panel: Annual mean of SST for the period 1982 to 2017 computed with OISST1, OISST0.25, HadISST (1°×1°), and Pathfinder (4km × 4km) from left to right respectively. Bottom panel is the corresponding standard deviation.

The annual standard deviation of the monthly anomalies of the SST datasets (**Figure 3.1**, lower panels), reveals a spatial difference of SST variability along the east coast of the South Atlantic. The SST in the Benguela Upwelling System and the SASH show less variability compared to the SST in the two coastal boundaries of the Benguela upwelling, ABF and Agulhas region. In the Benguela Upwelling System, the standard deviation is less than 0.7°C with the SST datasets except for Pathfinder where the standard deviation is about 0.9°C close to the coast. The SST in

the two coastal boundaries of the Benguela Upwelling System shows stronger variability. In the ABF, the standard deviation varies between 1.1°C and 1.3°C with OISST1 and OISST0.25, between 0.7°C and 0.9°C for HadISST1 and more than 1.5°C for Pathfinder. In the Agulhas Current region especially in the Agulhas retroflexion area, the standard deviation of SST is ~0.9°C for OISST1 and larger than 1.3°C for OISST0.25 and Pathfinder. In summary, Hadley SST has the lowest interannual variability along the east coast of the South Atlantic, while Pathfinder has the highest variability. Again except for HadISST1, these differences could be due to the difference between datasets and/or the methods used to reconstruct the dataset.

3.2.2 Annual cycle of SST

The monthly climatological SST, over the period 1982-2017, in the eastern part of the South Atlantic, is illustrated in **Figure 3.2** and **Figure 3.3**. A comparison of the annual cycle of SST for all datasets is shown in **Figure 3.3** for the four locations: ABF, NB, CB and SB. The shaded area in **Figure 3.3** represents one standard deviation. These figures show high variability of SST throughout the year depending on location. The highest variability is observed in the ABF (15-19°S) with a maximum value of SST of about 23-26°C observed in February-April and with a minimum value of SST of about 13-16°C observed in July-September. Relatively warm water is observed offshore while a narrow band of cool water is observed along the coast from 20°S to 35°S with minimum values of 13-14 °C observed at Lüderitz (~27°S) all the year where the strongest and most persistent upwelling of the Benguela Upwelling System occurs (Shannon and Nelson, 1996). The contrast of SST between the coast and offshore is very high in austral summer, earlier autumn, and can reach 5°C difference in March-April (**Figure 3.2)** indicative of upwelling. In the Benguela Upwelling System, the SST magnitude ranges from about 13 to 19 °C with the maximum in late austral summer (February-March). Minimum values of 13-15°C, are observed in austral winter-earlier spring season (June-September) along the coast and extended offshore. This, at first glance, does not match the general knowledge that upwelling in the region should be more intense in austral summer and the water at the coast should be cooler in austral summer when the upwelling favourable south-easterly wind is stronger. SSTs should also be warmer in austral winter in the Southern Benguela where north-westerly wind dominates which is not the case in **Figure 3.2** and **Figure 3.3**. However, the very cold coastal water may not be captured by

the low resolution of the datasets when compared with climatology obtained with the 500 m by 500 m climatology done by Dufois and Rouault (2012), but I note that the gradient of SST which is also used to characterized upwelling intensity by many authors is higher in austral summer than in austral winter indicating that even if the datasets do not capture the very cold water at the coast, they do pick up the rest of the upwelling. The SST offshore of the upwelling follows the expected influence of the annual change of solar radiation (Demarcq et al., 2003). Moreover, Pathfinder and AVHRR data have a warm bias near the coast (Dufois and Rouault, 2012). Looking at **Figure 3.3**, all SST products display the same annual cycle across all the regions. A comparison among datasets (**Figure 3.3**) reveals that, in the ABF and the Benguela Upwelling System, HadISST1 has the warmest SST all year long while OISST0.25 and Pathfinder have the coolest SST. In the ABF (**Figure 3.3 left top panel**), the maximum SST ranges between 20 and 24°C depending on datasets and is observed in March. The minimum SST ranges between 15 and 19°C within datasets and it is observed in August. In the NB (**Figure 3.3**, **right top panel**), maximum SST ranges between 17 and 20°C in February. Minimum SST ranges from 13 to 16°C with OISST1, OISST0.25 and Pathfinder while it is ~17°C in HadISST1 dataset. CB and SB have the same range of variability with a maximum from 16 to 20°C in February as in NB. However, CB exhibits the coldest values in austral winter with SST ranging between 13 and 15°C using OISST0.25 and Pathfinder (**Figure 3.3 left bottom panel**). As mentioned above, the HadISST1 exhibits the highest SST value in the annual cycle and is quite different from the other datasets in the Benguela Upwelling System especially in the CB and SB. Its standard deviation does not overlap with others. The SST difference of HadISST1 compared to OISST0.25 or Pathfinder is up to 4°C in CB and SB.

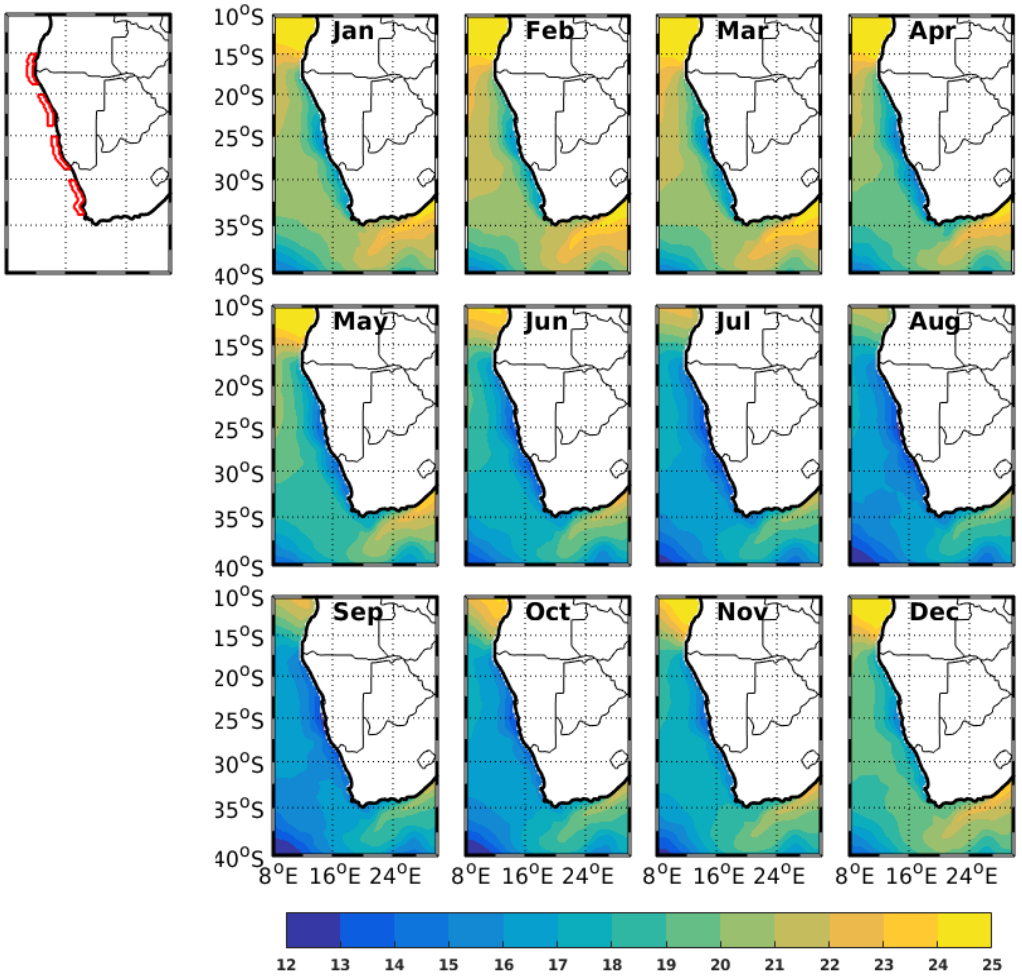

Figure 3.2: monthly SST (°C) climatology from 1982 to 2017 computed with OISST0.25 in the Benguela region. The zoom with the red boxes denotes the four domains used for analysis: ABF, NB, CB and SB**.**

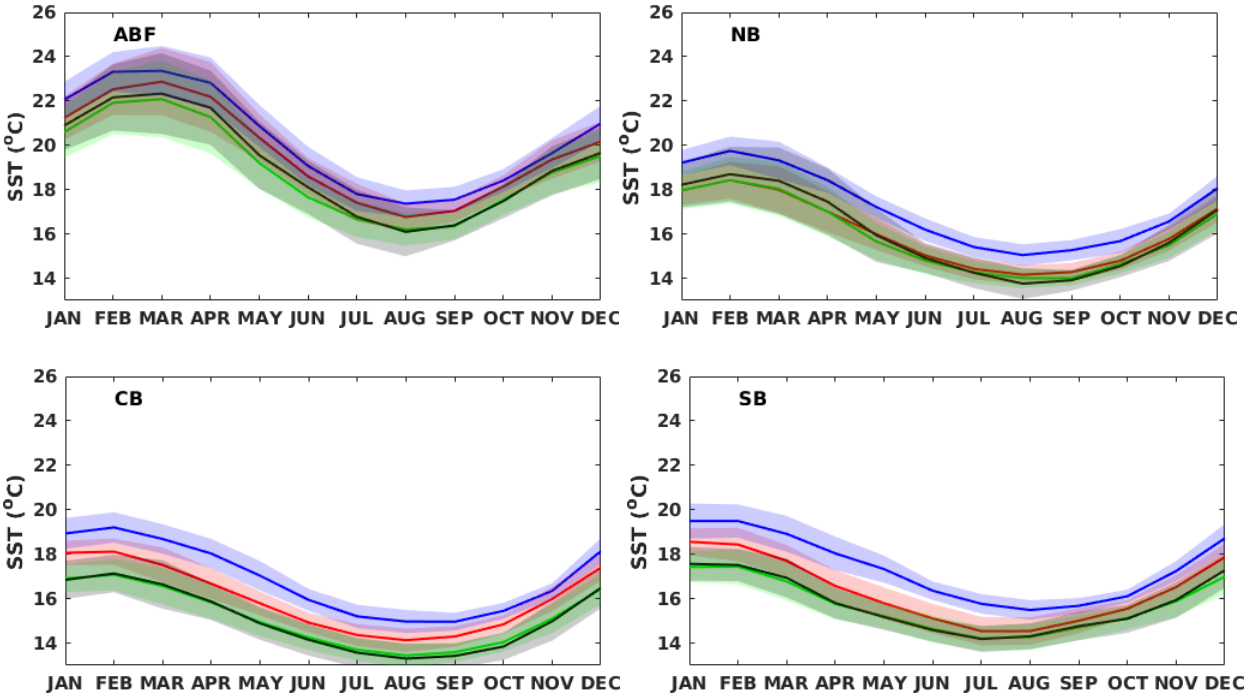

Figure 3.3: Annual cycles of SST (°C) in the Benguela Upwelling System off ABF, NB, CB and SB domains (see map in Figure 3.2) for OISST1 (red), OISST0.25 (green), HadISST1 (blue) and Pathfinder (black). Shaded areas represent the standard deviation.

3.2.3 Annual cycle of wind

3.2.3.1 Long-term means of wind

Figure 3.4 shows the annual mean of near-surface wind speed at the height of the 1000 hPa isobar of ERA5 for the period 1982-2017 (**Figure 3.4 a**) and the zonal average, from the coast to 3° off of the meridional wind of near-surface meridional wind of the five different reanalysis datasets used here: ERA5, Era-Interim, MERRA-2, JRA-55 and NCEP2 (**Figure 3.4 b**). Strong winds, up to 10 $m.s^{-1}$, are observed along the Namibian and South African west coasts, while weak winds are observed along the Angolan coast, in the centre of the SASH between 27°S-35°S and 0°E-6°E, and along the southern coast of South Africa (**Figure 3.4 a)**. The wind speed is about 3-4 $m.s^{-1}$ along the Angolan coast. It is less than 3 $m.s^{-1}$ in the centre of the SASH and along the south coast of South Africa. Along the west coast, the mean wind is mostly equatorward. It is southerly along

South Africa, southeasterly along Namibia and southwesterly along Angola. The maximum winds, about 9 m.s^{-1}, are observed in the CB and ABF regions.

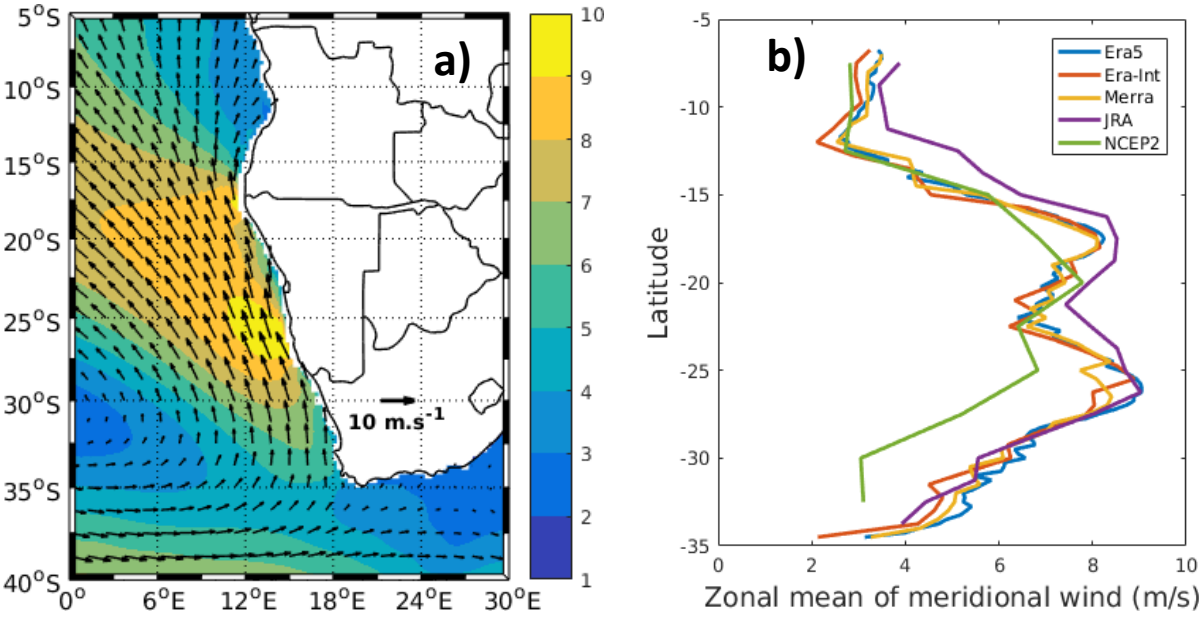

Figure 3.4: a) annual mean of wind speed of ERA5 (m.s^{-1}) at 1000hpa for the period 1982-2017, superimposed with the annual mean direction (black arrows). **b)** zonal average in the 3°-width coastal band of the annual mean of the meridional wind along the Angolan, Namibian, and South African west coast for the ERA5 (blue line), Era-Interim (red line), MERRA-2 (yellow line), JRA-55 (purple line), and NCEP2 (green line). The time period for the mean is 1982-2017 for all datasets, except for JRA-55 dataset which is 1982-2013.

A comparison of meridional wind along the coast among the datasets (**Figure 3.4 b**) shows that in the Benguela Upwelling System the patterns of coastal wind in all the datasets are in good agreement with ERA5, except for NCEP2 and JRA-55 in the Northern Benguela and Angola region. As mentioned in the previous section, weak equatorward meridional winds ranging from 2 to 4 m.s^{-1} are observed north of the ABF and in South Benguela. Between these two boundaries, a relatively stronger coastal meridional wind is observed, greater than 4 m.s^{-1}, with two maxima. One maximum is observed in the ABF and the second one is observed in the CB with values ranging between 8 and 9 m.s^{-1}. For NCEP2, the maximum wind observed in the ABF zone is slightly

south of ABF. Moreover, in the Benguela Upwelling System, the NCEP2 has the weakest wind with a difference of 2 to 4 $m.s^{-1}$ compared to other datasets. This may be due to the coarse resolution of NCEP2 (2.5°×2.5°).

3.2.3.2 Annual cycle of meridional wind

Figure 3.5 displays the annual cycle of the near-surface coastal meridional wind for the five different reanalysis datasets at the four locations (ABF, NB, CB and SB), as in **Figure 3.3** except that the coastal boxes are extended to 3° off the coast. All the products present the same pattern of the annual cycle except NCEP2 in ABF and NB. In ABF, all datasets show a relatively strong equatorward meridional wind ranging from 5 to 10 $m.s^{-1}$ throughout the year. Minimum values of meridional wind are observed in January-February. Two maxima are observed: one in April-May and the second in October in most datasets. However, the April-May maximum is not observed in NCEP2. As in the ABF, relatively strong meridional winds are also observed in NB throughout the year with a slight relaxation in June-July, confirming the persistence of upwelling throughout the year (Veitch et al., 2010). The meridional wind in NB has values that range from 4 to 10 $m.s^{-1}$. JRA-55 shows the highest values throughout the year in the ABF and NB. The meridional winds in CB and SB show a similar seasonal pattern of variability. Intense equatorward meridional winds are observed from October to March while relatively weak winds are observed from April to September. The maximum values are obtained in January and range from 9 to 11 $m.s^{-1}$ on average in CB and 6 to 9 $m.s^{-1}$ on average in SB. In CB, the minimum values are observed in June-July; the minimum values are about 6 to 8 $m.s^{-1}$ except for NCEP2 (~2 to 4 $m.s^{-1}$). Compared to NB, the meridional wind in CB is higher throughout the year indicating perennial and persistent upwelling throughout the year. In SB, the equatorward winds are very weak, less than 4 $m.s^{-1}$ in SB from April to September and reverse direction (< 0 $m.s^{-1}$) from May to July in NCEP2. The minimum values are observed in June-July when the centre of the SASH is either close to the Equator or on the western side of the South Atlantic basin (Sun et al., 2017). I also notice that NCEP2 shows the weakest wind in the annual cycle in CB and SB. Again, this relatively low wind speed could be due to the results of averaging strong northwesterly wind experienced during low-pressure systems and cold fronts and southerly wind experienced after cold fronts

and during high-pressure system conditions, bringing low wind or strong southeasterly winds at times, all of those leading to low averages.

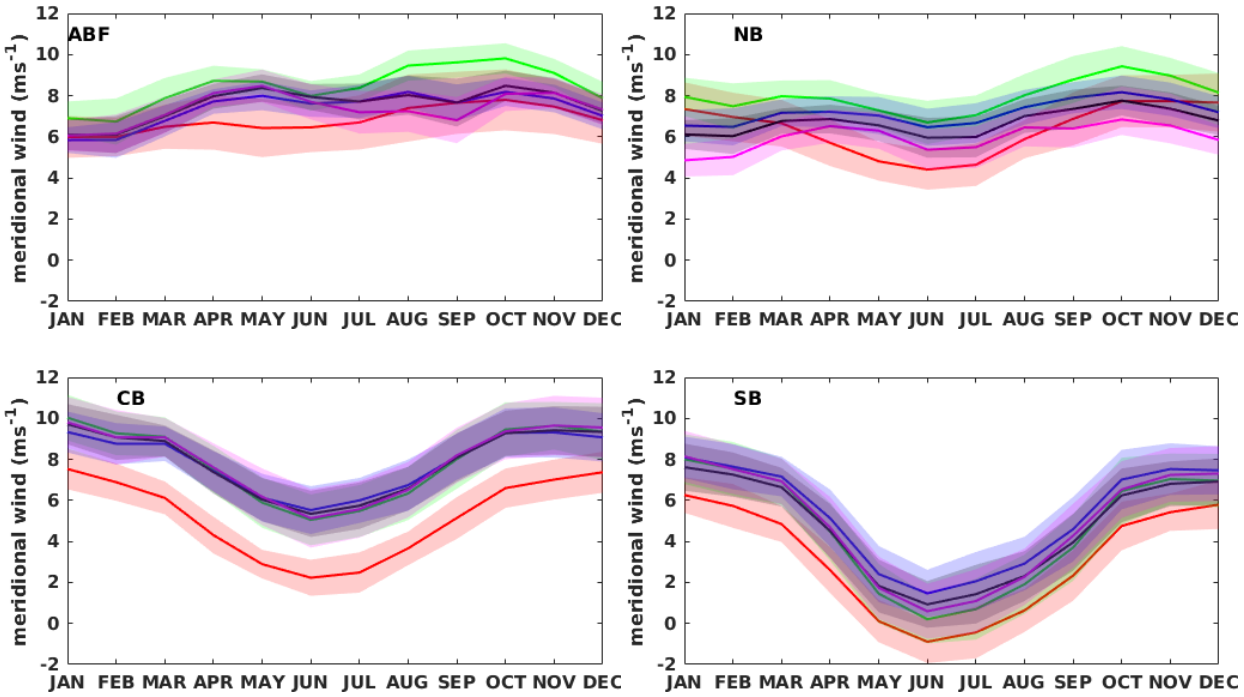

Figure 3.5: Annual cycles of meridional wind speed ($m.s^{-1}$) in the Benguela Upwelling System off ABF (15-19°S), NB (20-24°S), CB (25-29°S), and SB (30-34°S) for NCEP2 (red), JRA-55 (green), MERRA-2 (blue), Era-Interim (black), and ERA5 (magenta). Shaded areas represent the standard deviation. Each box is the average of meridional winds in the 4°-long domains in latitude and the 3°-width coastal fringe. Note that positive values mean equatorward.

3.3 TRENDS IN SST

3.3.1 Overall trends

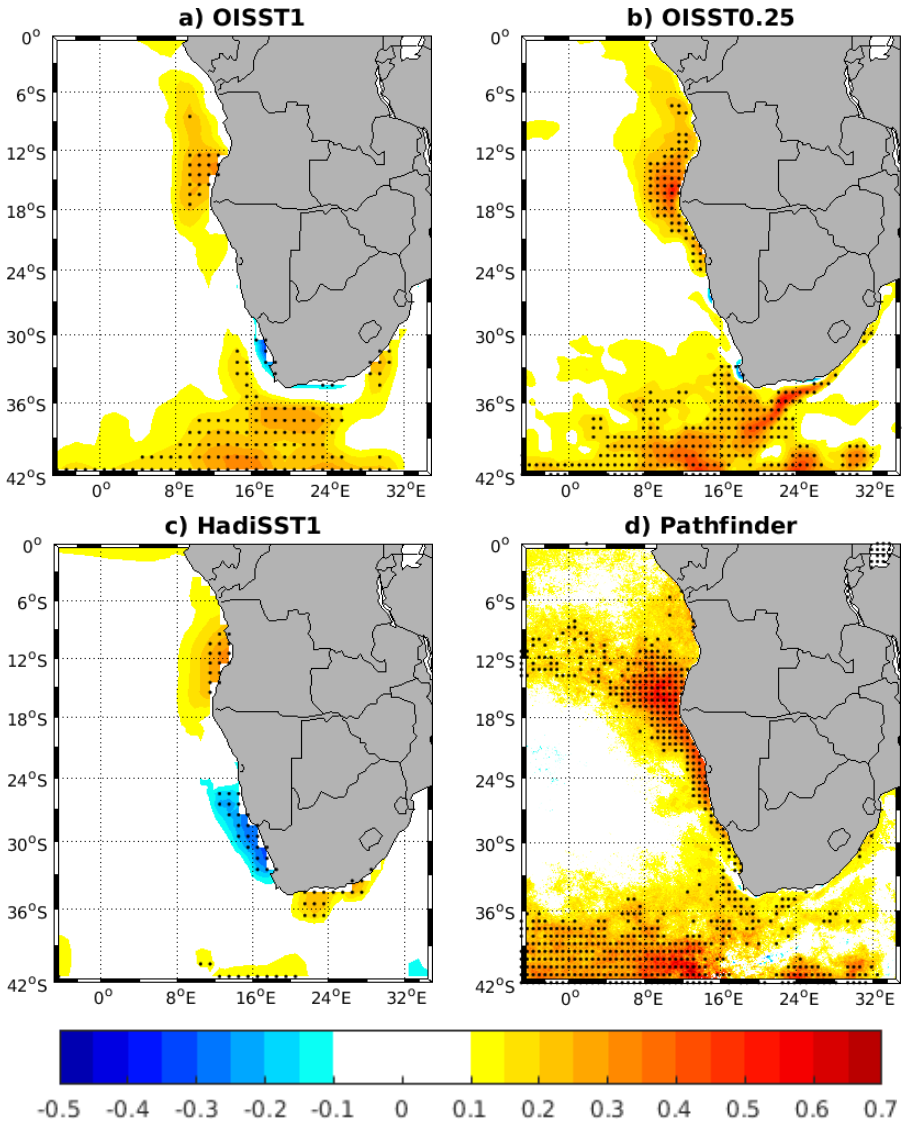

Figure 3.6: Linear trend in annual mean SST for the period 1982-2017 for a) OISST1, b) OISST0.25, c) HadISST1, and d) Pathfinder. The black points denote statistically significant values at 95% level using student's test based on linear regression.

The SST trends and their statistical significance for the period 1982-2017 are shown in **Figure 3.6**. Statistical significance at 95% level of confidence is calculated using student's test based on linear regression. Overall, statistically significant warming trends, ranging from 0.2 to

0.6°C per decade are observed along Angola and Northern Namibia from 6°S to 22°S in all datasets. Except for HadISST1, the datasets also agree that there is a significant warming trend observed in the open ocean and Agulhas Current south of 33°S. Disagreement in SST trends occurs among the datasets especially along the coast in the Benguela Upwelling System. A statistically significant cooling trend, ranging from 0.2 to 0.4°C, is observed in the Central and Southern Benguela using HadISST1 dataset while a warming trend is observed with the Pathfinder dataset almost everywhere in the Benguela Upwelling System (**Figure 3.6 c** and **d**). A cooling trend of lesser magnitude and spatial extent than HadISST1 is observed in the south of the Benguela using OISST1 and OISST0.25 (**Figure 3.6 a** and **b**). However, the cooling trend is not statistically significant in OISST0.25. The difference in trend at the regional scale for products (OISST1, OISST0.25, HadISST1, Pathfinder) that are based on the same AVHRR spaceborne instrument is a cause for concern.

3.3.2 Seasonal trends

To investigate how the SST trends vary depending on the season in the Benguela Upwelling System, Hovmöller diagrams of the monthly linear trend of SST in °C per decade, for each dataset, averaged within the 1°-width coastal fringe along the Angolan, Namibian, and South African west coasts, are shown in **Figure 3.7.** This 1° band off the coast is chosen to quantify trends within the upwelling for all datasets. **Figure 3.7** shows the seasonal dependence of the trends in SST in the Benguela Upwelling System. The warming trend observed in Angola and northern Namibia is present all year round, but the trend is not statistically significant from February to September. The warming trends are up to 0.7-0.9°C per decade in the austral summer (November to January). The cooling trend observed south of 30°S in most of the datasets is observed all year round in OISST1 and HadISST1, while they are observed from December to May in OISST0.25 and are statistically significant at that monthly scale. A statistically significant cooling trend of lesser magnitude is also observed south of 33°S for the Pathfinder dataset from December to May. The cooling trends observed in OISST1 and HadISST1 are statistically significant from December to September. They are more pronounced, up to -0.6°C per decade, in April to July with OISST1 while they are more pronounced in January-February and April-May for HadISST1.

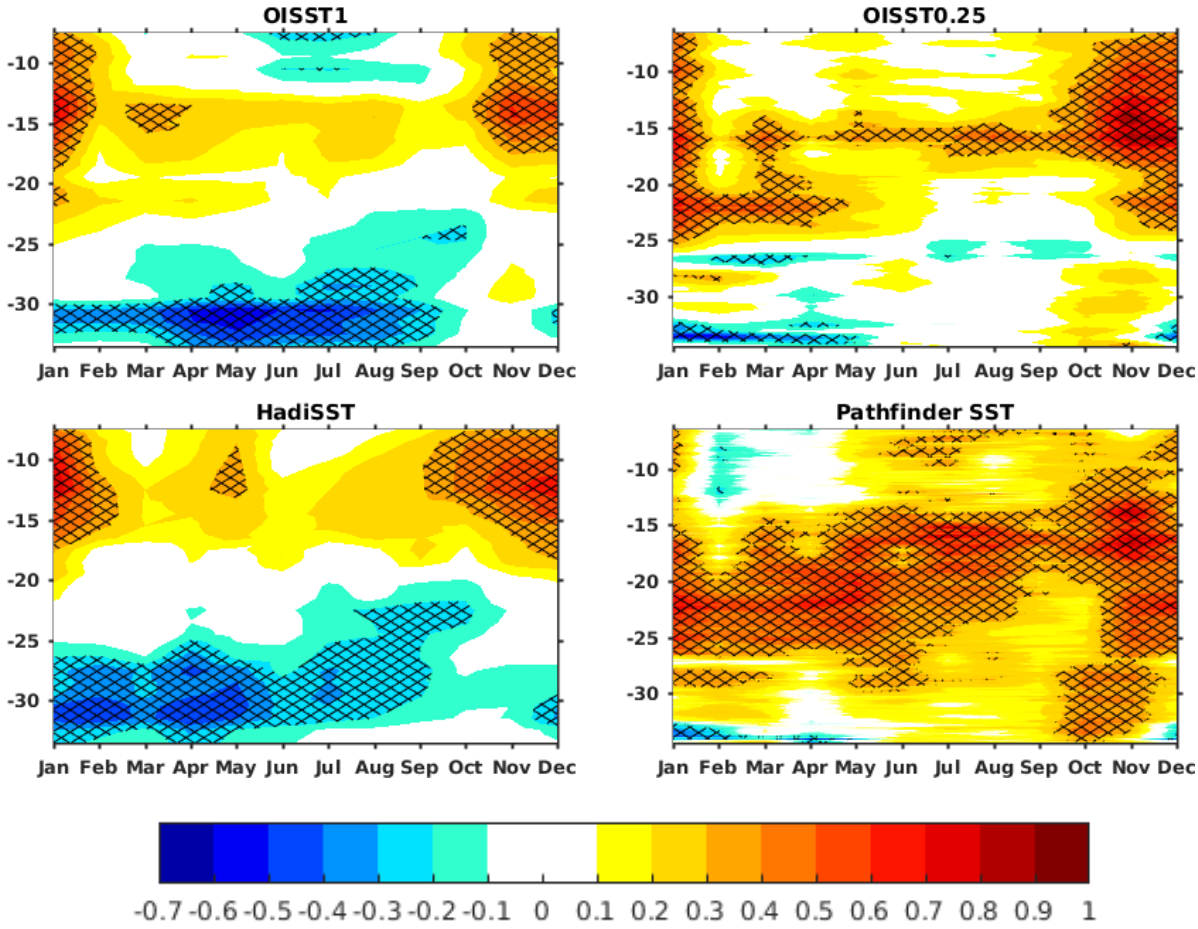

Figure 3.7: Hovmöller diagram of monthly linear trend of SST averaged from coast to 1 degree off the coast along the Angolan, Namibian and west of South African coasts for OISST1 (left top panel), OISST0.25 (right top panel), HadISST1 (left bottom panel) and Pathfinder (right bottom panel). The period considered is 1982-2017 for all data. Cross lines denote statistically significant values at 95% level using student's test based on linear regression.

3.4 COMPARISON OF MONTHLY TIMESERIES OF SST ANOMALIES IN THE FOUR DOMAINS TO UNDERSTAND THE DIFFERENCE IN SST TREND

To understand the differences in trends observed among the datasets in the Benguela Upwelling System, timeseries of monthly SST anomalies for the four SST datasets in ABF, NB, CB, and SB boxes are shown in **Figure 3.8** and correlations between SST anomalies among datasets in the same domains as in **Figure 3.8** are shown in **Table 3.1**. Note that all the correlations are

statistically significant at the 95% level. There is a good agreement among datasets in the ABF. The correlations between SST anomalies among datasets in the ABF are greater than 0.8 except for the correlation between HadISST1 and Pathfinder which is 0.76 (**Table 3.1**). There is also agreement among datasets in NB. However, the correlations between SST anomalies among datasets are slightly lower than the ones in the ABF. The lowest correlations are observed between HadISST1 and the other three datasets. The Pearson correlations are respectively 0.64, 0.60 and 0.5 between HadISST1 and OISST1, HadISST1 and OISST0.25 and between HadISST1 and Pathfinder. The correlation is greater than 0.8 between OISST1 and OISST0.25, and also between OISST0.25 and Pathfinder. Discrepancies among datasets are observed in CB and SB. In CB, HadISST1 starts with a warm bias of up to 2.5°C compared to OISST0.25 or Pathfinder (**Figure 3.8**). The correlations between HadISST1 and the other three datasets are even lower than 0.5. HadISST1 correlation is 0.47 with OISST1, 0.37 with OISST0.25 and 0.19 with Pathfinder (**Table 3.1**). However, there is quite a good agreement between OISST1, OISST0.25, and Pathfinder. In SB, the agreement among datasets is quite good compared to CB except that HadISST1 and OISST1 start with warm bias compared to OISST0.25 or Pathfinder. Besides the correlation between HadISST1 and Pathfinder which is about 0.42, all the correlations are larger than 0.5. Again, the different methods of producing datasets could be the cause of the discrepancies in trends among datasets. For example, HadISST1 and OISST1 used *in-situ* and operational AVHRR data while OISST0.25 used *in-situ* data, Pathfinder AVHRR data from 1985-2005 and operational AVHRR data from 2006 onwards (see section 2.1.1). Moreover, the lowest correlation between HadiSST1 and other datasets is due to the fact that HadiSST1 is less influenced by the AVHRR, whereas AVHRR is the major component of other SST products.

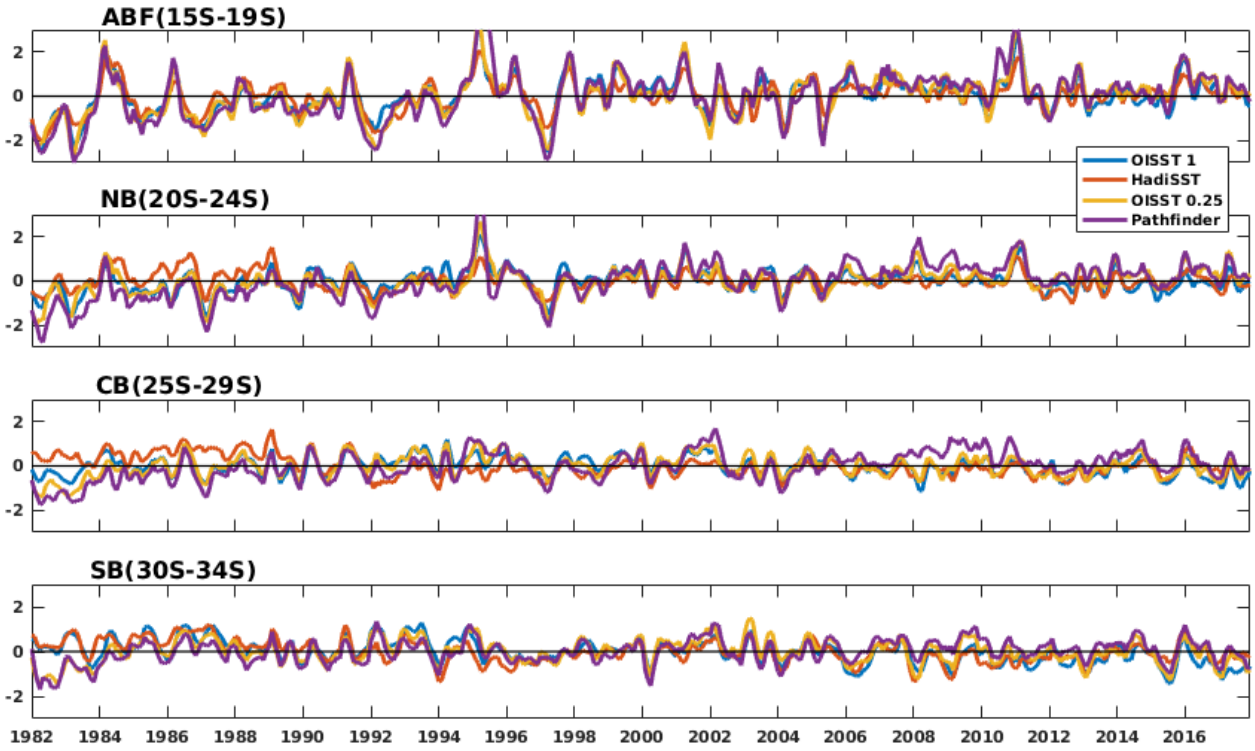

Figure 3.8: Moving average over 3-month windows of SST anomalies from 1982 to 2017 in four different boxes (from top to bottom ABF, NB, CB, and SB, see map in Figure 3.2) for the four datasets: OISST1 (blue), HadISST1 (red), OISST0.25 (yellow), and Pathfinder (Magenta)

Table 3.1: Pearson Correlation between anomalies of SST among datasets (HadISST1, OISST1, OISST0.25, and Pathfinder) in ABF, NB, CB and SB boxes (see map in Figure 3.2).

ABF				
	HadISST1	**OISST1**	**OISST0.25**	**Pathfinder**
HadISST1	1	0.82	0.82	0.76
OISST1		1	0.91	0.88
OISST0.25			1	0.9
NB				
HadISST1	1	0.64	0.60	0.50
OISST1		1	0.83	0.77
OISST0.25			1	0.86
CB				
HadISST1	1	0.47	0.37	0.19
OISST1		1	0.86	0.61
OISST0.25			1	0.78
SB				
HadISST1	1	0.72	0.55	0.42
OISST1		1	0.74	0.57
OISST0.25			1	0.85

Similar trends analysis over the period 1986-2017 (**Figure 3.9**) shows quite a good agreement between OISST1, HadISST1 and OISST0.25. Pathfinder trend results are still far from

other datasets but show a similar pattern. This could be due to the fact that Pathfinder data have a lot of missing values (**see Figure 2.1**) and also, Pathfinder is not corrected with *in situ* data and could be more related to skin temperature which may be more affected by global air temperature and present a warmer trend than the other datasets.

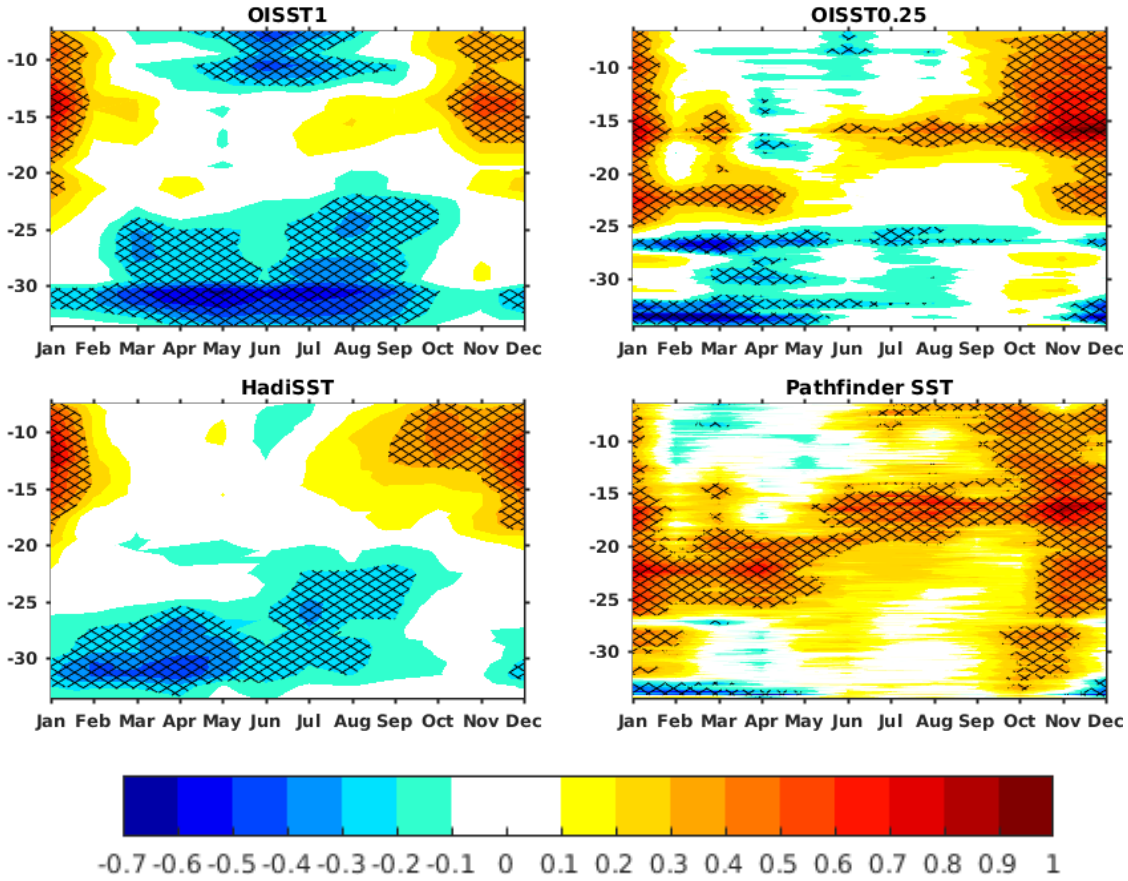

Figure 3.9: Same as figure 3.7 but for the reduced period 1986-2017

In conclusion, there are some discrepancies between datasets. HadISST1 is less correlated with the other three SST datasets. There is even a difference between the two OISST products. Most of the discrepancy is also found at the beginning of the time series, especially from 1982 to 1985. The CB is the domain with the most discrepancy followed by SB. These discrepancies may be at the origin of the difference in trends between datasets. However, trend analysis over the period 1986-2017 shows quite a good agreement between OISST1, HadISST1, and OISST0.25 and demonstrates that the 1982 to 1985 dataset needs to be removed for trend analysis. A general warming trend is found in Southern Angola and Northern Benguela and a cooling trend is found

in Central and Southern Benguela. Even the Pathfinder which at first seems a bit different has a similar seasonal pattern with a warm bias compared to OISST.

3.5 TRENDS IN WIND

3.5.1 Overall trends in wind speed

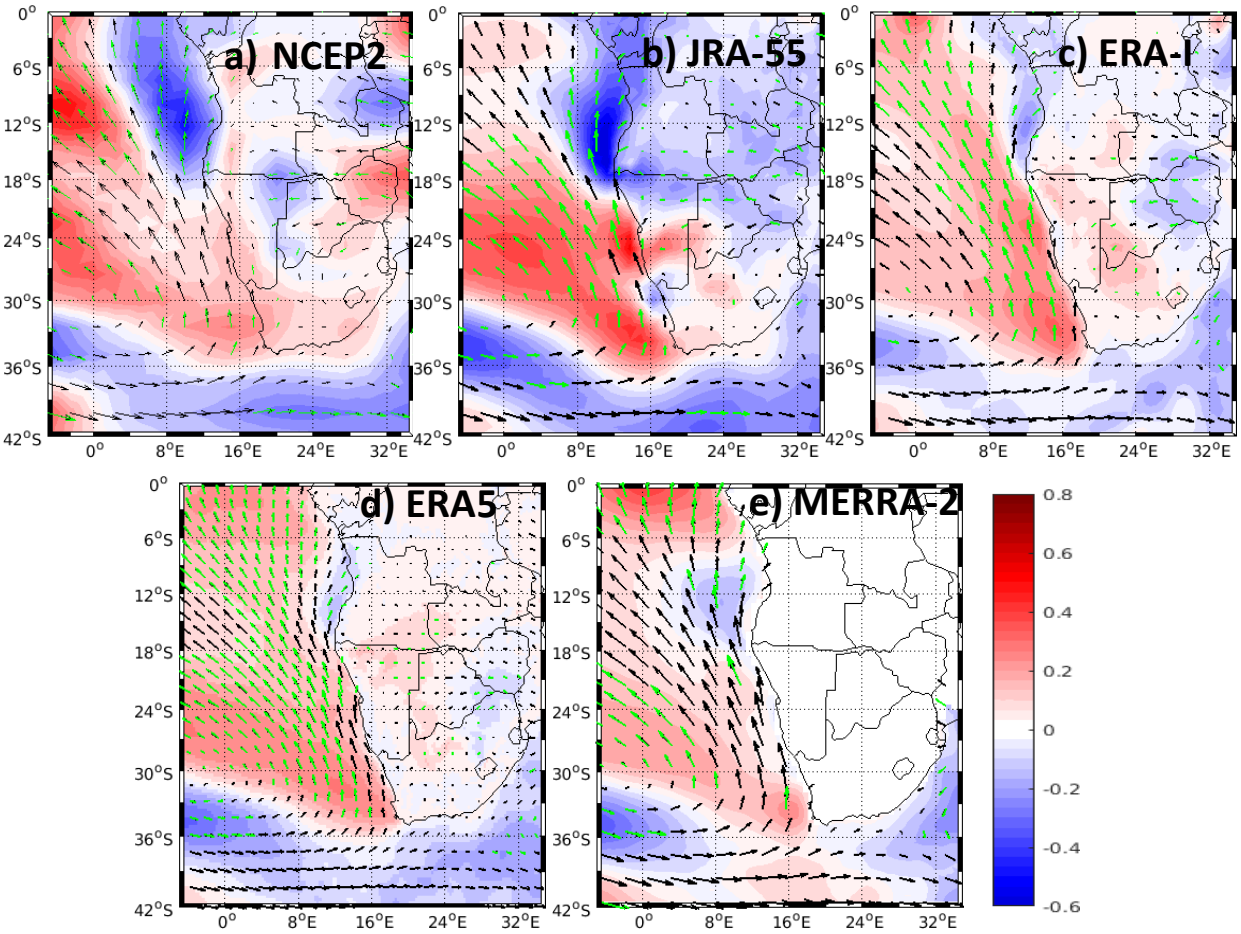

Figure 3.10: Linear trends in mean wind speed (m/s per decade) for **a)** NCEP2, **b)** JRA-55, **c)** Era-Interim, **d)** ERA5, and **e)** MERRA-2 with the associated climatological direction superimposed (green and black arrow). Green arrows denote where the trend values are statistically significant at 95% level using Student's test based on linear regression. The period considered is 1982-2017 for all datasets, except for JRA-55 which is 1982-2013.

Here I analyze and compare the linear annual and seasonal wind speed trends of the five reanalysis atmospheric datasets. **Figure 3.10** shows the wind speed and direction trends and the annual mean direction over the period 1982-2017 for the same datasets. Noted that JRA-55 has a shorter period of 1982-2013. Statistical significance at 95% level of confidence is calculated using Student's test based on linear regression and is shown by the green arrows. Globally, there is good agreement in trends among datasets, although the JRA-55 trends tend to be the largest, while MERRA-2 trends tend to be the smallest. Positive trends up to 0.7 $m.s^{-1}$ per decade are observed in the Benguela upwelling and the open ocean while negative trends up to -0.5 $m.s^{-1}$ are observed along the Angolan coast and in the open ocean south of 35°S. The negative trends along the Angolan coast are more pronounced and are statistically significant using JRA-55 and NCEP2. The positive trends observed along and near the coast of Namibia and the South African west coast, are not statistically significant. This could be due to a problem in the reanalysis datasets, calculated using model outputs near the coast. In addition, the observed low values in JRA-55 wind trends around 30°S near the coast seems spurious as JRA-55 winds indicate a significant positive trend almost everywhere in the Benguela Upwelling System. Indeed, most of the statically significant values are not found near the coast but offshore and near the Angolan coastal zone. However, there is an overall impression of intensification of southerly and southeasterly wind speed in the eastern part of SASH and a decrease of wind speed off Angola to the north of the Benguela Upwelling System.

3.5.2 Seasonal trends in wind speed

As it was done for the SST trend analysis (see section 3.1.2), to understand how the wind trends vary seasonally and to relate the wind trends to the SST trends (**Figure 3.7**), Hovmöller diagrams of monthly linear trends of meridional winds for each dataset, averaged within a 3°-width coastal fringe along the west coast of Angola, Namibia and the South African are shown in **Figure 3.11.** This figure shows the seasonal dependence of wind trends in the Benguela Upwelling System. Although there is a good agreement in the annual trends of wind speed among datasets (**Figure 3.10**), discrepancies are observed in the seasonal trends (**Figure 3.11**). This may be due to modelling problems of reanalysis in resolving the dynamics close to the coast and also to different spatial resolutions and different techniques of modelling. For instance, NCEP2 and JRA-

55 have coarser resolution (2.5° and 1.25° respectively) while ERA5 has a finer resolution (0.25 °). The negative trends along the Angolan coast (**Figure 3.10**) occur almost all year round and are up to -0.7 $m.s^{-1}$ per decade in all datasets (**Figure 3.11**) with different degrees of intensity and timing, except for ERA5 which shows no trend in the coastal meridional wind. These negative trends are statistically significant throughout the year with JRA-55 and in the austral winter period from July to September with NCEP2, but they are not statistically significant with ERA-Interim. In MERRA-2, these negative trends are observed in the austral winter and autumn periods from June to October and are statistically significant only in June. This may explain some of the warming SST trends there. However, the timing of the lowest trends of wind speed (austral winter) (**Figure 3.11**) does not correspond with the timing of the highest SST trend (austral summer) (**Figure 3.7** and **3.9**). South of ABF, roughly, there seems to be an intensification of upwelling favourable winds at different months and different locations, depending on the dataset considered. For instance, in the Northern Benguela and central Benguela, JRA-55 and Era-Interim show an intensification of upwelling favourable winds up to 0.5 $m.s^{-1}$ from February to September, while ERA5 shows an intensification from May to September. Unlike JRA-55 and Era-Interim, NCEP2 shows no trend from September to February and intensification for the rest of the year. However, there seems to be a general tendency for increased wind in the Southern Benguela in all datasets from December to April which corresponds to the SST cooling trends (**Figure 3.7** and **3.9**). Moreover, from August to November, no positive or negative trends are observed in Southern Benguela in most of the datasets, except for NCEP2. In JRA-55, negative trends are more pronounced in the second part of the year compared to the positive trend in the first part of the year (**Figure 3.11**) and could be at the origin of negative trends at the annual scale observed around 30°S (**Figure 3.10**).

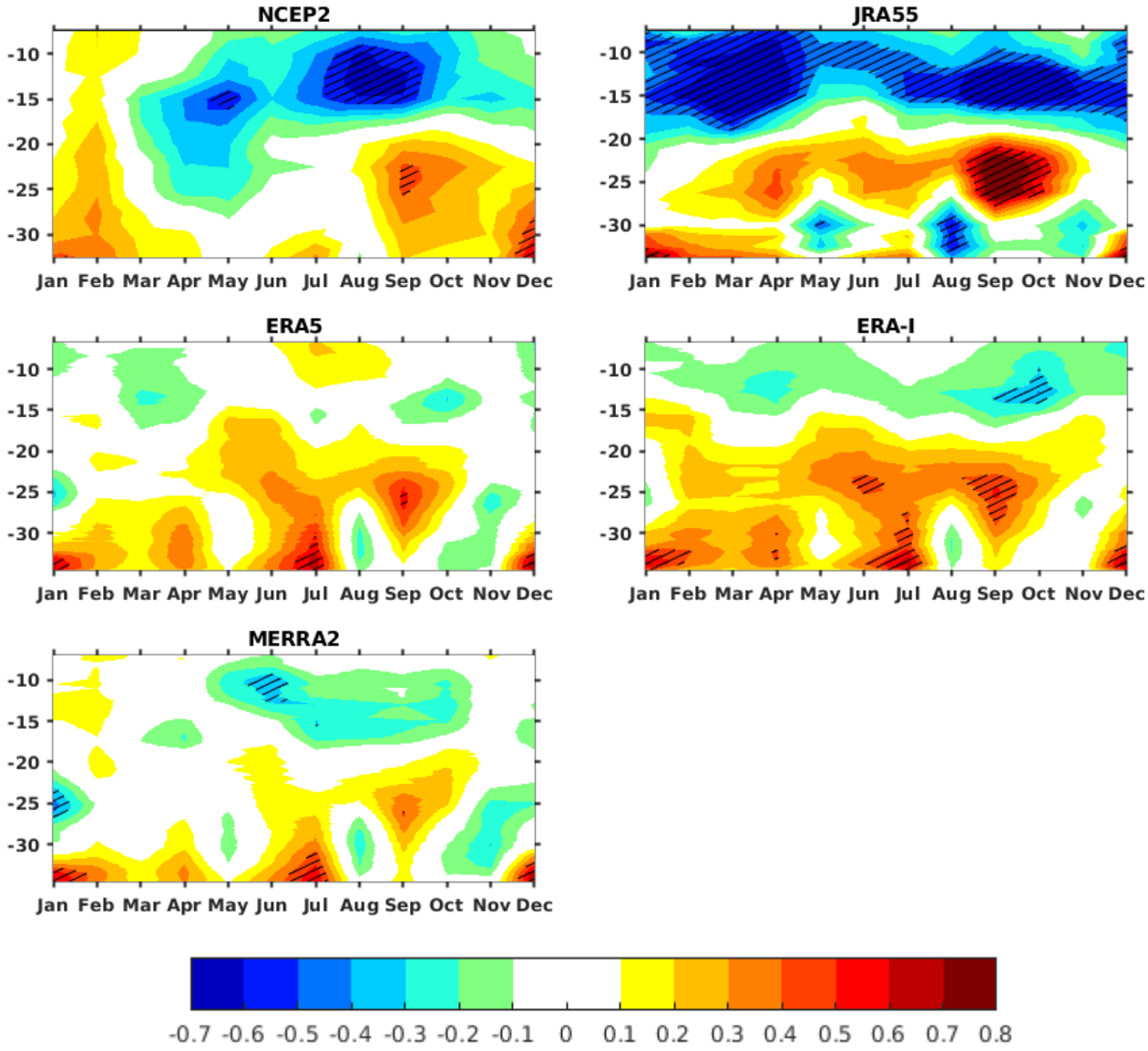

Figure 3.11: Hovmöller diagram of monthly linear trends of meridional winds averaged from the coast to 3 degrees offshore along the Angolan, Namibian, and South African west coast. The hatched parts denote statistically significant values at 95% level using Student's test based on linear regression. The period considered is 1982-2017 for all data except JRA-55, which is 1982-2013.

Due to opposite signs of wind speed trends observed seasonally, I now investigate the seasonal wind speed trend at the regional scale by considering two seasons, austral summer (DJFMA) and austral winter (JJASO) (**Figure 3.12**). As mentioned above, annual and monthly

negative trends of wind speed up to -0.6 $m.s^{-1}$ per decade are observed along the Angolan coast and in the ABF region, in both seasons and all datasets. Negative trends seem to be stronger north of the ABF along the Angolan coast. This could have warmed up the entire Angolan coast and, since the water flow is mostly poleward within the Angola Current, warm water could be advected slowly poleward to the ABF region and further south, especially in austral summer (Rouault, 2012). These negative wind speed trends are more pronounced and statistically significant in the austral winter (JJASO) period. In the Benguela Upwelling System, I observe that in austral summer (DJFMA), statistically significant positive trends up to 0.7 $m.s^{-1}$ are observed in the Southern Benguela in all datasets, in agreement with the SST cooling. Discrepancies are observed in the Northern Benguela. While some datasets such as ERA5 and MERRA-2, show negative trends, others show positive trends. However, the positive or negative trends observed in Northern Benguela are not statistically significant. A closer look at the trends in the Benguela Upwelling System shows that the trends in austral summer seem to suggest a poleward shift and or intensification of the SASH. In austral winter, positive trends are observed in the entire Benguela Upwelling System. However, the positive trends are statistically significant only in the Northern Benguela in all datasets except MERRA-2. Consequently, no trends at the annual scale are observed in the Northern and Central Benguela with MERRA-2 (**Figure 3.10**), which could be due to the negative trend in austral summer and the positive trend in austral winter.

Although there are discrepancies among SST and wind datasets, the comparison of wind trends and SST trends above shows that there are agreements between SST and wind trends mainly at the seasonal scale along the Angolan, Namibian, and South African west coasts. For instance, positive trends in SST observed in Southern Angola and the ABF or part of NB regions are matched with negative trends in the equatorward wind in most datasets. Also, the cooling trends observed in the south of the Benguela Upwelling System are more pronounced from December to June in most SST datasets, in good agreement with the increasing trend of equatorward winds in all wind datasets during the same period.

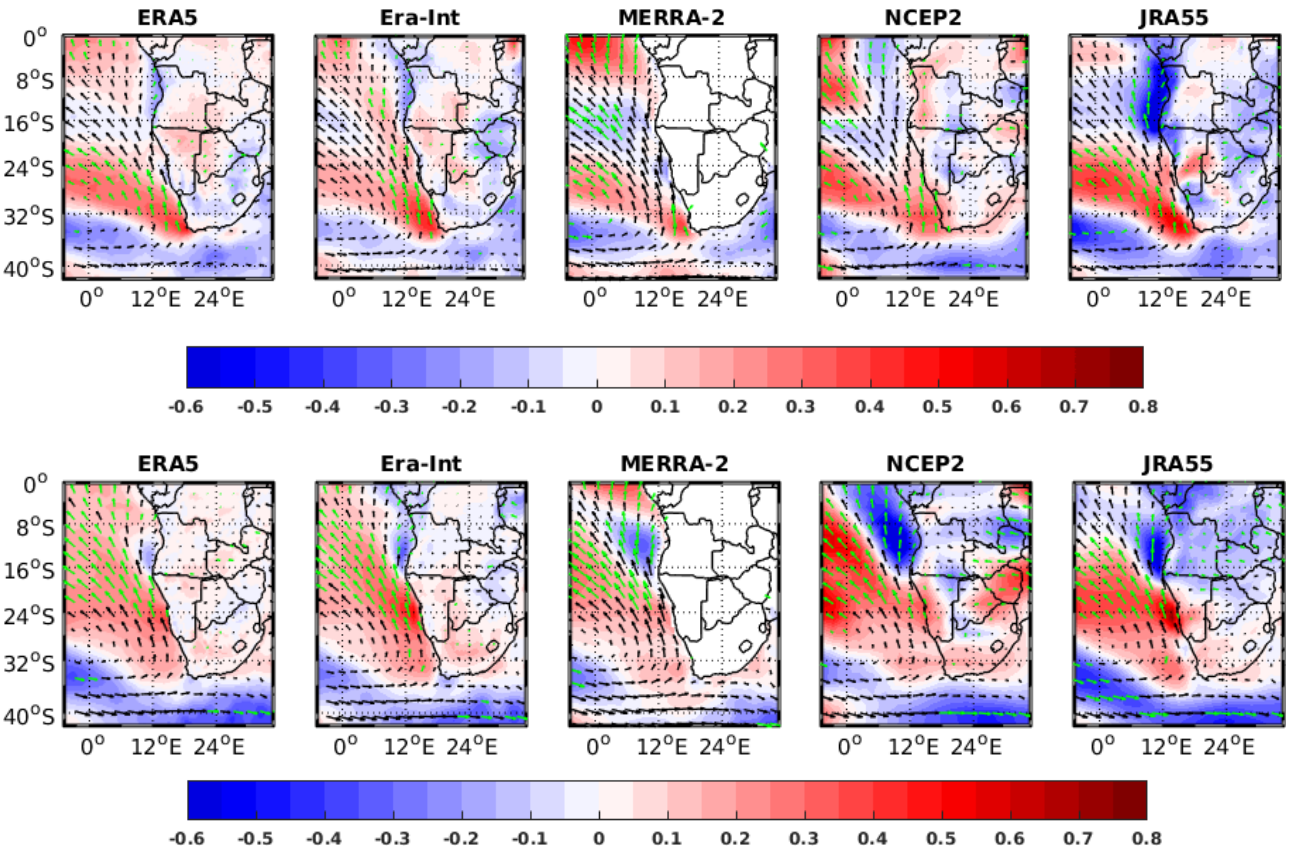

Figure 3.12: Same as Figure 3.9 but for austral summer period DJFMA (Top panels) and austral winter period JJASO (bottom panels).

3.6 Regression and Correlation between wind and SST

Because of some discrepancies between wind trends and SST trends at the seasonal scale and the problem of reanalyzed wind validity, especially near the coast, and to further investigate the relation between wind and SST in the Benguela upwelling system and offshore, I perform a regression and correlation analysis of wind onto coastal SST indices. **Figure 3.13** shows the regression of the monthly anomaly of wind speed onto the OISST0.25 SST anomalies averaged within ABF, NB, CB and SB boxes. The analysis is performed for December-January-February (DJF), March-April-May (MAM), June-July-August (JJA) and September-October-November (SON). The contour lines represent the statistically significant correlation values between wind speed and SST. The arrows represent the 95% statistically significant regression wind vectors. Note that the data are not detrended. However, detrended data (not shown) do not show any difference

compared to non-detrended data. The results estimated for the other datasets also lead to similar conclusions to the one described below.

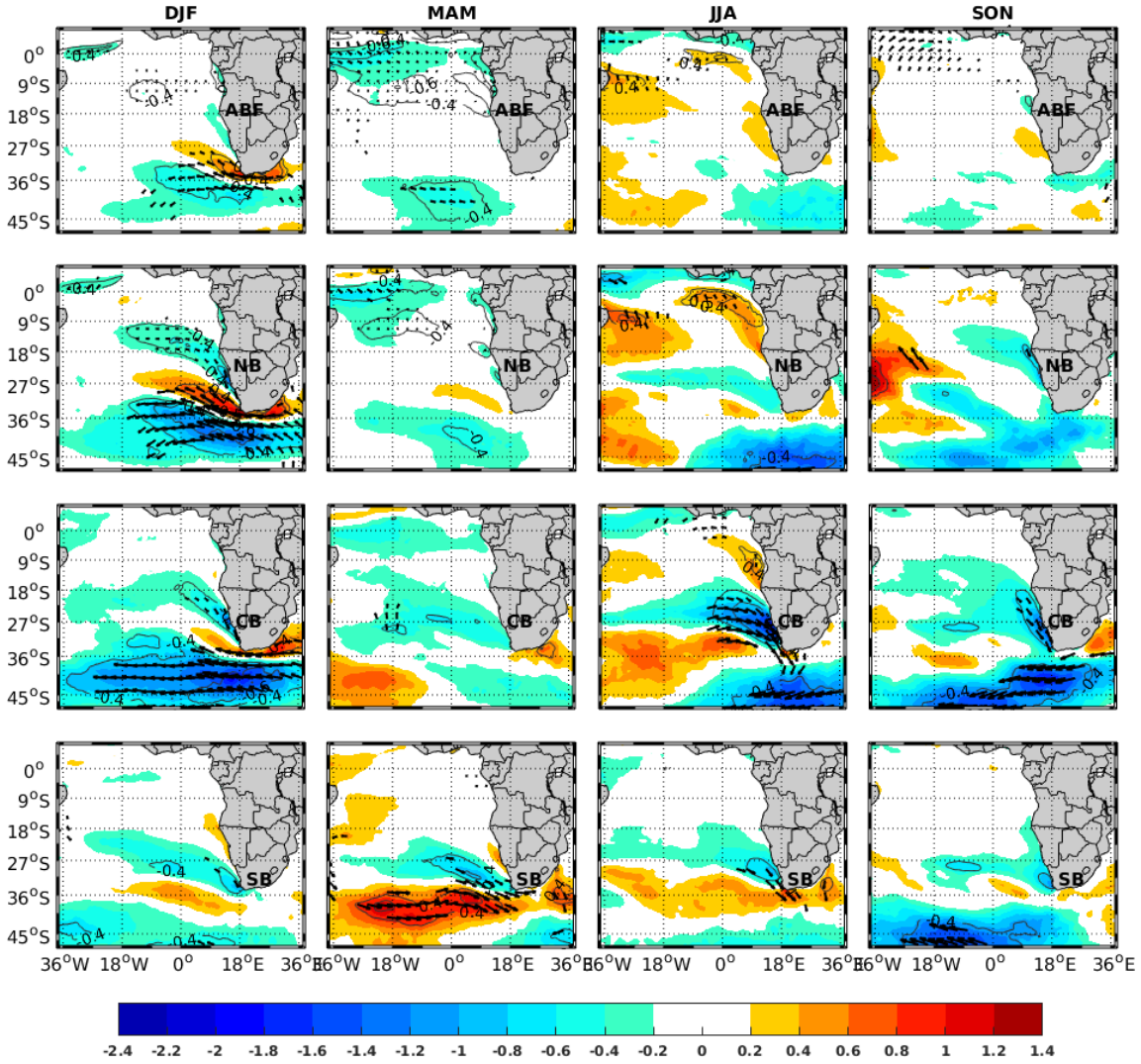

Figure 3.13: Regression (m.s^{-1} per °C) of monthly anomaly of ERA5 wind speed onto OISST0.25 monthly anomaly averaged in ABF (first-panel line), NB (second-panel line), CB (third-panel line), and SB (fourth-panel line) domains (see map in **Figure 3.2)**. This analysis is performed at 4 different seasons (left to right respectively): in December-January-February (DJF), March-April-May (MAM), June-July-August (JJA) and September-October-November (SON). The contour lines denote 95% statistically significant correlations for wind speed and arrows represent the 95% 95% statistically significant regression wind vectors.

Wind speed regressed onto ABF or NB SST anomaly (**Figure 3.13 first** and **second-panel lines**) shows that the change in ABF or NB SST is related to changes in the easterly wind along the equator and anomalous winds in the South Atlantic, south of 27°S in both the SASH and the mid-latitude westerly wind to the south suggesting a shift of the SASH in austral summer and autumn. In ABF and NB regions, the impact of SASH surface wind on SST is more important in austral summer while in austral autumn (March-April-May), the influence of the easterly wind along the equator is more important. The influence of the easterly equatorial wind on the region has been linked to Benguela Niños with weaker easterly winds leading to warming at the ABF and NB regions. Conversely, Benguela Niñas are linked to stronger easterly wind and cooler than normal water. The regression values in austral autumn indicate that 1°C positive anomaly in ABF or NB SST corresponds to a maximum easterly wind negative anomaly of 0.6-0.8 $m.s^{-1}$ at the Equator and *vice versa*. The correlation between easterly wind at the equator and AB SST or NB SST is negative and greater than -0.4. The impact of the SASH wind is more pronounced in NB compared to the ABF area, which is logical. Indeed, the NB region is in a strong wind-driven upwelling system while the ABF zone is a transition zone between a tropical region and an upwelling region. The ABF has weaker winds than NB and is also under the influence of a poleward warm current leading to warmer SST. The regression of wind speed onto NB SST in the South Atlantic suggests a shift as some regions have higher wind speeds in the Southern Benguela and then weaker wind speeds south of the southern tip of Africa. These results suggest that in austral summer a poleward shift of the SASH decreases the southerly and southeasterly winds in ABF and NB which in turn increases the SST in these regions. This shifting behaviour of the SASH is found in other EBUS (Rykaczewski et al., 2015). The regression of wind speed onto CB SST and SB SST anomaly (**Figure 3.13 third** and **fourth-panel line**) shows that the change in CB SST and SB SST is related to local wind and also SASH wind; this is observed in all seasons except in MAM where the regression onto the CB SST is not statistically significant. However, in SB, the regression coefficients are higher and statistically significant in MAM compared to other seasons. As in NB, wind speed onto SB SST shows higher westerly wind south of the continent and less southeasterly wind to the Southern Benguela. These results confirm that a poleward shift of the SASH increases the southerly and south-easterly winds in the Southern Benguela, which cool the SST in the

coastal region. Contrary to the Southern Benguela, the poleward shift of SASH decreases the wind speed in the Northern Benguela which warms up the SST. In austral winter JJA, the 1°C positive anomaly in CB SST corresponds to a maximum of northwesterly wind anomaly of ~1.4-1.8 $m.s^{-1}$ in the CB region. The negative correlation between CB SST and CB wind speed is about - 0.6- 0.7.

3.7 INTENSIFICATION AND POLEWARD DISPLACEMENT OF SASH

Several factors can lead to the intensification of the continental-oceanic pressure gradient, for instance, the continental warming (Bakun, 1990) or the poleward displacement of the SASH (Rykaczewski et al., 2015) which could lead to the positive wind speed trend observed in the Benguela Upwelling System and negative wind speed trends to the north of ABF. Extension and intensification of the SASH could also be at play rather than a shift because the wind increase extends to the whole Benguela current while, given the length of the Benguela Upwelling System, a shift would lead to a decrease in one part and an increase in the other part. Regression analysis of wind anomalies onto SST anomalies in different domains (see Section 3.5) suggests that a poleward shift of SASH would influence wind in the Benguela Upwelling System in opposite wind directions, which in turn would oppositely impact local SST. To study long-term changes in SASH, surface geopotential height is analyzed in this section. I first consider two seasons: austral summer (DJFMA) and austral winter (JJASO), and then for each season, I calculate and compare the long-term mean of the surface geopotential height over two 18-year long periods: (1982-1999) and (2000-2017), using Era-Interim, ERA5, MERRA-2, and NCEP2 **(Figure 3.14** and **3.15**). I did not use the JRA-55 data because its time period only extends to 2013. The statistically significant difference at 95% is calculated using the Welch's t-test, shown by the magenta contour lines, in **Figure 3.14.**

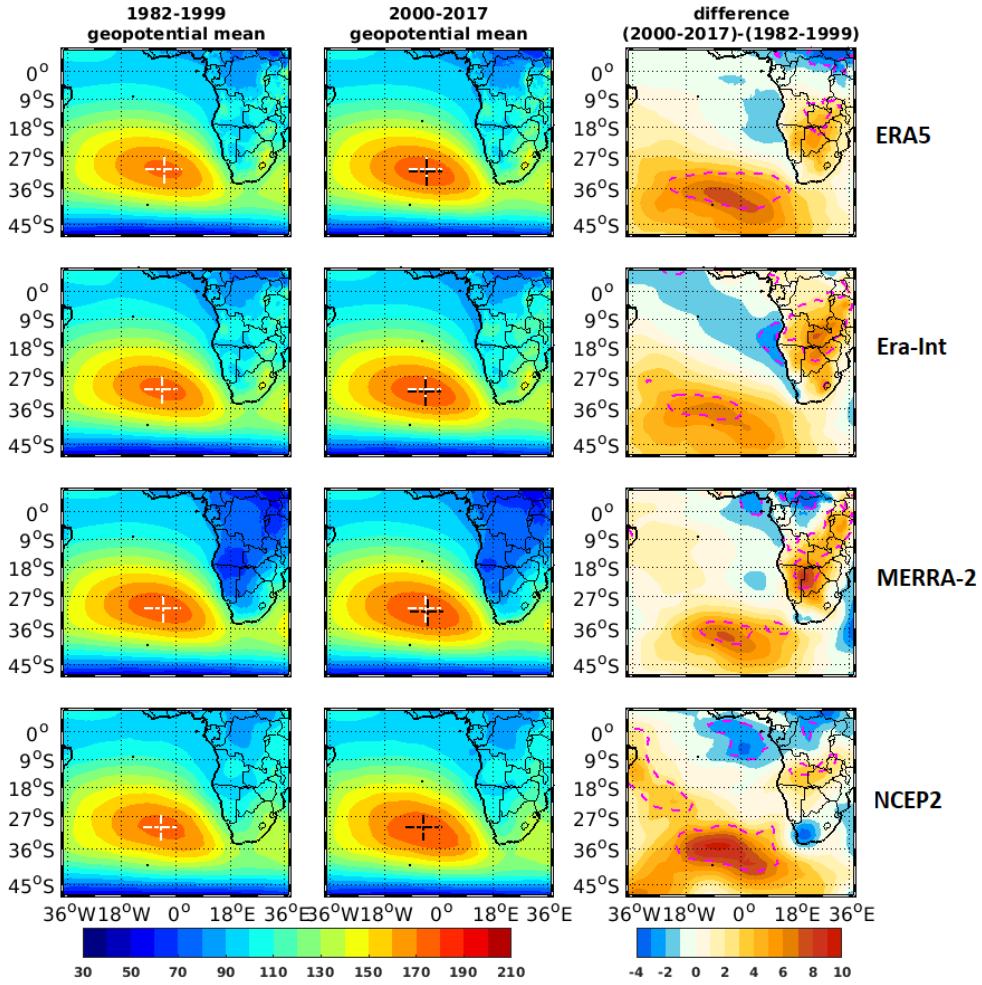

Figure 3.14: Austral summer (DJFMA) long-term mean of 1000 geopotential height (m) over the period 1982-1999 (left panel), the period 2000-2017 (middle panel), and the difference of the long-term mean between the period 2000-2017 and 1982-1999 for top to bottom: ERA5, Era-Interim, MERRA-2, and NCEP2 reanalyses respectively. The white and black cross lines represent the position of the maximum in mean geopotential height for the period 1982-1999 and 2000-2017 respectively. The magenta contour lines denote where the long-term means of geopotential height of the two periods are significantly different at the 95%-level according to Welch's t-test.

In austral summer (DJFMA), the two long-term means show that the SASH is confined within the South Atlantic basin between 15°S and 40°S latitude and 36°W and 18°E longitude. The centre of the SASH is about 30.5°S ± 0.5° and 4.5°W ± 0.5° for the first period 1982-2017 and shifts poleward by about 1° in the second period 2000-2017 for all datasets except NCEP2 which

has too coarse a resolution (2.5°×2.5°) to pick up a 1° displacement. Moreover, the core of the SASH in the period 2000-2017 is expanded to the south in all datasets. The difference of the long-term mean between 2000-2017 and 1982-2017 **(Figure 3.14, right panel**) reveals that the long-term mean geopotential height has increased in the second half period 2000-2017 by up to 10 m over the ocean south of 18°S in all the datasets, while a decrease of long-term mean geopotential height in the second half period up to -4 m is observed in the equatorial part of the ocean (9°S to 9°N) and along the Angolan and Namibian coasts in most datasets. This suggests an intensification of the SASH in the south more than a shift, which is consistent with the increase in upwelling-favourable wind in the south. The increase of geopotential height in the south would have led to an increase of the pressure gradient from southwest to northeast, leading to the observed south to south-east increase in wind. The increase of geopotential height over the open ocean is more pronounced south of 30°S; it is statistically significant and may be a sign of intensification and poleward extension of the SASH. MERRA-2 shows less augmentation of the geopotential height over this period compared to other datasets which are consistent with MERRA-2, having a smaller increase in wind speed. Disagreements among the datasets are observed over land. A statistically significant increase of geopotential height up to 10 m, over the period 2000-2017 compared to the period 1982-1999, is also observed on the continent in the central part of Africa in all datasets while a statistically significant decrease of geopotential height up to -4 m over the same period 2000-2017 is observed in the equatorial part of the continent in most datasets, except Era Interim. There is no increase or a slight non-significant decrease of geopotential height in the south of the continent, which again is consistent with the increase in wind speed south of the Benguela Upwelling System and decrease of SST. As the land temperature increases due to global warming, one would expect the surface pressure to decrease. It seems therefore that the increase in wind speed is due to change in the SASH rather than change over the land in austral summer.

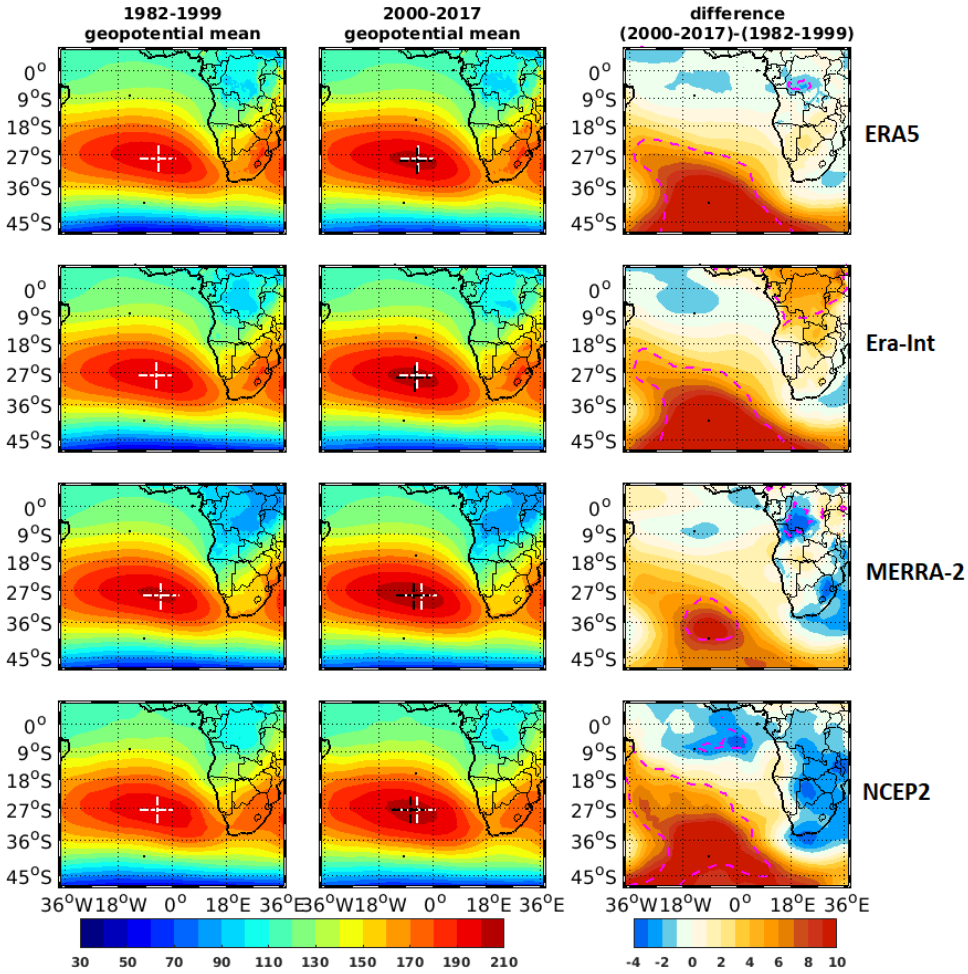

Figure 3.15: same as Figure 3.14 but for austral winter period (JJASO).

In the austral winter period (JJASO, see **Figure 3.15**), the SASH is more intense and extends toward the adjacent continent compared to the summer period (DJFMA, see **Figure 3.14**). The SASH in JJASO is connected with the Mascarene high over the Indian Ocean through Southern Africa when land surface temperatures over the latter are cooler than over the adjacent South Atlantic (Sun et al., 2016). The SASH is also closer to the equator in JJASO compare to DJFMA. The centre is located at 28°S ± 0.5° latitude and 4.5°W ± 0.75° of longitude in the first half period 1982-1999 and shifts by about 0.5° poleward in ERA5 and Era-interim. No poleward change is observed with MERRA-2 and NCEP2. However, all datasets show a westward displacement of ~0.5° to 2.5° depending on the datasets. Similar to the austral summer, the difference of the long-term means between 2000-2017 and 1982-2017 in JJASO shows that the long-term mean

geopotential height has increased up to 10 m in the second period 2000-2017 over the ocean south of 9°S in all datasets **(Figure 3.15, right panel**). This increase of the long-term mean geopotential height in the second period is more pronounced south of 27°S suggesting an extension southward of the SASH. A decrease of JJASO long-term geopotential height, up to -4 m, in the second period 2000-2017, is also observed along the equator and on the continent in most datasets except Era Interim which manifests a statistically significant increase of the austral winter long-term geopotential height over the continent during the period 2000-2017.

Next, I analyze the linear trend of the latitudinal position and magnitude of the center of the SASH (**Figure 3.16** and **3.17**). The SASH center is determined each month by the position of the maximum of the geopotential height in the South Atlantic region within the 45°S-0°S - 40°W-15°E region. **Figure 3.16** shows the timeseries of the latitudinal position (left panel) and magnitude (right panel) of the SASH centre for ERA5, Era-Interim, MERRA-2, and NCEP2 reanalyses. The black solid lines denote the linear trends. The trend analysis results are summarized in **Table 3.2**. All datasets agree on intensification and a poleward displacement of the SASH with positive trends in magnitude and negative trends in latitudinal position of the SASH centre. The positive trends in the magnitude of the SASH centre are statistically significant at the 95% level in all datasets. The trend is 0.165m per decade, 0.216m per decade, 0.166m per decade and 0.299m per decade for ERA5, Era-Interim, MERRA-2 and NCEP2, respectively. The positive trends in the magnitude of the SASH centre are observed all year round in all datasets (**Figure 3.17**). The positive trends in the magnitude of the SASH centre are statistically significant at the 95% level in January, July, and September in most datasets (**Figure 3.17**). The negative trends observed in the latitudinal position are also statistically significant at the 95% level in most of the datasets except Era-Interim where it is statistically significant at a 90% level (**Figure 3.16)**. The trend value is -0.029^{o} per decade, -0.014^{o} per decade, -0.015^{o} per decade and -0.02^{o} per decade for ERA5, Era-Interim, MERRA-2 and NCEP2, respectively. The negative trends in the latitudinal position of the SASH centre are observed in most months of the year in most datasets (**Figure 3.17**).

Table 3.2: Linear trend analysis results of latitudinal position and magnitude of the SASH centre for each different dataset: Era5, Era-Interim, MERRA-2 and NCEP2. T-stat indicate the student test statistic. Significant trends are shaded in grey.

	Decadal trend	Decadal trend unit	Standard Error	t-stat	P-value	R^2
Latitudinal position of SASH centre						
Era5	-0.029	°/decade	0.001	-2.893	0.004	0.020
Era-Int	-0.014		0.0008	-1.719	0.086	0.006
MERRA-2	-0.016		0.0009	-1.837	0.066	0.007
NCEP2	-0.020		0.001	-2.066	0.039	0.010
SASH centre Magnitude						
Era5	0.165	m/decade	0.004	4.143	<0.001	0.040
Era-Int	0.216		0.005	4.346	<0.001	0.042
MERRA-2	0.166		0.005	3.274	0.001	0.024
NCEP2	0.299		0.004	6.051	<0.001	0.079

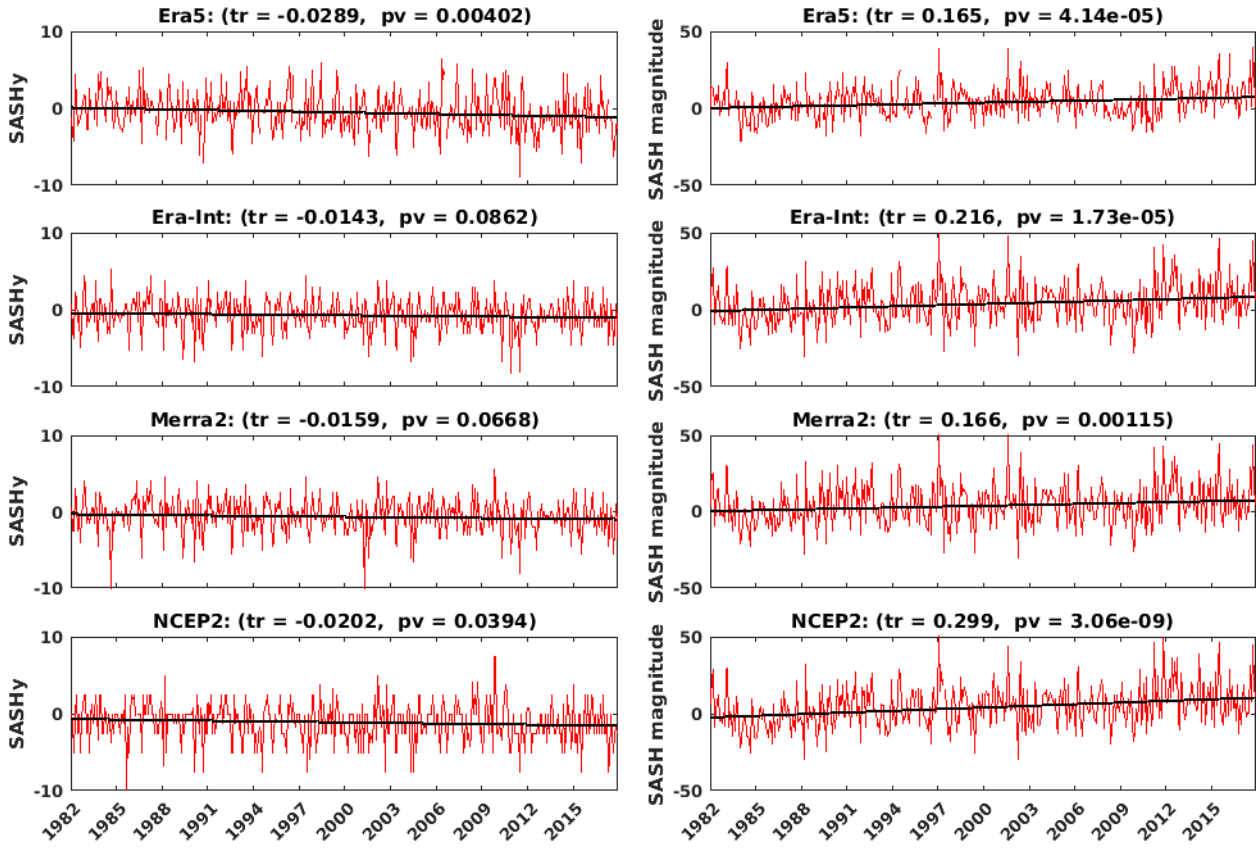

Figure 3.16: Anomalies of the meridional position (SASHy) (left panel) and magnitude (right panel) of the SASH center for the period 1982-2017 for, top to bottom: ERA5, Era-Interim, MERRA-2, and NCEP2, respectively. Solid black lines indicate linear trends.

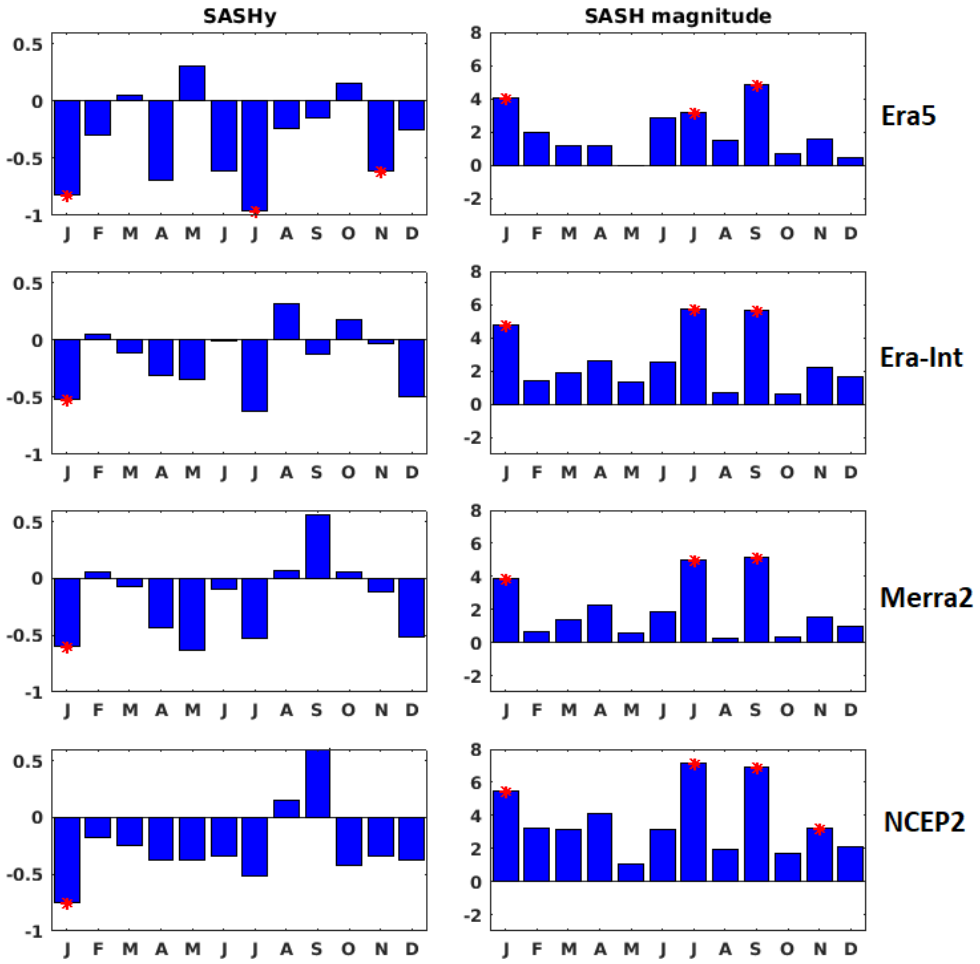

Figure 3.17: Linear trends (° per decade) in the meridional position of the SASH (left panel) and its magnitude (right panel) for each month of the year (blue bars) over the period 1982-2017 for (top to bottom): ERA5, Era-Interim, MERRA-2 and NCEP2, respectively. The red stars indicate statistically significant trends at the 95 % level using student's test based on linear regression.

3.8 Decadal variability of SST in the Benguela Upwelling System.

This section aims to investigate whether the SST trend is linear or whether it is part of decadal variability although the period of study of 37 years is rather short for this. However, it would be interesting to know if the trends reported by Rouault et al. (2010) and Blamey et al. (2015) continue. To do so, the non-detrended monthly SST anomalies in ABF, NB, CB and SB boxes (from Figure 3.8) are low-pass filtered using a 5-year running average. Filtered time series are shown in **Figure 3.18**. All datasets appear to present decadal variation in all the domains.

However, the variation is different from one domain to another and from one dataset to another, especially in the Benguela Upwelling System. In the ABF all datasets depict the same variations. Negative SST anomalies are observed from 1984 to 1993 and positive SST anomalies up to 0.5°C are found from 1994 to 2001 and from 2005 to 2015. From 2001 to 2005 the SST anomalies are almost nil or negative. Although decadal variation is observed, the warming trend dominates in the ABF. In NB discrepancies among datasets start to be observed. While negative SST anomalies, from 1984 to 1992, are observed with OISST1, OISST0.25, and Pathfinder, positive SST anomalies are observed for HadISST1. In general, no clear decadal variations are observed in all datasets in NB. However, OISST1 presents a reversed SST trend. A positive trend is found over the period 1984-1998, while a negative trend is observed over the period 2000-2015 which may be due to decadal variability. In CB the SST anomalies are negative from 1984 to 1990 and 2006 to 2015 and positive from 1992 to 2004 with OISST1 and OISST0.25. Pathfinder has the same pattern of variation until 2005 when it starts to diverge. It shows a positive SST anomaly from 2006 to 2015 while other datasets show negative SST anomalies. This divergence of Pathfinder over the period 2006 to 2015 is also observed in SB and may explain the pronounced warming trend observed in the entire Benguela Upwelling System with Pathfinder (see Section 3.3). Indeed, Pathfinder has the coolest bias early in the period of study from 1982 to 1992 and the warmest bias later from 2006 to 2017. In the SB region, all datasets present positive SST anomalies of up to 0.4 °C from 1985 to 1995 and from 1999 to 2004, while negative SST anomalies up to -0.4 °C are observed from 2006 to 2016, except with Pathfinder. From 1996 to 1999 the SST anomalies are around zero in most datasets.

In conclusion, the moving averages with a 5-year window in different domains of the Benguela Upwelling System indicate that SST anomalies in the Benguela Upwelling System exhibit decadal variation, although there are discrepancies among datasets over the study period. However, it is difficult to pronounce on the time scale of the variability, so signal decomposition analysis is needed. For that, I perform wavelet analyses.

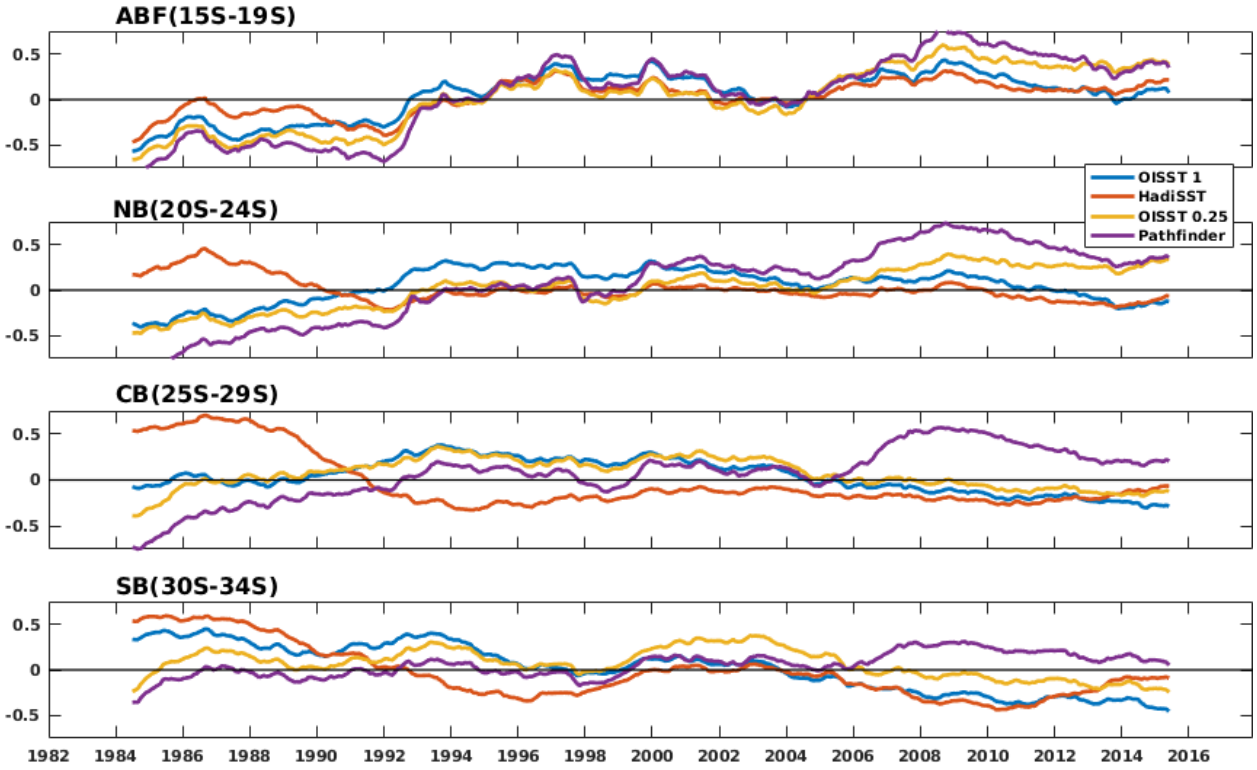

Figure 3.18: 5-year running average of SST anomalies from 1982 to 2017 in the four different boxes (from top to bottom: ABF, NB, CB, and SB) and for the four SST datasets: OISST1 (blue), HadISST1 (red), OISST0.25 (yellow), and Pathfinder (Magenta).

Figure 3.19, 3.20, 3.21, 3.22 represents a comparison of wavelet analyses of the detrended anomalies of SST using OISST0.25, OISST1, HadISST1, and Pathfinder in ABF, NB, CB, and SB domains, respectively. The left panel is the local wavelet spectrum which represents the changes of wavelet power in terms of scale with respect to time and the right panel is the global wavelet spectrum which is the time average of all the local wavelet spectra for each time scale. The red, green, blue, and black lines are the global wavelet spectra of OISST1, OISST0.25, HadISST1, and Pathfinder, respectively. The time scales SST variability appear to differ in different boxes according to the global wavelet spectra (right panel of **Figure 3.19, 3.20, 3.21, 3.22**). Three dominant peaks of variability are observed depending on the domain and the dataset at interannual time scales ranging between 2-8 years and at decadal time scales within 11-14 years and 23-28 years. Although the increasing variance is statistically significant in some domains, it is difficult to conclude on the 24-28 years scale, as the length of the timeseries is only 36 years

which does not cover enough frequencies of the 24-28 years scale. Longer timeseries of at least 70 years are required for the analysis of this time scale. The interannual scale of 2-8 years is present in all datasets and different domains (**Figure 3.19, 3.20, 3.21,** and **3.22**). However, the scale of 4-8 years has more energy and is statistically significant in most domains; it can be linked to ENSO, Benguela Niños or Atlantic Niños. Moreover, the timing period of increasing variance is different among the domains and the datasets. For instance, in ABF and NB regions (**Figure 3.19** and **3.20**), OISST0.25 and Pathfinder display significantly increased variance from 1990 to 2000 while HadISST1 shows greater variance since the 1980s. In CB, significantly increased variance is observed from 1982 to 1991 with OISST0.25 (**Figure 3.21b**) while it is observed from 1994 to 2010 with Pathfinder (**Figure 3.21d**). In the SB domain (**Figure 3.22**), all datasets except HadISST1, display significantly increased variance from 1992 to 1997. Decadal variability at the 11-14 years scale is present in most domains depending on the datasets, according to the global wavelet spectrum (right panel of **Figure 3.19, 3.21, 3.22**). It is observed in the ABF coastal zone with all datasets, in the CB domain with HadISST1 and Pathfinder, and in the SB region for OISST0.25, HadISST1 and Pathfinder. However, the increasing variance of this 11-14 years scale is only statistically significant in CB and SB boxes for HadISST1 (**Figure 3.21c, 3.22c**). Moreover, this time scale of 11-14 years, which is not significant in most domains, maybe due to the short period of study, is a known scale of variability in the South Atlantic High-pressure system and basin-wide SST (Venegas et al., 1997). Decadal variability at the 23-28 years scale also seems to occur in most domains with some datasets, for instance in ABF and NB with OISST1 (**Figure 3.19a, 3.20a**), in CB with OISST1, OISST0.25 and HadISST1 (**Figure 3.21a, b, c**), and SB with OISST0.25, as demonstrated by the global wavelet spectra (right panel of **Figure3.19 to 3.22**). This scale of variability was reported by Dieppois et al. (2016) for both austral winter and austral summer rainfall variability in Southern Africa and was linked to Pacific Ocean variability. This will be studied in more detail with a longer dataset in chapter 5.

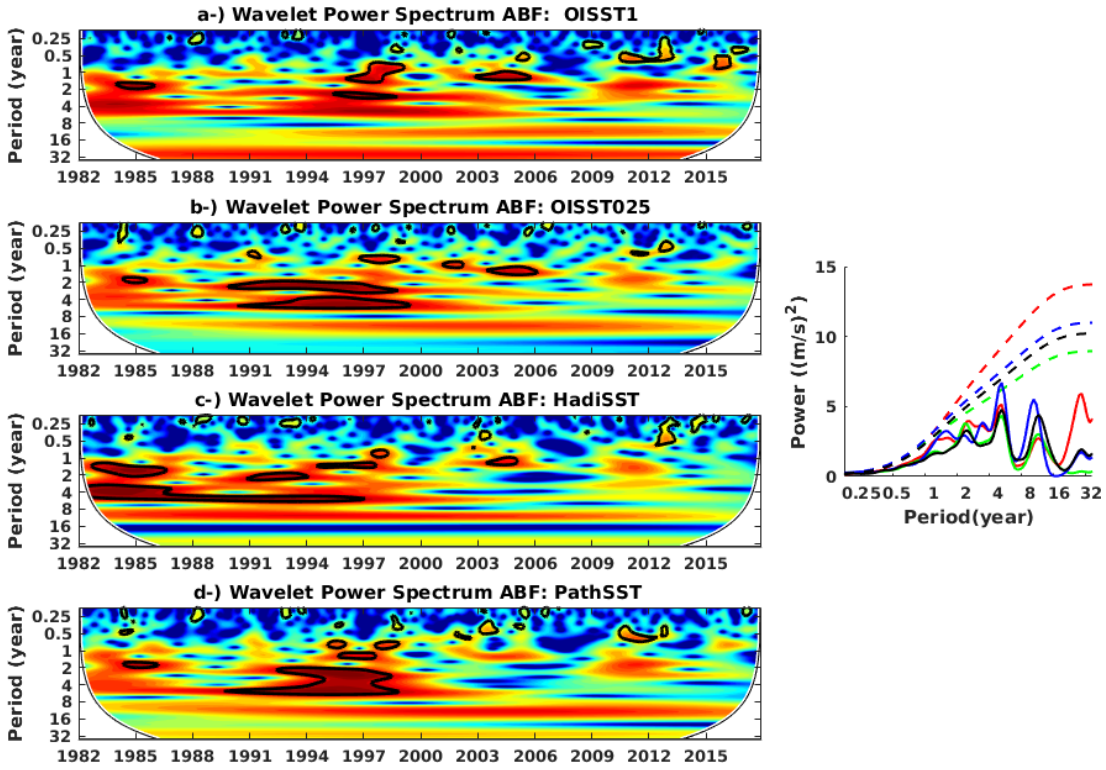

Figure 3.19: Wavelet analysis of detrended anomalies of SST averaged in the Angola Bengula Front box. Left panels show wavelet power spectrum for a) OISST1, b) OISST0.25, c) HadISST1, and d) Pathfinder. The bold contour lines show the 95% confidence limits based on Monte Carlo simulations of a red noise background spectrum. The black thin line (the so-called cone influence) delineates the area under which power can be underestimated as a consequence of edge effects. Right panel shows the global wavelet power spectra for OISST1 (red), OISST0.25 (green), HadISST1 (blue), and Pathfinder (black). The dotted lines indicate the red noise spectra with regards to the first-order autoregression.

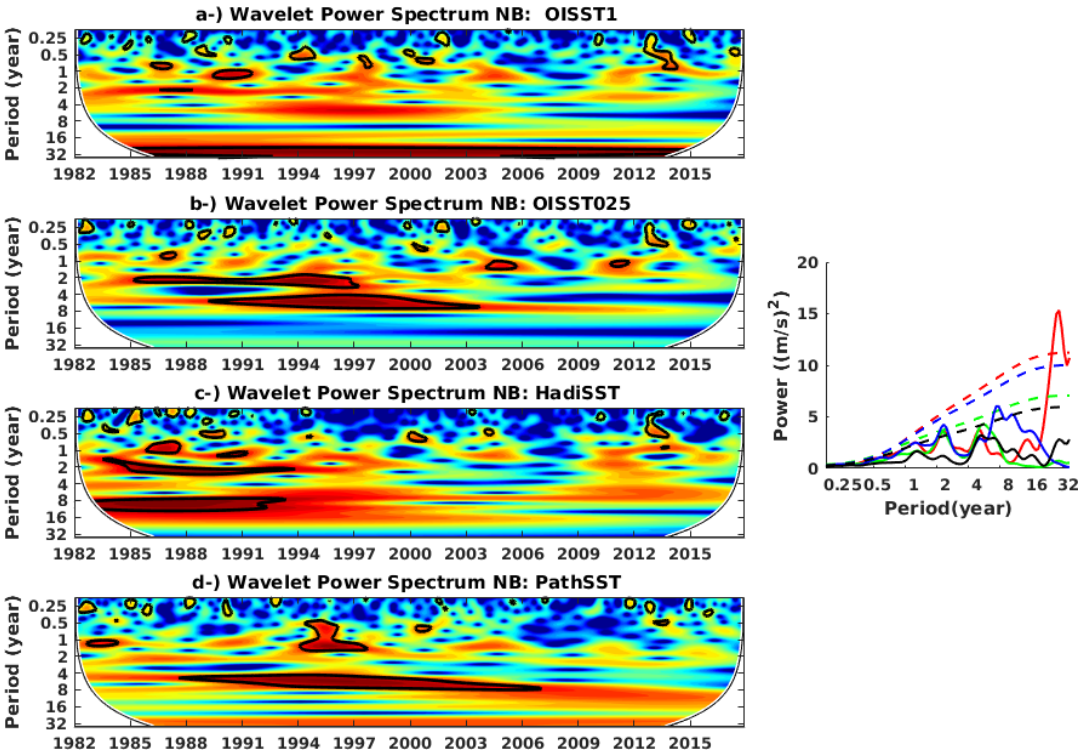

Figure 3.20: Same as figure 3.19 but in the Northern Benguela box.

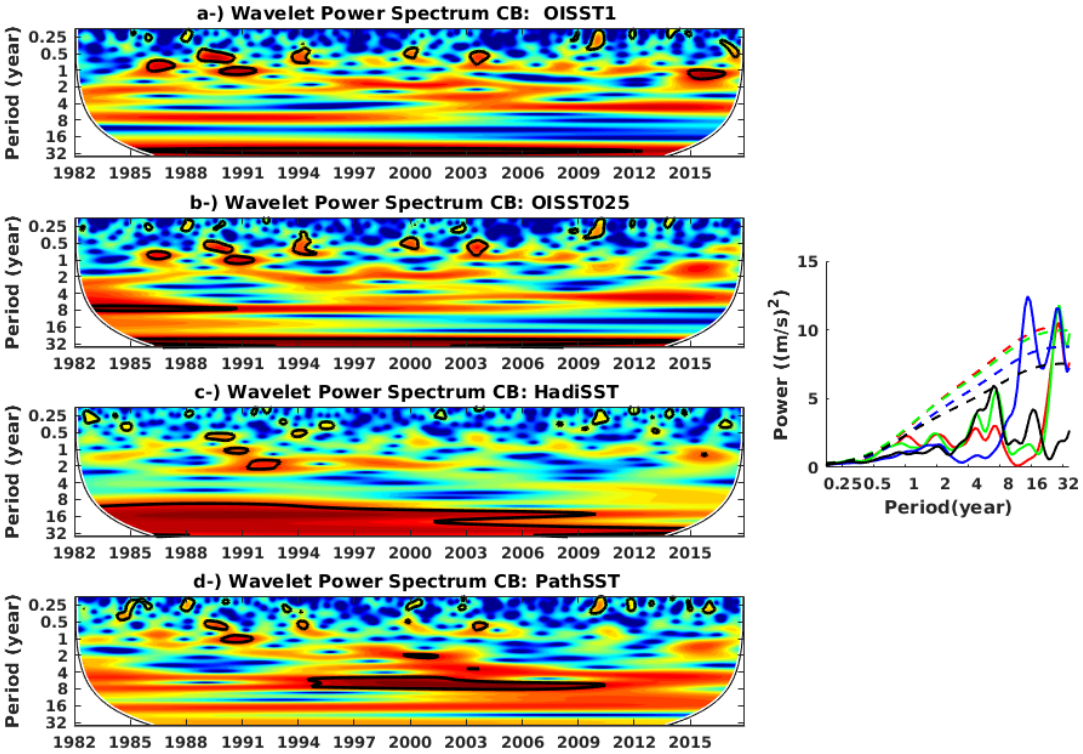

Figure 3.21: Same as figure 3.19 but in the Central Benguela box.

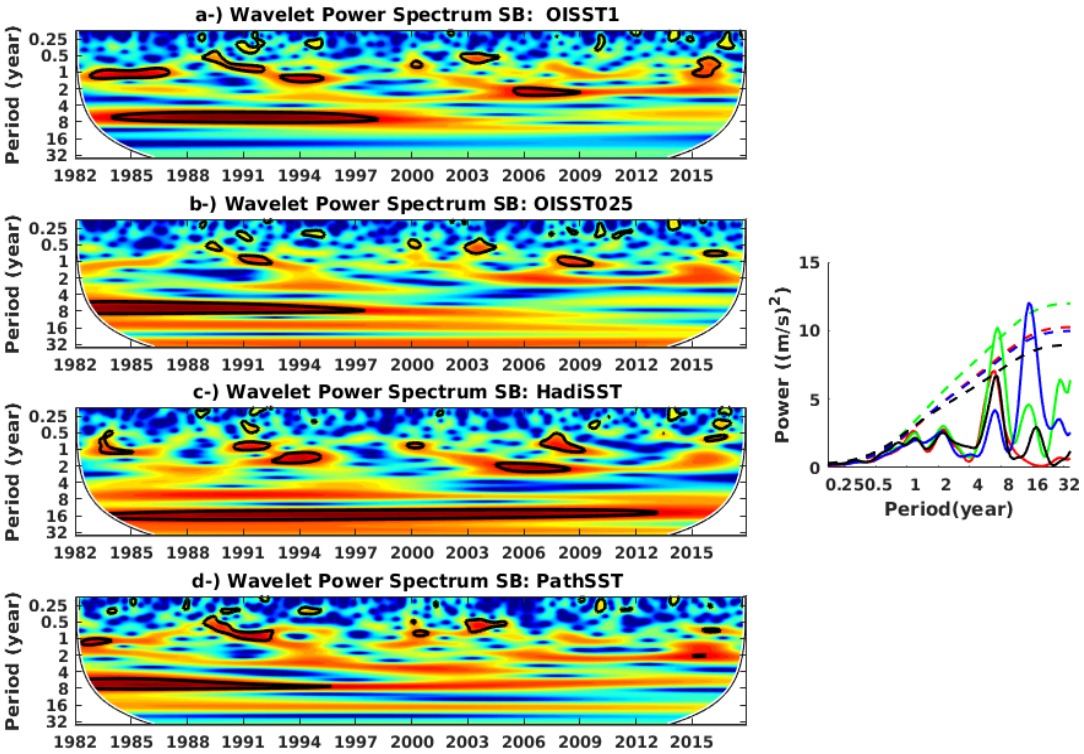

Figure 3.22: Same as figure 3.19 but in the Southern Benguela box.

3.9 DISCUSSION AND SUMMARY

In this chapter, the long-term change in the Benguela Upwelling System, over the period 1982-2017, has been investigated using a comparison method based on four different satellite-based oceanic SST datasets (OISST1, OISST0.25, HadISST1, and Pathfinder, see **section 2.1.1**) and five atmospheric reanalyzes of wind and geopotential height datasets (NCEP2, JRA-55, Era-Interim, MERRA-2, and ERA5, see section 2.1.2). I first looked at how these SST and wind data represent the Benguela upwelling mean characteristics. All SST data represent the Benguela Upwelling System and the Agulhas Current differently. However, the high resolution of OISST0.25 and Pathfinder provides a better representation of the Benguela Upwelling System mean conditions as they reveal the major upwelling cells in the Benguela Upwelling System as well as the Agulhas Current (**Figure 3.1**) very well. In the annual cycle, all datasets have the same variability with relative lower SST in austral winter than summer in the entire Benguela Upwelling System. However, higher resolution SST datasets have lower values of SST while coarse resolution

datasets (HadISST1 and OISST1) have higher values of SST and the difference is large in the Benguela Upwelling System. For instance, in south Benguela, water is colder at the coast in austral summer when upwelling is more active than in winter even though the shortwave radiation is higher in summer than winter. However, this is not observed in any SST dataset, not even in Pathfinder which has a 4x4 km resolution. This could be because the coldest water is too close to the coast for Pathfinder to pick up that effect. Also, upwelling is not observed every day. For example, in summer, when the upwelling favorable wind collapses the water can get warmer than in winter because of higher solar in summer compared to winter. For similar reasons, when there is a strong upwelling event in winter, water will be as cold as for summer. All this makes the representation of a realistic seasonal cycle of SST using satellite remote sensing derived dataset in the Benguela Upwelling System a challenge, especially near the coast. This misrepresentation of the seasonal cycle is a cause of concern. While Dufois and Rouault (2012) and Pfaff et al. (2019) have shown a more realistic representation of the local coastal SST seasonal cycle in the vicinity of False Bay (Western Cape, South Africa) and the Cape peninsula upwelling using 500m x 500 m resolution MODIS SST, they also detect differences of up to 3°C between MODIS and Pathfinder in the bay outlining further problem for the Pathfinder dataset used in my thesis. For instance, Pathfinder and OISST0.25 have a cold bias at the beginning of the study period from 1982 to 1985 especially, and Pathfinder ends the study period from 2006 to 2017 with the warmest bias (**Figure 3.8 and 3.18**). This would affect the consistency of trends and decadal variability in OISST0.25 and Pathfinder. However, trend analyses over the period 1986-2017 yield good agreement of warming or cooling trends among datasets, except for Pathfinder. In addition, the magnitude, the spatial extension and the seasonal timing of the cooling or warming trend are slightly different from one dataset to another (Figure 3.9). There may be many reasons that could explain the differences in SST and SST trends among datasets. The main upwelling occurs in a narrow band of 25 to 150 km off the coast (Shannon and Nelson, 1996; Chavez and Messié, 2009; Fennel et al., 2012), so the SST data with coarse resolution might not distinguish nearshore upwelling temperatures from offshore temperatures. Furthermore, as the satellite does not provide complete daily gridded coverage across the Benguela coastal area, HadISST1, OISST1, and OISST0.25 use various strategies of interpolation and *in-situ* data to fill the

gaps of missing values. For example, the interpolation scheme of the OISST1 and HadISST1 datasets use data interpolation and correlation with a radius of 300km to replace missing values. Moreover, HadISST1 and OISST1 use *in-situ* and operational AVHRR data while OISST0.25 use *in-situ* data, Pathfinder AVHRR data from 1985-2005, and operational AVHRR data from 2006 onward. The OISSTs and HadISST1 have also not been reanalyzed to make them homogenous or to correct them retrospectively. OISSTs are operational products. Another reason that could explain the differences among datasets is the temporal resolution of data used in the reconstruction of the dataset. For example, OISST0.25 is reconstructed based on daily data (Reynolds et al., 2007) while OISST1 and HadiSST1 are reconstructed based on weekly and monthly data respectively (Reynolds et al., 2002; Rayner et al., 2003). Thus, the monthly mean of high temporal resolution OISST0.25 is more likely to capture the daily variations of SST, characteristic of upwelling events, including duration and intensity, compared to lower temporal resolution OISST1 and HadiSST1. Different bias correction and interpolation methods using satellite and in-situ data in the reconstruction of the datasets could be another factor of uncertainties among data. Also, methods to interpolate missing data are different and could lead to difference. Lastly, Pathfinder is not corrected with *in situ* data and may be more related to skin temperature which could be affected by global air temperature and present a warmer trend than the other datasets. Concerning wind datasets, all wind data represent the winds in the Benguela upwelling quite well except NCEP2 and JRA-55 in northern Benguela. NCEP2 underestimates winds in the entire Benguela upwelling system while JRA-55 overestimate the wind in northern Benguela (**Figure 3.4**). These discrepancies may be due to the coarse resolution of NCEP2, but JRA-55 has a higher resolution than NCEP1 and 2 and ERA40. Imbol Nkwinkwa Njouodo et al. (2021) has shown some differences also between ERA-interim and the other more recent higher resolution reanalysis in the Benguela and South of Africa. A good example of the difficulties of model wind at the coast concerns the Benguela low-level coastal jet (BLLCJ). Several studies have shown that the BLLCJ is poorly represented in reanalysis or WRF model and is sensitive to spatial resolution (Desbiolles et al., 2014; Small et al., 2015; Patricola and Chang, 2017) resulting in misrepresentation of winds speed and direction along the Benguela coast. This misrepresentation of coastal wind speed and direction in the Benguela upwelling system could

be one of the reasons for the difference in trend among datasets observed along the Benguela coast. The differences in coastal trends can also arise from the ingestion of in-situ data in reanalysis as the reanalysis models use different input datasets for the reconstruction of reanalysis datasets. The difference in coastal trends can also arise from the orography. Orography at the coast is a challenge for model and reanalysis or ocean modeler. The comparative approach to analyzed trend in this chapter is very useful to address if indeed the Benguela Upwelling System wind speed has effectively changed during these 36 years and also to address the uncertainties inherent in the estimation of the long-term trend. I demonstrate in this chapter that the change varies in space and depends on the season. Cooling trends are observed in the southern part of the Benguela Upwelling System and are present throughout the austral summer (**Figure 3.9**). These cooling trends are consistent with an intensification of equatorward winds due to the intensification and the poleward expansion of the SASH (**Figure 3.14**). Similar trends have also been reported in previous studies (Narayan et al., 2010; Rouault et al., 2010; Blamey et al., 2012; Tim et al., 2015; Vizy and Cook, 2016; Abrahams et al., 2021). Warming trends are observed in the northern part of the Benguela and ABF. Vizy and Cook (2016) explain the warming in the Northern Benguela and ABF by a decrease in wind speed due to a poleward shift of the SASH. In my study, the SST warming in the Northern Benguela and ABF is observed only in austral spring and summer (September to February) (**Figure 3.7** and **3.9**), but I observed no trend in winds during this period in most of the wind datasets (**Figure 3.11**), although a poleward shift of the SASH was observed in my study (**Figure 3.14** and **3.16**). However, a decrease in wind speed north of the ABF may have led to a warming of Angolan water advected to the south and leading to warming at the ABF and Northern Benguela. Furthermore, the regression analysis of SST and wind (**Figure 3.13**) suggest that in austral summer a poleward shift of the SASH would decrease southeasterly winds in the Northern Benguela which in turn would increase SST in the area, but no trend is found in the coastal winds in austral summer in the Northern Benguela.

Lastly, I found that the warming or cooling trends in the Benguela Upwelling System are not linear. The trend decreases and can reverse signs in some domains, illustrating the occurrence of decadal variability (**Figure 3.18**). For instance, in CB, the warming trend is observed over the period 1982-2000 while a cooling trend is observed after the 2000s in most SST datasets.

The time scales of variability in the Benguela Upwelling System during the period of study are investigated using wavelet analysis and demonstrate that, in addition to a 2 to 8 years periodicity signal that appears in all datasets and all domains in the Benguela Upwelling System, signals of 11-14 years and 23-28 years also appear in most of the datasets (**Figure 3.19, 3.20, 3.21** and **3.22**). However, the time period of the observed datasets is too short to conclude firmly about decadal variability. Thus, a longer period, at least 100 years, will be needed to firmly study the decadal variability studies in chapter 5. The 2 to 8 years signal is the general time scale of ENSO events which has been shown to impact the BUS at the interannual scale (Rouault et al., 2010; Dufois and Rouault, 2012; Blamey et al., 2015) so it could be due to ENSO, but interannual variability is not the focus of the thesis. In the next chapter, I will investigate the origin of the warming trend in the ABF and Northern Benguela. The warming trend in the Agulhas Current has been studied by Rouault et al. (2009) but there is no study of warming in the coastal ABF region and the Northern Benguela except the study of Vizy et al. (2018). I will then study the decadal variability in this system to see whether 10-14 year and 23-28 year periodicities are found in longer datasets.

CHAPTER 4

4 ORIGIN OF THE RECENT WARMING ALONG THE ANGOLA - NAMIBIA COAST

4.1 INTRODUCTION

The Angola Benguela Front (ABF), is a very dynamic area, characterised by a high-temperature gradient of up to 4°C per degree latitude (Colberg and Reason, 2006; Veitch et al., 2006). It fluctuates in position and intensity seasonally (Veitch et al., 2006) which strongly affects the local marine ecosystem (Verheye and Ekau, 2005; Chavez and Messié, 2009; Huenerlage and Buchholz, 2013).

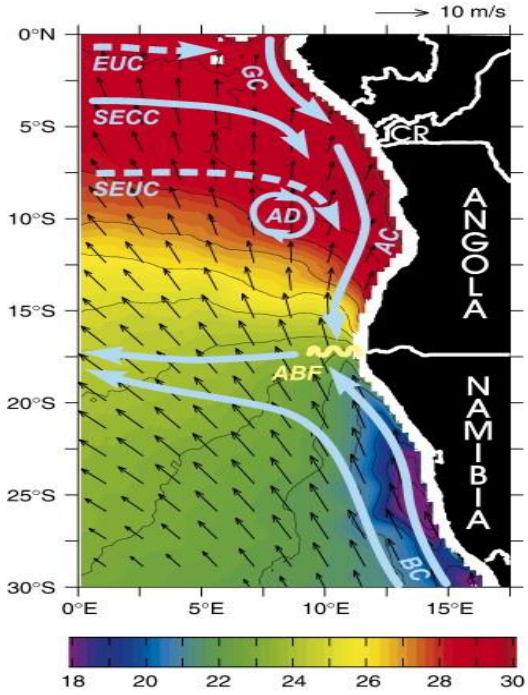

Figure 4.1: Schematic of the major oceanographic features in the South East Tropical Atlantic in late austral summer with mean 1988–2006 March TRMM TMI SST and 1999–2006 QuikSCAT wind speed and direction. Major features are Equatorial Under Current (EUC), South Equatorial Counter Current (SECC), South Equatorial Under Current (SEUC), Gabon Current (GC), Congo River

(CR), Angola Current (AC), Angola Benguela front (ABF) and Benguela Current (BC). SST is plotted every degree from 18 to 30 °C. Maximum wind speed is 8 m/s in the south and minimum wind speed is 3 m/s just north of the ABF. Figure from Rouault et al. (2007).

A lot of research, in the past decades, has focused on the SST variability at the interannual timescales in the ABF including the Angolan and Northern Namibian coasts. It showed that Benguela Niños and Niñas are the main mode of interannual variability in SST (Florenchie et al., 2003; Rouault et al., 2018) in the austral summer and autumn, which has a strong impact on atmospheric circulation and rainfall (Rouault and Richard, 2003; Imbol Koungue et al., 2017; Rouault et al., 2018). Rouault (2012) found that there is a bi-annual advection of warm water into the North Benguela upwelling system across the ABF which has an important role to play in the advection of warm water in the Northern Benguela and is a key mechanism behind Benguela Niños and Niñas, together with coastal trapped wave propagations and the associated modification of the coastal current and thermocline depth (Rouault et al., 2007; Bachèlery et al., 2016; Imbol Koungue et al., 2017; Rouault et al., 2018; Imbol Koungue et al., 2019; Bachèlery et al., 2020). Koseki et al. (2019) investigated the dynamical and thermodynamical processes responsible for the seasonal cycle of the ABF and found that the ABF shows a semi-annual cycle with two maxima associated with two different processes. The first maximum, observed in April-May, is due to the enhancement of tilting associated with the meridional gradient of vertical velocity, and the second in November-December is driven by the intensification of the southward Angola Current associated with the development of the Angola Dome. Indeed, the Angola Dome is a relatively cold region centered around 8°S and 6°E and surrounded by relatively warm water. The Angola Dome was identified for the first time by Mazieika, in 1967 in subsurface around 20 to 100 m in austral summer and does not exist in austral winter. However, the seasonality, the position of Angola Dome and the mechanism driving the Dome are still in debate. Although some argue it is observed in austral summer (Mazeika, 1967), some argue it is well developed between March to August due to surface net heat budget consideration (Doi et al., 2007). On the decadal scale, in spite of the strong warming revealed and discussed in Chapter 3, there is little work focused on the ABF area. This may be because of a lack of long-term observational data and the

challenge of models to simulate the ABF properly in that region. Coupled and non-coupled models in the tropical Atlantic are known to suffer from a warm coastal bias extending to Angola and Namibia with the ABF having the warmest bias (Li and Xie, 2012; Richter et al., 2012; Toniazzo and Woolnough, 2014; Richter, 2015; Koseki et al., 2018). In Chapter 3 of this thesis, I have shown that the SST along the Angolan and north Namibian coasts exhibits statistically significant warming trends from October to January while no trend, or no statistically significant warming trends, are observed for the rest of the year. Vizy and Cook (2016) have attributed the warming along the Angola-Namibia coast to the net downward atmospheric heat flux. Another study of Vizy et al. (2018) has investigated the decadal change of the ABF based on annually averaged data using a regional climate model coupled with an intermediate-level mixed-layer ocean model. They found a warming trend in the SST along the Angolan coast and a cooling trend along the Namibian coast, which intensifies the gradient of temperature at the ABF of ~0.05 to 0.13 °C/100-km per decade, and a southward shift of 0.05° to 0.55° latitude per decade in the annual mean ABF position for these last three decades. Furthermore, Vizy et al. (2018) suggested that the warming trend north of the ABF is associated with a weakening of the vertical entrainment leading to less cooling of surface water. The cooling trend south of the ABF would be associated with the intensification of horizontal advection of cooler water from the Benguela Current. However, they did not investigate changes at the seasonal or monthly scale. In addition, investigating trend at a seasonal scale allow more detailed information on the quantification and also the origin of the change as different mechanisms occur at different seasons. This chapter aims to use all parameters involved in the surface and subsurface ocean heat budget to identify the mechanisms responsible for the long-term trend in the Angola-Namibia region identified in Chapter 3 at the seasonal scale. Trends along the Angolan and Namibian coast are different from one season to another. A warming trend is observed from September to February and a cooling trend is observed for the rest of the year. Assessing the mechanism responsible for the SST trend in the Angola-Namibia region can help to understand the origin of changes in the ecosystems in the region or establish a scenario for the region for the future.

A tropical Atlantic configuration of the OGCM NEMO model ((Madec et al., 2017), hereafter NEMO) is used for this study. This model has been extensively used in the region to

study the coastal interannual variability since 1958 (Imbol Koungue et al., 2019). Imbol Koungue et al. (2019) showed that this model configuration reproduces Benguela Niños and Benguela Niñas remarkably well since 1958. This chapter is structured as follows: Firstly, I validate NEMO SST trends by comparing the simulated trends with observed trends estimated from ensemble means of OISST1, OISST0.25 and HadISST1 (referred hereafter to observations). Because of the problems in the observed SST during the 1982-1985 period revealed in Chapter 3 and because the model configuration stops in 2015, I focus on the 1986-2015 period. The model is then used to evaluate the mean contribution of temperature rates of changes associated with different components of the heat budget. This evaluation helps to identify the potential important heat budget term involved in the long-term changes of mixed layer temperature or SST. Trend analysis is then done on the most important variables (currents, heat transport, net heat flux at the surface, vertical velocity, mixed layer depth) involved in the heat budget that is driving the SST long-term changes in the Angola and Northern Namibia region. Note that the mean mixed layer depth of the region is about 30 m. The detailed and seasonal trend analysis will provide insight into potential mechanisms causing the trends in SST. Finally, I will highlight the role of the Angola Dome in the austral summer warming of the Angola - Namibia region.

4.2 COMPARISON OF SST TREND IN NEMO WITH OBSERVATIONS IN THE ABF

Figures 4.2 and **4.3** show the observed and modeled SST trends at annual and seasonal scales. Statistical significance at the 95% level of confidence (contour line) is calculated using the Student's test based on linear regression. At the annual scale, NEMO warming trends range from 0.1 to 0.4°C per decade in the Angolan sector north of 17°S in agreement with the observations. South of 16°S along the Namibian coast there is a cooling trend ranging from 0.05 to 0.2°C per decade in the NEMO model, while a warming trend is observed in the observations of up to 0.2°C per decade along the Namibian coast, which is a cause of concern. At the seasonal scale, the warming trend observed along the Angolan coast (6°S to 17°S) is found throughout the entire year except in austral winter in the model and austral winter and autumn in the observations. The warming trend ranges from 0.1 to 0.9°C per decade depending on the month. The warming trends are more pronounced and are statistically significant in the austral summer (November to

January) while they are weaker and not statistically significant for the rest of the year in both the model and the observations.

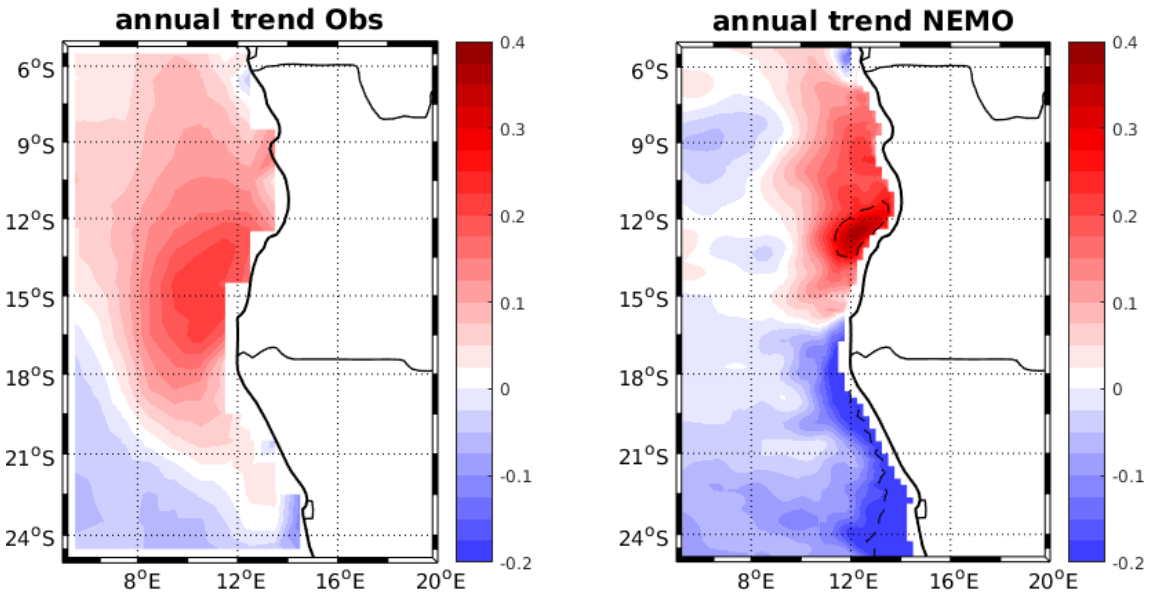

Figure 4.2: Linear decadal trends in annual mean SST (°C per decade) for the period 1986-2015 for ensemble mean OISST 0.25, OISST1, and HadISST1 (left panel) and NEMO (right panel). The dashed contour line denotes statistically significant values at the 95% confidence level using Student's test based on linear regression.

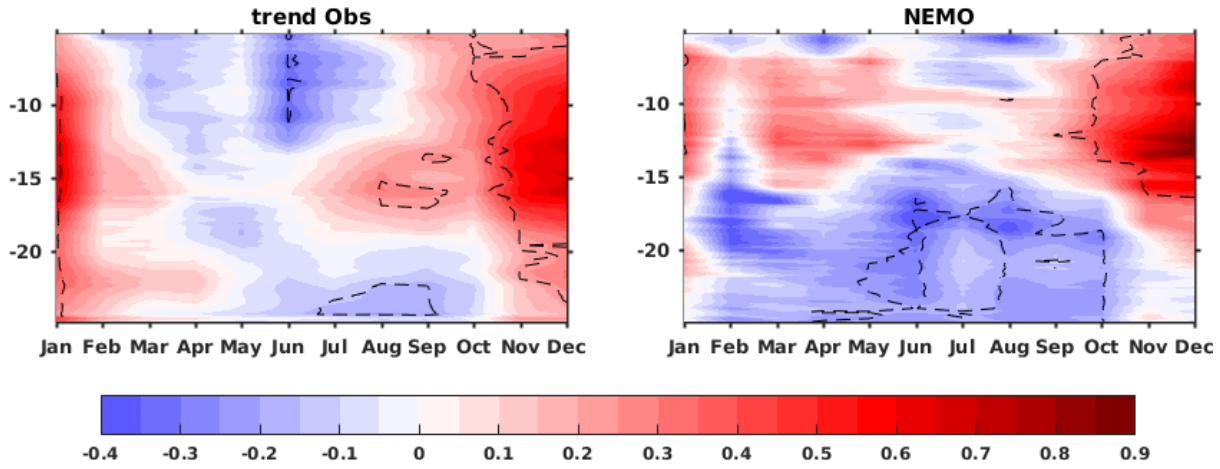

Figure 4.3: Hovmoller diagram of the monthly decadal linear trend of SST (oC per decade) for the observation (left panel) and NEMO (right panel) Trends are estimated over the 1986-2015 period for the SST averaged from the coast to 1 degree offshore along Angola and Namibia coasts.

Dashed contour lines denote statistically significant values at the 95% confidence level using the Student's test based on linear regression.

South of 18^{o}S, a cooling trend is found throughout the year using NEMO, except from December to January when a positive but very weak trend is depicted. There is also a cooling trend south of 18^{o}S in the observations from April to October, while there is a warming trend for the rest of the year. The cooling trend is pronounced up to -0.4^{o}C per decade in the model and is statistically significant in late austral winter and spring. The cooling trend is also statistically significant south of 22^{o}S from July to September in the observations. Overall, the warming trend in the observations persists over the summer with higher amplitude along the Angolan and Namibian coasts making the overall annual decadal SST trend positive in most parts of the Angolan and Namibian coasts.

In conclusion, the NEMO model represents the annual warming trend in the Angolan sector well but does not represent the warming trend in the ABF and Northern Namibia. At the seasonal scale, the model shows a good representation of the austral summer warming trend and the winter cooling trend in the ABF and Northern Namibia except that the model overestimates the cooling trend. This is probably due to unrealistic higher than normal trends in wind forcing, which can increase upwelling and the equatorward horizontal motion of cold water to the north a bit too much.

4.3 UPPER-OCEAN HEAT BUDGET ANALYSIS IN THE MIXED LAYER

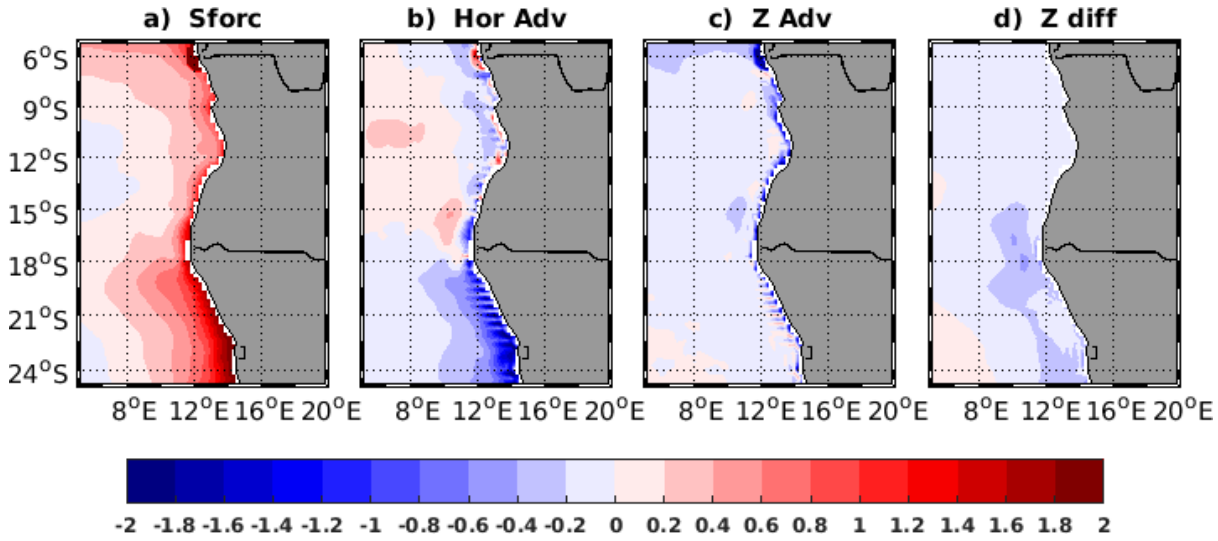

Figure 4.4: Climatology of NEMO temperature rates of change (1986-2015) associated with the **a)** net surface heating term, **b)** horizontal advection of heat, **c)** vertical advection of heat, and **d)** vertical diffusion of heat (10^{-1} °C.day^{-1}). Note that the lateral diffusion parameter is not shown as it does not have any impact on the climatology or the trends.

To investigate the processes involved in regulating the SST at the climatological scale in the ABF zone, I evaluate the mean contribution of temperature rates of changes associated with different components (Figure 4.4) of the upper-ocean heat budget in the mixed layer based on the decomposition detailed in **Chapter 2** (see Eq. 2.1). This will help to understand the mechanisms responsible for the trend later on. These components of the upper-ocean heat budget are the net surface heating term (Sforc in eq 2.1), the horizontal advection of heat, the vertical advection of heat, the vertical diffusion of the heat, the vertical entrainment, and lateral diffusion, respectively. Note that the lateral diffusion and vertical entrainment of the heat term are not shown here as their contributions do not account much for the upper-ocean heat budget climatology. From the climatological point of view, the net surface heating term (**Figure 4.4a**) warms the ocean, especially along the coasts of Angola and Namibia where upwelling occurs most likely due to strong short-wave radiation and low turbulent heat fluxes characteristic of the EBUS. The warming is stronger at the coast compared to the open ocean. Horizontal advection

of heat, except in the open ocean off the Angolan coast and some parts along the coast, cools the ocean (**Figure 4.4b**). This cooling is associated with horizontal advection of heat and is very strong along the Namibian coast, compensating the net surface heating term. The other two terms (vertical advection and vertical diffusion of the heat) also cool the ocean surface layer (**Figure 4.4c, d**). However, these two terms (vertical advection and vertical diffusion of the heat) contribution do not contribute much for the upper-ocean heat budget climatology except the vertical advection along the coast. A decomposition of the horizontal advection into zonal and meridional advection (Figure 4.5) reveals that the cooling associated with horizontal advection along the Angolan and the Northern Namibian coast is mainly due to the zonal advection (Figure 4.5 a). Indeed, the zonal advection of heat, except in the open ocean off the Angolan and some parts along the Angola coast between 11°S and 13°S, cools the ocean. The cooling associated with the zonal advection is very strong up to -0.2°C.day^{-1} along the coast because of the strong negative zonal SST gradient observed (not shown) highlighting the strong upwelling in the region. On other hand, the meridional advection of heat warms the ocean almost everywhere in Angola region except the coastal area between 11°S and 14°S. The maximum values of meridional advection of heat in Angola region are observed along the coast, especially at the mouth of the Congo River, coastal region between 9°S and 11°S and ABF coastal area. These regions coincide with a region of high meridional SST gradient (not shown). The meridional advection of heat also warms the ocean along the coast of Northern Namibia (north of 23°S) and cools the open ocean off the Namibia coast.

In conclusion, the net surface heating, horizontal advection, and vertical advection appear to be the most important terms for the long-term changes of the mixed layer temperature or SST. The net surface heating term increases the SST of the coastal ocean while the horizontal advection and vertical advection decrease the SST of the coastal ocean of Angola and Northern Namibia. In the following sections, different parameters involved in the different terms of the heat budget will be analysed to understand the annual cycle trend in the Angola and Northern Namibia region.

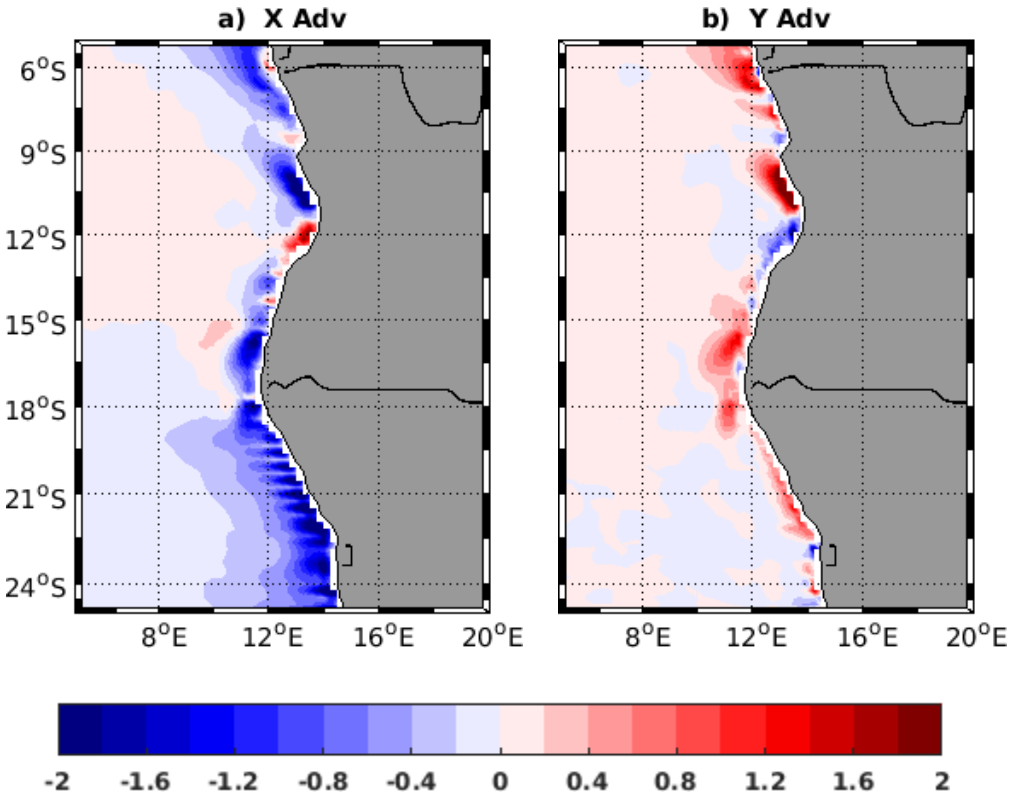

Figure 4.5: Same as Figure 4.4 but with a) zonal advection and b) meridional advection (10^{-1} $^{o}C.day^{-1}$)

4.4 UPPER-OCEAN HEAT CONTRIBUTION IN SEASONAL SST TREND

Before quantifying the contribution of net surface heat flux (Q_{net}) and the mixed layer depths changes to SST trends at the seasonal scale, I first present in **Figure 4.6** the maps of the seasonal SST trends shown in **Figure 4.3**. Warming trends up to 0.8°C per decade occur along the Angola-Namibia coast as well as in the open ocean in early austral summer from November to December. These warming trends are not statistically significant south of 21°S. Warming trends also occur in late austral summer, from February to April, in the Angolan sector and offshore of Namibia while negative trends occur along the Namibian coast. The cooling or warming trends along the Angolan and Namibian coasts in late austral summer are not statistically significant. In austral winter, from May to August, cooling trends up to -0.4 °C per decade, are observed in most parts of the ocean along the Angolan and Namibian coasts as well as in the open ocean. However, weak warming trends of about 0.2°C occur along the Angolan coast in May and August. In early

austral spring, cooling occurs in the open ocean and along the Namibia coast while warming trends up to 0.5°C per decade are found in the open ocean and along the Angolan coast. The cooling trends in the Namibian sector are only statistically significant along the coast.

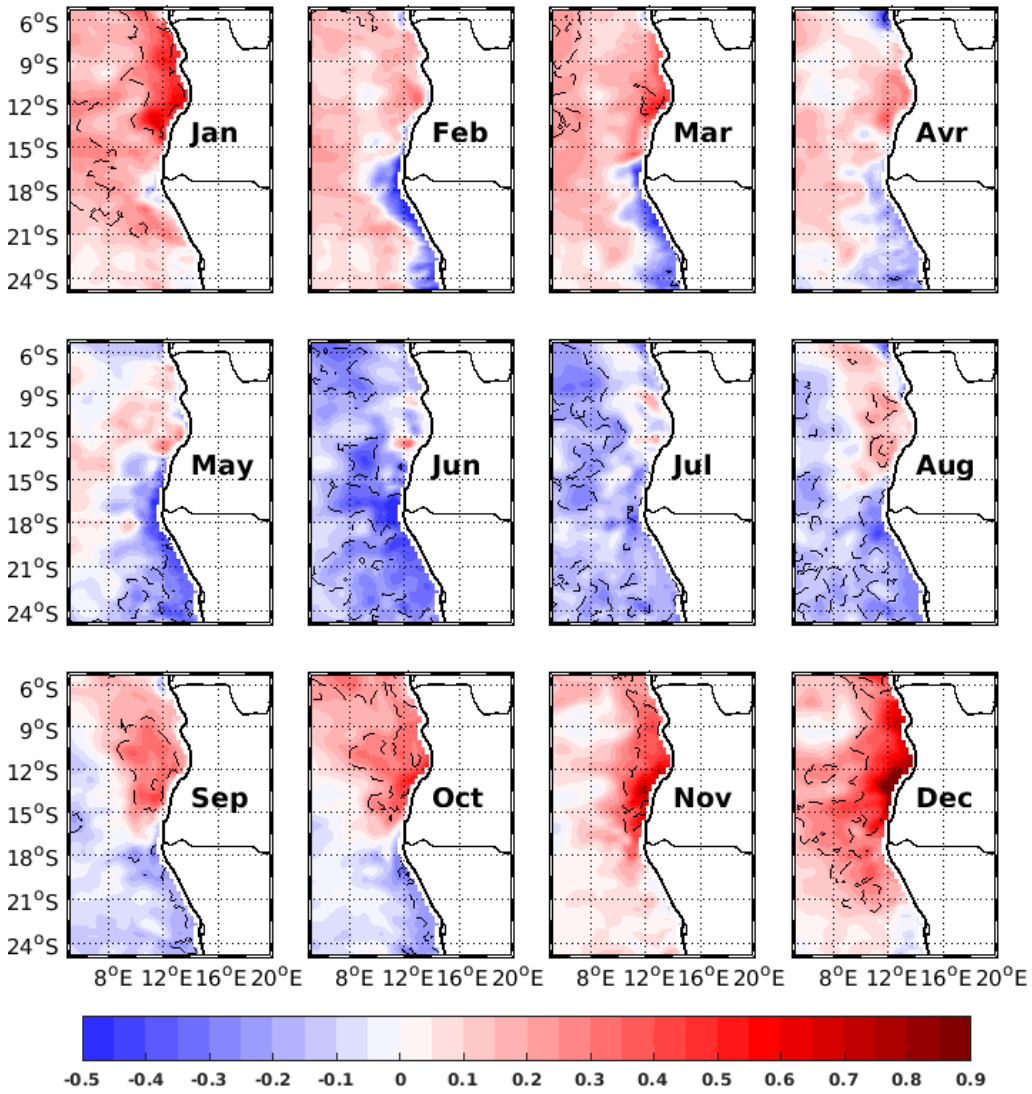

Figure 4.6: Monthly decadal trends of SST (°C per decade) from NEMO over the period 1986-2015. Dashed contour lines denote statistically significant values at the 95% confidence level using Student's test based on linear regression.

Secondly, I quantify the contribution of the Q_{net} to the SST trend. To do so, I estimate the month to month SST change (dSST) derived from Q_{net} (see section 2.2.4 in Chapter 2 for details) and then I analyse the trends of dSST (**Figure 4.7**). Note that the spatial patterns of the seasonal

Qnet trends match very well with the spatial patterns of the seasonal dSST trends. This suggests that the trends in dSST are due to change in Qnet and MLD does not play a role in dSST trend. The mixed layer depth trends are then investigated at the end of this section.

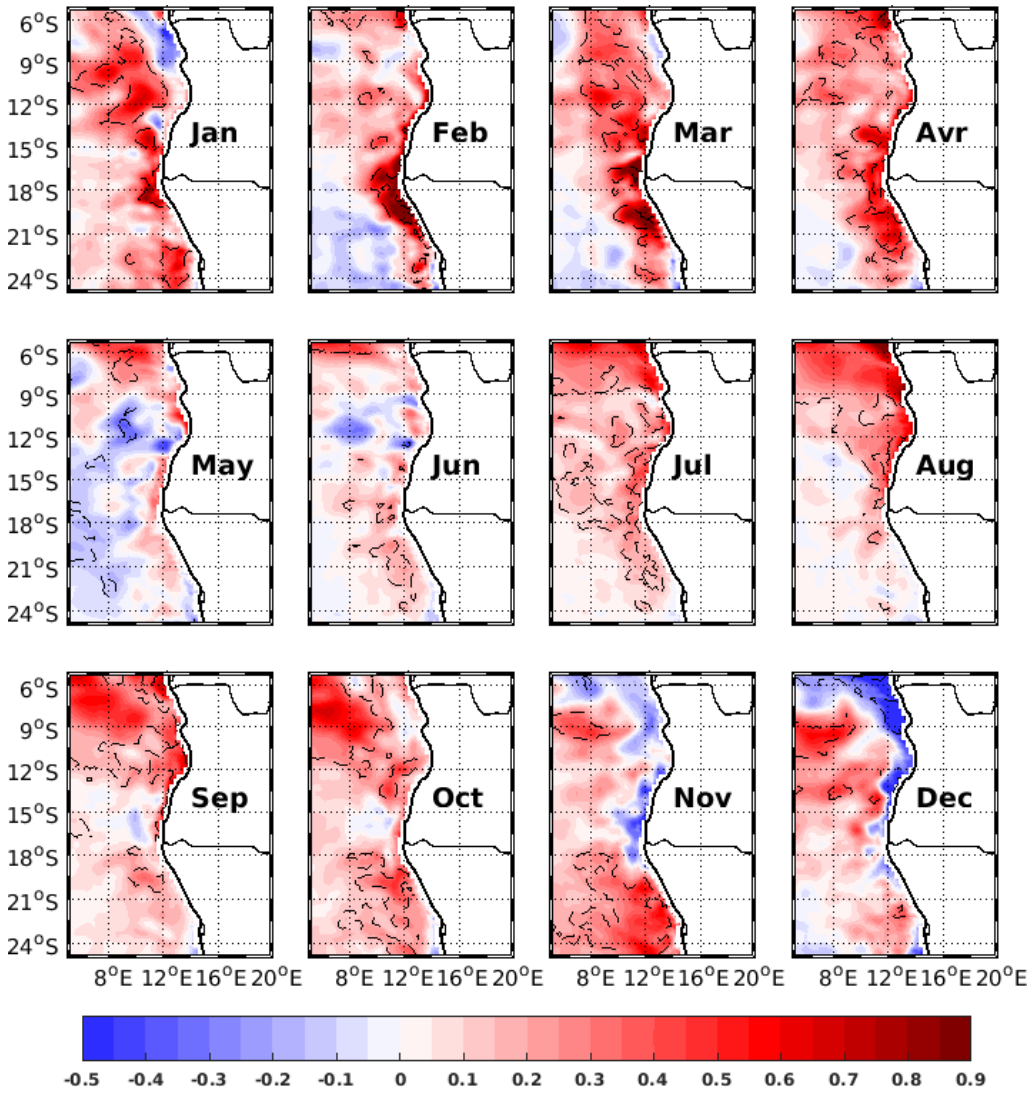

Figure 4.7: Monthly decadal trends of NEMO dSST (°C per decade) estimated from Qnet (see section 2.2.4). Dashed contour lines denote statistically significant values at the 95% confidence level using Student's test based on linear regression.

The trend analysis of dSST, reveals that in the Angolan sector (north of 15°S), dSST shows a positive trend, up to 0.8°C per decade in late austral summer to early Autumn (February to April) and late austral winter to early spring (July to October) meaning that positive trends in Q_{net}

contribute to the positive trends in SST. The biggest contributions to positive trends in Q_{net} occur from July to August, when the SST shows cooling in July or weaker warming trends in August (**Figure 4.6**). Positive trends in dSST are also observed in the Angolan open ocean in early austral summer (November, December, January). However, along the Angolan coast north of 15°S, negative trends in dSST, up to -0.5°C per decade, occur in the same period. This suggests that in austral summer, Q_{net} has decreased over the 1986-2015 period which would cool down the SST. However, as the SST shows a pronounced warming trend in the region (**Figure 4.6**), the cooling due to Qnet is compensated by something else. In other words, the negative trend of Q_{net} in the Angolan sector suggests that changes in Q_{net} are not responsible for the warming trend along the Angolan coast in austral summer. In the ABF, close to the coast, the trends in dSST are positive all year round except in November and December when negative trends are observed. The biggest values of the dSST trend are observed from February to April when they exceed 0.9°C, suggesting that the trend in Q_{net} would have contributed to the warming trend of the ABF coastal zone all year round, except in early summer when negative trends in Q_{net} are found. In February-March, despite the important contribution of the trend in Q_{net} to the positive trend in dSST, the SST in the ABF coastal zone (**Figure 4.6**) shows a negative trend. Furthermore, in austral winter dSST shows positive trends in the ABF coastal zone while SST shows negative trends. Again, this suggests that Q_{net} is not the main factor for the SST change in the ABF coastal zone over the 1986-2015 period. In the Namibian sector (south of 19°S), the dSST trend is positive throughout the entire year. However, the positive trend is weak in austral winter, less than 0.3°C per decade, and not statistically significant.

As the net surface heating term is also a function of the mixed layer depth, I also analyse its contribution to the SST trend. Figure 4.8 shows the seasonal mixed layer depth trends of the model. Figure 4.8 indicates negative mixed layer depth trends at rates of -1 to -5 m per decade through most months of the year in the Angola region. Relatively small positive mixed layer depth trends of up to 1.5 m per decade are found in early summer (October to December) off northern Angolan coast to about 9°S in late summer (January-February) in the open ocean of Angola region. However, these positive trends are not statistically significant. The maximum values of negative mixed layer depth trend in the Angola region are observed in the winter period. In

northern Namibia, along the coast, the mixed layer depth is shoaling at the rate of up to -2 m per decade in summer (November to April) while relatively small positive deepening mixed layer depth trends up to 2 m per decade is found in winter. However, these positive or negative trends are not statistically significant at 95 % level. Overall, in Northern Namibia, negative mixed layer depth trends are found from October to May and positive trends with the same magnitude are found in the rest of the year making the annual trend almost null (not shown) while in the Angolan region negative trend is observed almost year-round making the annual trend negative with the rate up to -2 m per decade. The shoaling of the mixed layer depth contributes to the warming associated with the net surface heating term while a deepening of the mixed layer depth contributes to the cooling associated with the net surface heating term. However, a comparison of the annual cycle of the mixed layer trend (**Figure 4.8**) and dSST trend (**Figure 4.7**) does not show a similar pattern in most parts of the study region. For instance, dSST shows a negative trend in the open ocean from May to June while the mixed layer depth contributes to the positive trend of dSST. Other examples are observed in October in the Namibia region and November-December along the Southern Angolan coast. These contradictory results confirm as I mentioned earlier that the MLD does not play a role in dSST. The trends in dSST are due to change in Q_{net} as the spatial pattern of seasonal Q_{net} trend (not shown) matches very well with the spatial patterns of the seasonal dSST trends.

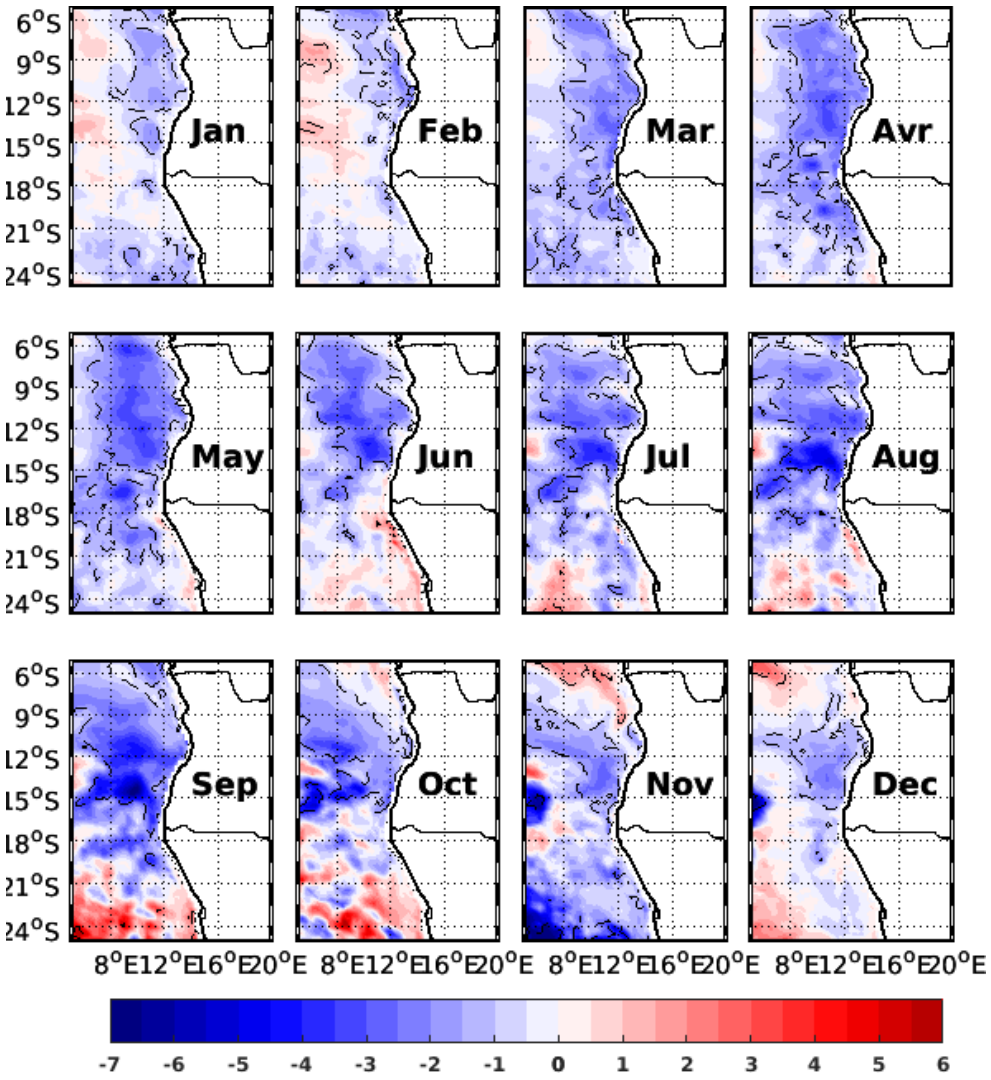

Figure 4.8: Monthly decadal trends of NEMO mixed layer depth (m per decade). Dashed contour lines denote statistically significant values at the 95% confidence level using Student's test based on linear regression.

In summary, trends in dSST are due to changes in Qnet. The long-term mean mixed-layer heat budget analysis appears to demonstrate that the net surface heating term is the main driver of the warming trend observed in the Angolan and ABF areas. The seasonal trend analysis of dSST in Figure 4.6 demonstrates that trends in Qnet cannot sufficiently explain the SST change in the Angolan and Namibian coastal zones, especially in early austral summer. Indeed, the SST trends have the highest values in austral summer although the Qnet trends tend to cool the SST.

4.5 ROLE OF HORIZONTAL CURRENTS IN SEASONAL SST TREND

4.5.1 Climatology of horizontal current

Figure 4.9 shows the seasonal climatology of horizontal currents (arrows) and the meridional currents (shading colour) of the model. The current is averaged from the surface to 250 m depth as in Rouault (2012). In the Namibian sector, south of 17°S, the current is predominantly westward throughout the year, but it is weak during early winter (May to July). In the coastal area of the Angolan sector, the current is more variable and follows the coastline all year round. Two seasons of poleward flow, late austral summer (February-April) and austral spring (September- November), up to -10 $cm.s^{-1}$, are distinguished north of 15°S. However, in March-April and November, an equatorward flow is observed close to the coast. For the rest of the year, the current flows equatorward and is up to 18 $cm.s^{-1}$. The equatorward flow is strongest in June, contributing to the development of the upwelling in this region, while the poleward flow is strongest in October. In the Angolan open ocean between 5°S and 10°S, the current flows mostly westward all year round. In the ABF, the current is poleward all year round with a weakening flow in austral winter (May to July). The strongest poleward flow about -12 $cm.s^{-1}$ occurs from September to November.

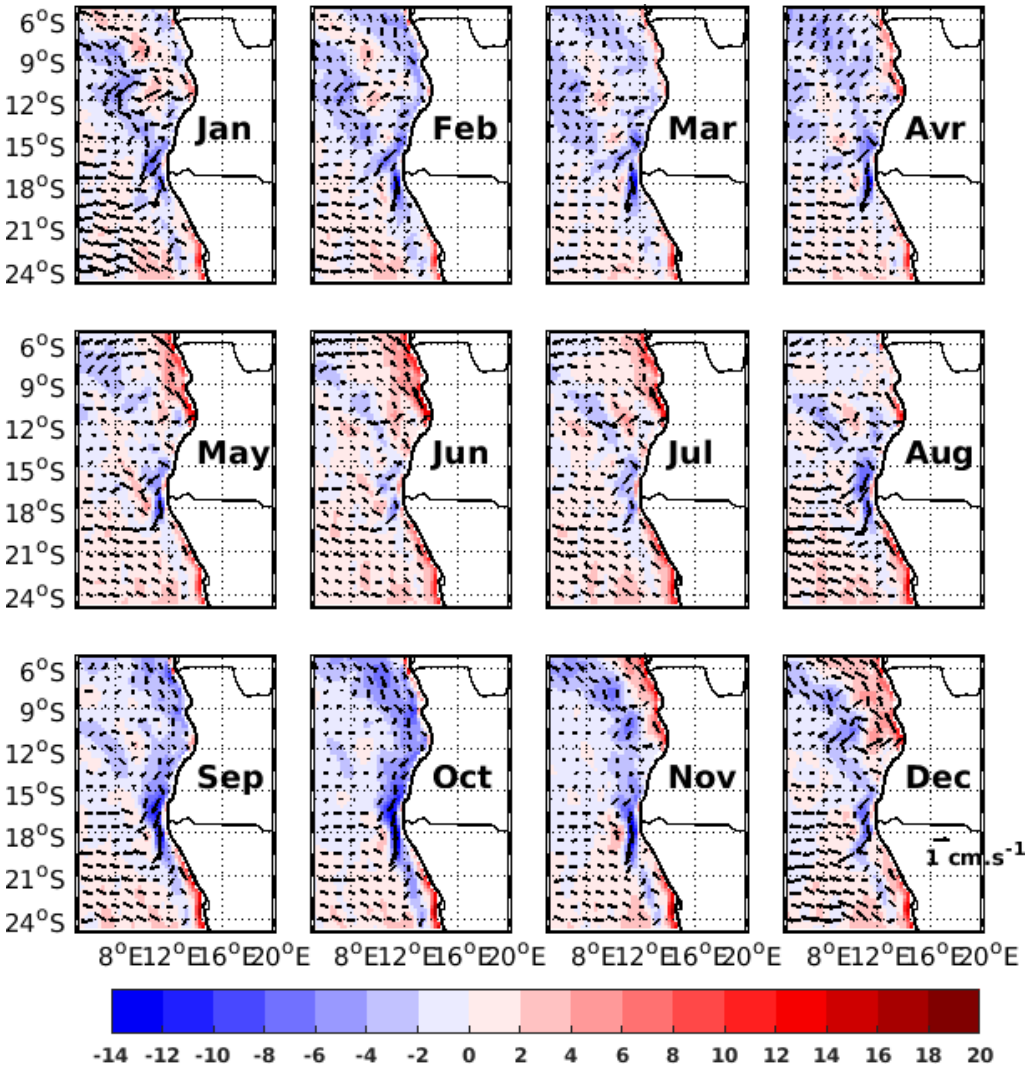

Figure 4.9: Seasonal climatology of NEMO horizontal current (cm.s^{-1}, arrows) and meridional current (cm.s^{-1}, shading) averaged vertically from the surface to 250 m depth. Positive values indicate equatorward flow.

4.5.2 seasonal trend of horizontal current

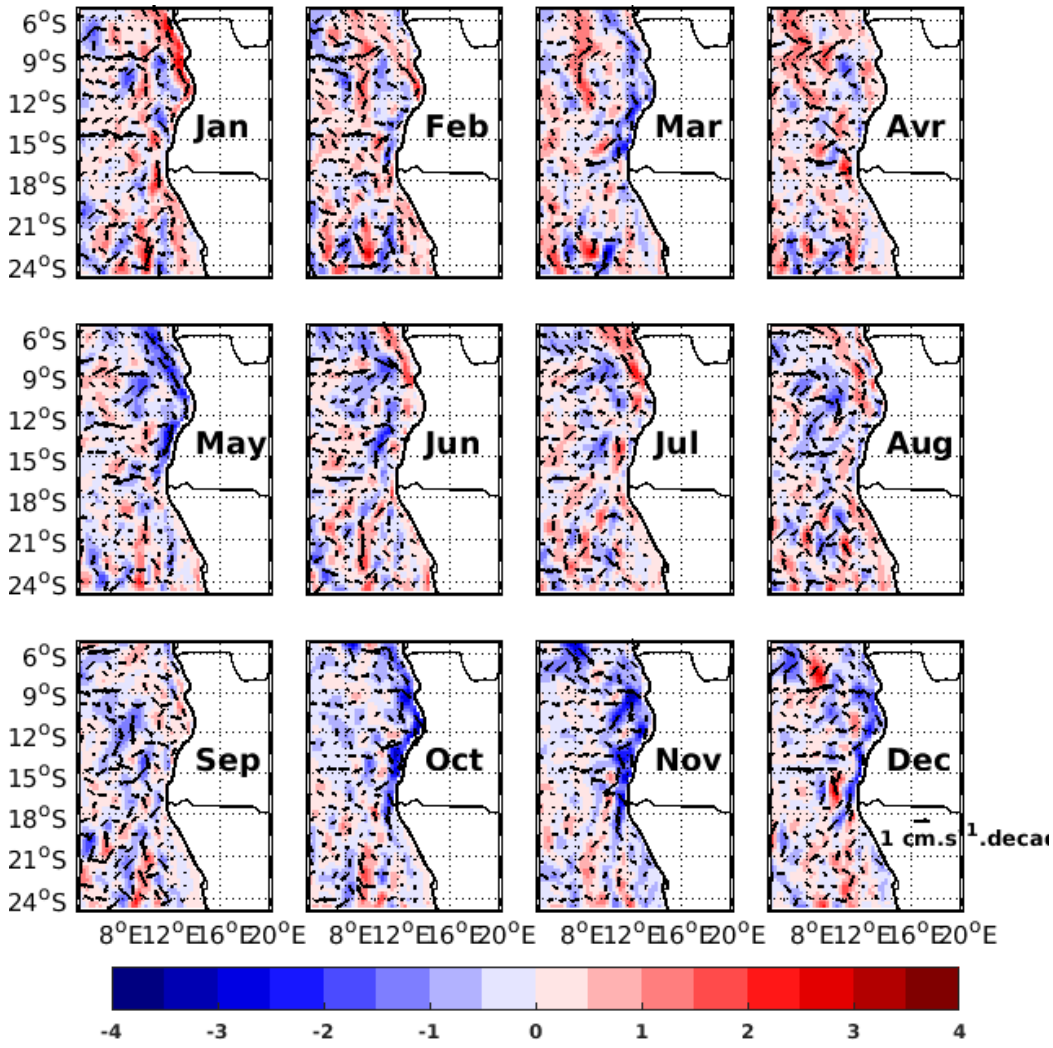

Figure 4.10: Seasonal trends of NEMO horizontal current (cm.s^{-1} per decade, arrows) and meridional current (cm.s^{-1} per decade, shading) averaged vertically from the surface to 250 m. Positive values indicate equatorward trends.

Figure 4.10 displays the seasonal horizontal current trends of the model. Alternation of poleward and equatorward trends is observed depending on the season along the Angolan coast. During the late austral spring and early summer, the currents along the coast of Angola display a strong poleward trend. This poleward trend extends to the ABF and intensifies the poleward current that flows along the coast in October-November. It also reduces the equatorward flow closer to the coast in November and December. Contrary to what is observed in early austral

summer, in late austral summer (January and February), the current shows equatorward trends along the Angolan coast. This equatorward trend intensifies the equatorward flow observed in January and decreases the poleward flow in February along the Angolan coast. In early austral winter (May to June) the current along the Angolan coast exhibits a poleward trend before showing an equatorward trend in late winter (July to September). The poleward trend observed in May-June decreases the equatorward flow observed in this period while the equatorward trend in July-August increases the equatorward flow in the period. In the Namibian sector, no significant trends occur. However, negative trends close to the coast take place in austral spring from October to December.

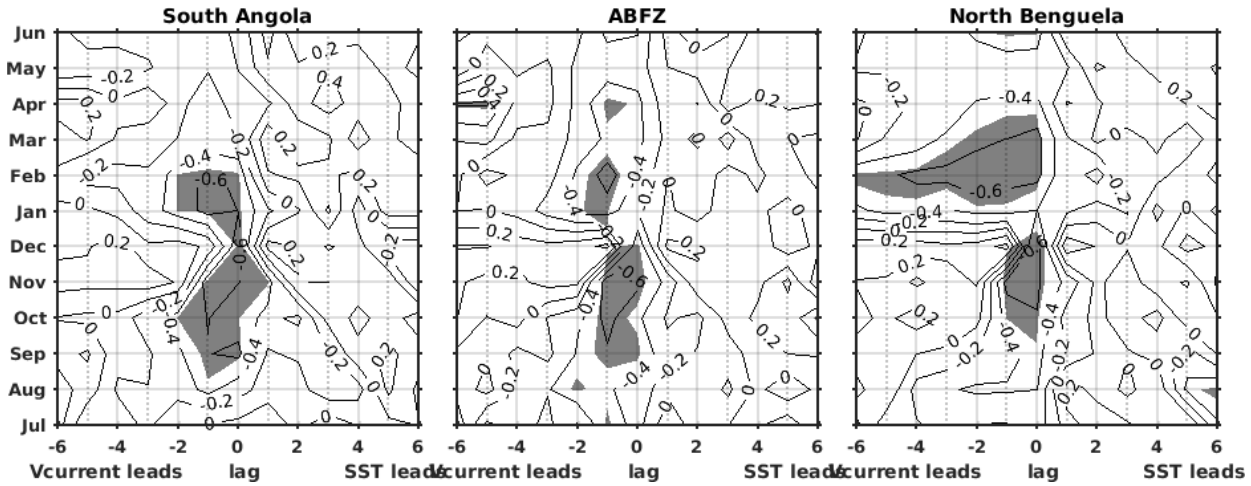

Figure 4.11: Lag correlation between normalized anomalies of the meridional current averaged vertically from the surface to 250 m and normalized SST anomalies in (left) South Angola (10^{o}S-15^{o}S), (middle) ABF (15^{o}S-19^{o}S), and (right) North Benguela (20^{o}S-24^{o}S). Noted the meridional currents and SST are averaged from the coast to 1^{o} offshore. Shaded areas represent statistically significant correlations at the 95% confidence level (Student t-test).

A close look at the seasonal horizontal currents focusing on the meridional component as the dominant component of the horizontal current along the coast helps to confirm that the warming trends of SST that occur in summer (November to January) are explained by the intensification of poleward flow which brings warm water southward. The reduction of equatorward flow in the Namibian sector and close to the Angolan coast, in November-December, brings relatively cooler water equatorward into the Angola-Namibia coastal domain.

There is a 1-month lag between the poleward trend observed in the currents and the warming trend in the SST. This 1-month lag between the poleward trend in the current and the warming trend in SST could be a direct consequence of the lag correlation between current and SST at the interannual scale. To confirm that, monthly lag correlations between SST anomaly and meridional current anomaly are plotted in three different domains: Southern Angola, ABF and Northern Benguela (**Figure 4.11**). Note that the correlations are plotted without removing the long-term trend. However, the same results are obtained when the long-term trend is removed (not shown). In South Angola, the lag correlation is statistically significant at the 5% confidence level in austral spring and summer. Negative statistically significant correlations up to -0.7 are observed when the meridional current anomalies lead the SST anomalies by 1-month. In December, the correlation peaks to – 0.8 at lag 0. In the ABF, except in December and May, negative statistically significant lag correlations of up to -0.7 are found when the meridional current anomalies lead SST anomalies with 1-month lag. In Northern Namibia, the lag correlation is statistically significant from November to April. However, from January to March there are significant lag correlations with up to 5-month lags when the meridional current anomalies lead the SST anomalies.

4.6 ROLE OF VERTICAL CURRENTS

4.6.1 Climatology of vertical current

To investigate the impact of vertical current on the SST trend, I analyse the currents in the upper mixed layer. As I am interested in what occurs along the coast, I study the vertical profile (0 to 100 m) of the vertical current along the Angola Namibia coast. **Figure 4.12** represents the seasonal climatology of the vertical profile of the vertical current along the Angola-Namibia coast. The current is averaged from the coast to 1^{o} offshore and positive values indicate upward currents. In **Figure 4.12**, a clear upward current is observed throughout the year off Namibia and in the ABF. The model thus realistically simulates the quasi-permanent upwelling along the Namibian coast (Mackas et al., 2006; Chavez and Messié, 2009; Tim et al., 2015). The upward current indicative of the coastal upwelling is weak in late austral summer (January to March) along the Namibian coast when the subtropical atmospheric high-pressure system has moved to

its southernmost position, and the upward current is very strong in late austral winter and spring (August to October) when upwelling is strongest. Along the Angolan coast, the vertical upward current is more seasonal. It is strong in late austral autumn-early winter (April to July) and early summer (November-December) while for the rest of the year downward currents are observed. The upward current in the Angolan sector is weak compared to what occurs in the Namibian sector. The upward and downward current seasons along the Angola coast coincide with the seasons of the passage of upwelling and downwelling coastal trapped waves, respectively (Tchipalanga et al., 2018).

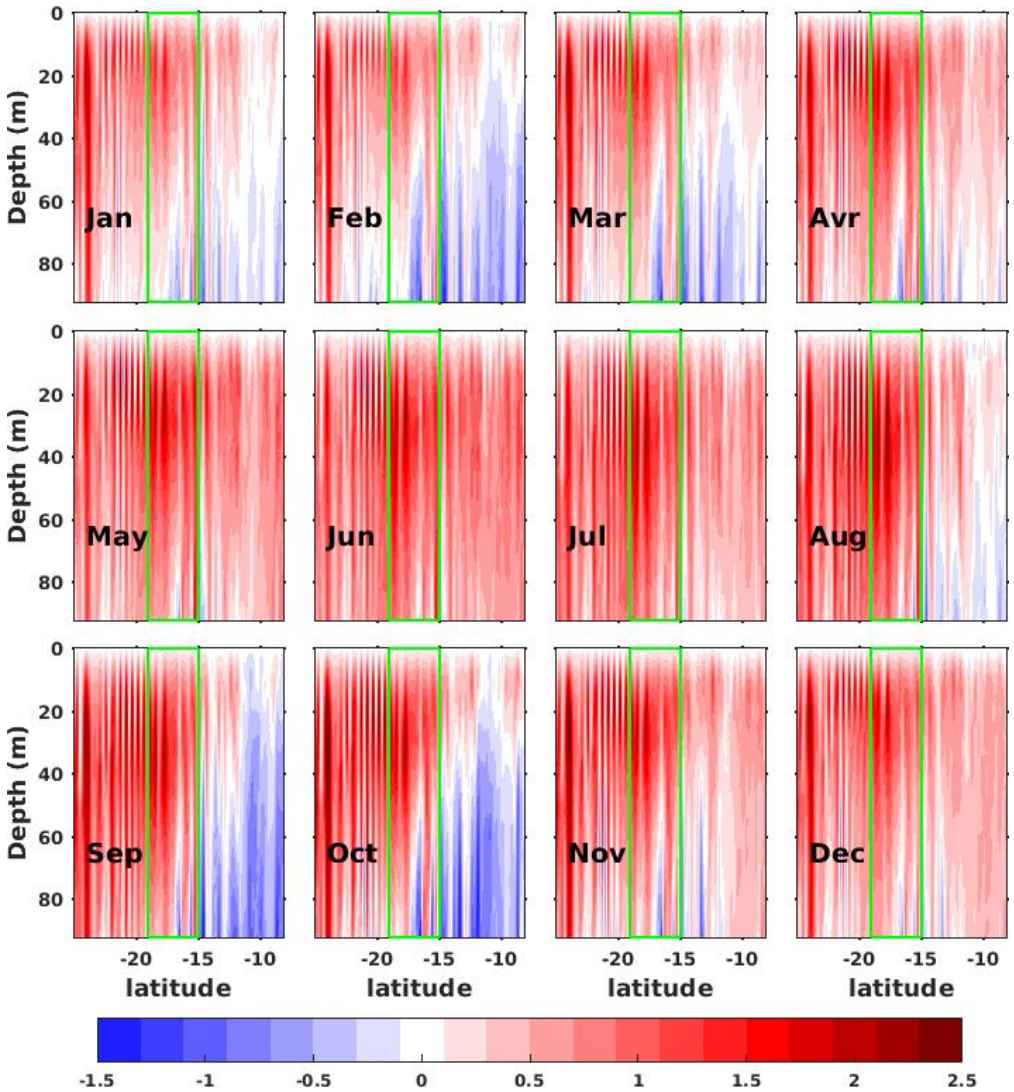

Figure 4.12: Seasonal climatology of NEMO vertical profile of vertical current (10^{-5} m.s^{-1}) along the Angola-Namibia coast. The green box highlights the ABF. Positive values indicate upward vertical current.

4.6.2 Seasonal trends of vertical currents

Figure 4.13 represents the annual cycle of decadal trends in vertical current velocities. Along the Namibian coast, the upward vertical current during austral summer months (November to January) has become weaker over the 1986-2015 period at a rate of -1.5×10^{-6} m.s^{-1} per decade, whilst during the same period the upward current from May to September and February to March has been intensifying at a rate of 2 ×10^{-6} m.s^{-1} per decade. Along the Angolan coast and ABF, two seasons of negative trends and two seasons of positive trends are found. Negative trends are observed from late austral spring to early summer (October-December) and autumn (March-May). Except for October, this negative trend tends to decrease the upward current observed in that period, which in turn is expected to decrease the temperature in the mixed layer. However, the contribution of the vertical advection of heat to the seasonal SST trend (not shown) indicates that despite a negative trend, the upward current does not have a significant impact on the SST trend. A positive trend in the upward current occurs in austral winter (June-September) and late summer (January-February). However, in February a negative trend is also observed north of 10^{o}S. The positive trend in winter illustrates the intensification of the upward current.

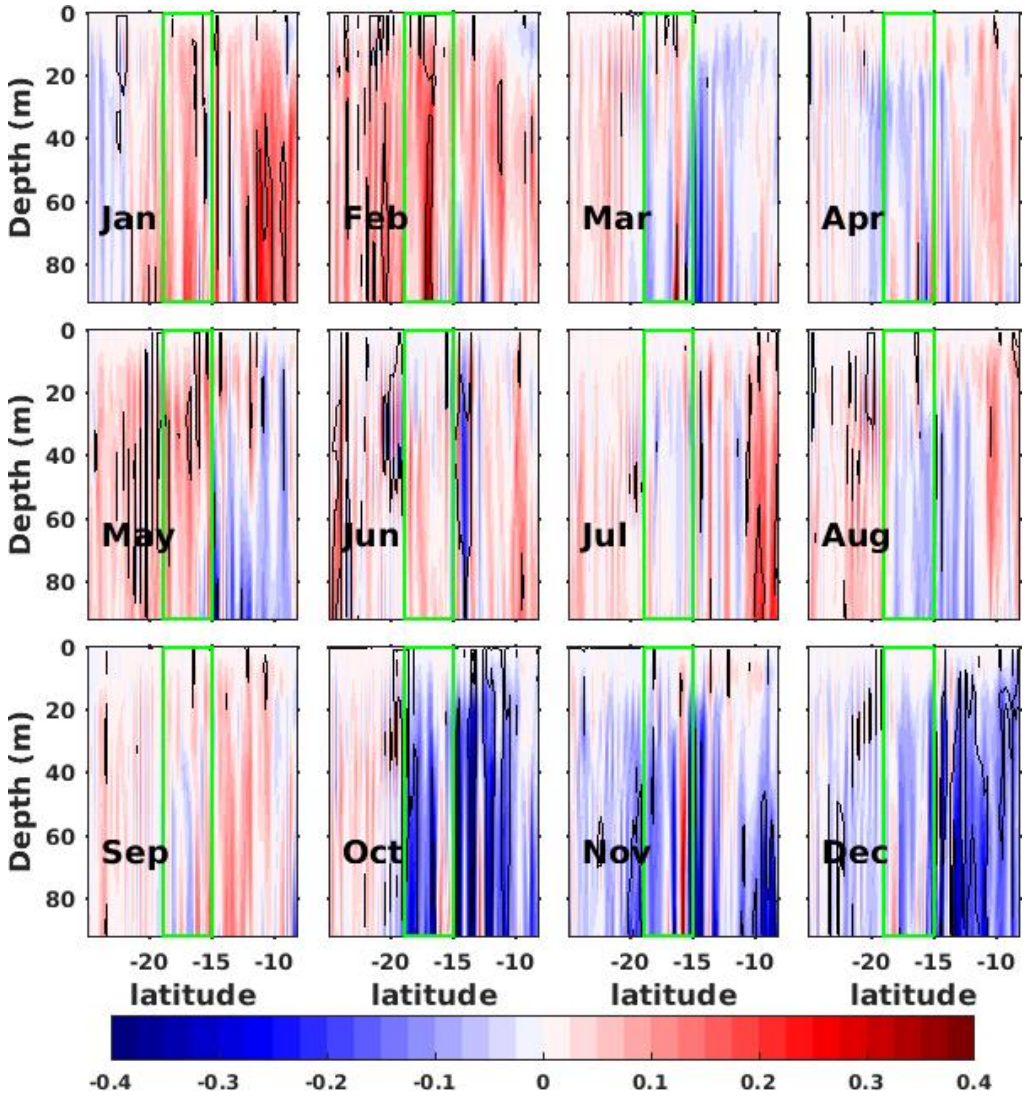

Figure 4.13: Seasonal trend of NEMO vertical profile of vertical current (10^{-5}.m.s^{-1} per decade) along the Angola-Namibia coast. The green box indicates the latitudinal extent of the ABF and the black dashed contour lines denote statistically significant values at the 95% confidence level using Student's test based on linear regression.

4.7 ROLE OF THE ANGOLAN DOME IN SUMMER WARMING OF THE ANGOLA-NAMIBIA COAST

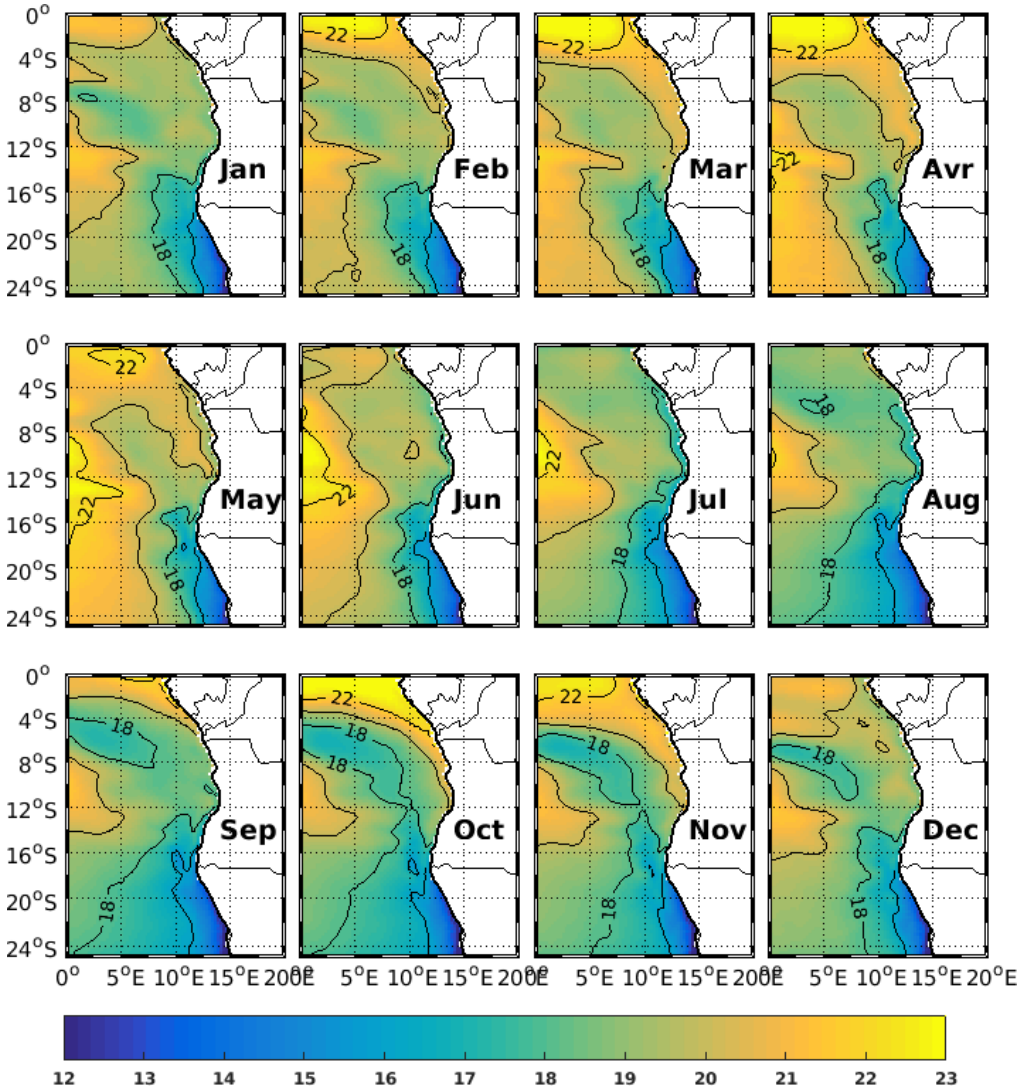

Figure 4.14: Monthly climatology of NEMO subsurface temperature averaged between 30 m and 60 m depth over the 1986-2015 period in the Angola-Namibia region. Contour lines highlight the isotherms with intervals of 1°C starting from 16°C.

An analysis of the vertical profile of modelled SST along the Angola-Namibia coast (not shown) indicates that the warming trend in SST in summer along the Angolan and Namibian coasts is also observed in the subsurface temperatures, especially along the Angolan coast. while the warming trend in the Angolan sector during the rest of the year is only observed in the mixed layer. To understand the mechanisms accountable for the subsurface warming in austral

summer, I analyze the model subsurface temperatures. **Figure 4.14** shows the monthly climatology of NEMO sub-surface temperature averaged between 30 and 60 m depth over the 1986-2015 period, in the Angola-Namibia ocean. Relatively cold water of ~12-14^{o}C is observed along the Namibian coast through the year while warmer water up to 21^{o}C is observed along the Angolan coast with a maximum value observed in March-April. In the open ocean, relatively warm water is observed. However, between 2^{o}S and 12^{o}S, the presence of a strong dome-like cold region centred around 6^{o}S and 2^{o}E is observed from September to December that becomes less pronounced from January before disappearing in early austral winter (May to July). This is one component of the Angola Dome as described in Doi et al. (2007). Indeed, Doi et al. (2007) suggested that the Angola Dome is composed of two domes; one found around 6^{o}S and 2^{o}E and the second one found around 16.5^{o}S and 10.5^{o}E. This Angola Dome is associated with the cyclonic curve of the South Equatorial Under Current which feeds the Angola Current (Peterson and Stramma, 1991; Wacongne and Piton, 1992). Moreover, the presence of the Angola Dome from September to April coincides with the poleward Angola Current (**Figure 4.9**). The cooler is the subsurface temperature in the Angola Dome region (**Figure 4.14**), the stronger is the poleward Angola Current (**Figure 4.9**). The Angola Dome by definition is a region with relatively cold water. The Dome is intensified when the region is coming cooler which happen with an intensifying cyclonic current which re-enforces the Angola current. The trend analysis of subsurface temperature in the domain (**Figure 4.15)** demonstrates a statistically significant cooling trend in the region of the Angola Dome that could lead to a strengthening of the Angola Dome current from September to December. The intensification of the South Equatorial Under Current strengthens the clockwise circulation around the dome which in turn intensifies the Angola Current. North of the Dome there is a positive trend in subsurface water propagating into the Angolan and Namibian coasts from October to January.

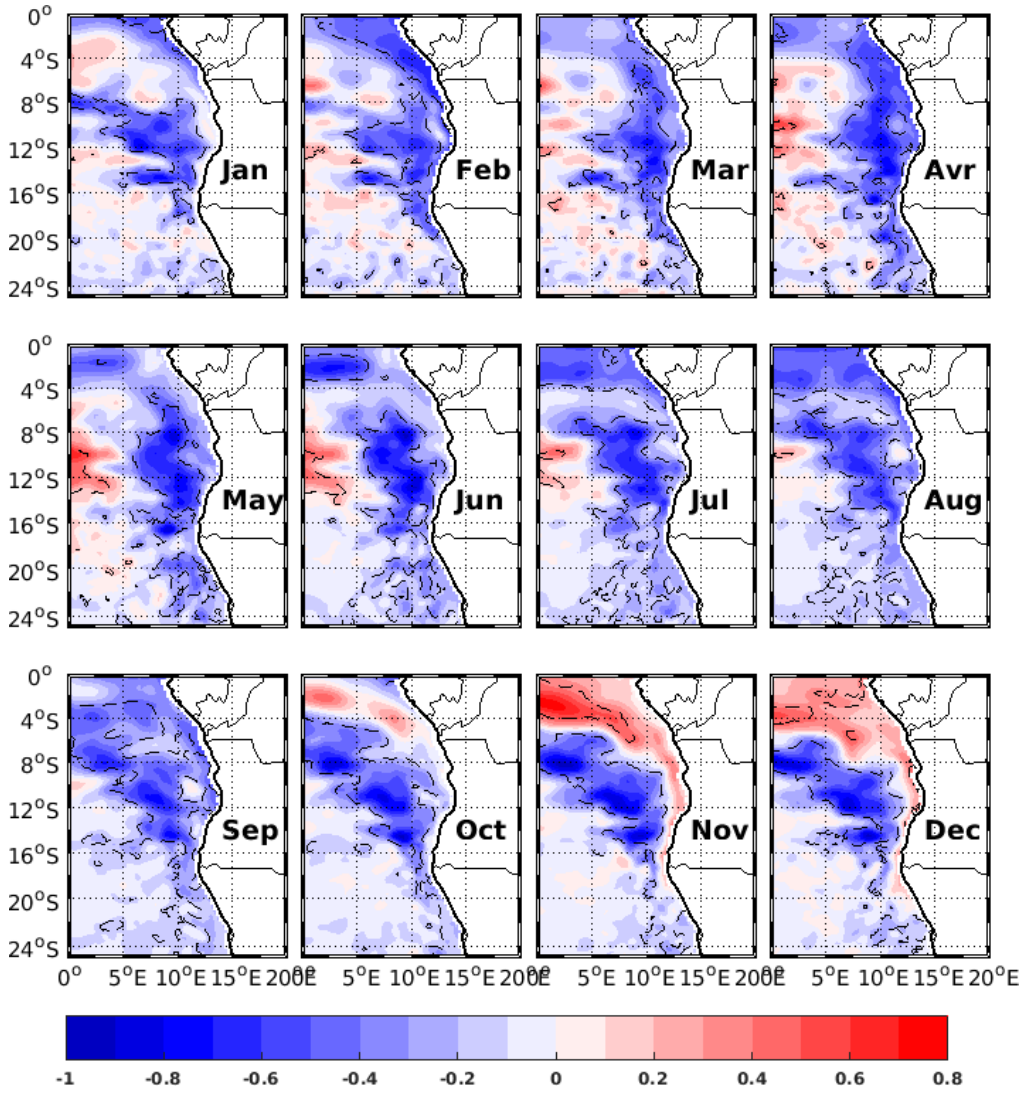

Figure 4.15: Seasonal trends of NEMO subsurface temperature (°C per decade) averaged between 30 m and 60 m depth over the 1986-2015 period in the Angolan-Namibian region.

4.8 DISCUSSION AND CONCLUSION

In this study, the long-term changes in the ABF are explored and the main processes driving these changes and their seasonal dependence are investigated. To do so, the OGCM NEMO3.6 model is used in its Tropical Atlantic configuration. In the first step, the model SST trend is compared with the observational data over the 1986-2015 period on both annual and seasonal scales. On the annual scale, the model represents the warming trend in the Angolan sector well. In Northern Benguela, the model shows a cooling trend while the observations show a warming

trend. However, the cooling and warming patterns in NEMO outputs are consistent with the trend in GODAS, ORA-S4, and CRCM reported in Figure 2 in the study of Vizy et al. (2018). At the seasonal scale, the NEMO SST trend is consistent with the observed SST trend, despite the cooling trend in the model being stronger than the cooling trend in the observations. This is most likely due to an unrealistically higher than the normal trend in wind forcing that can increase the upwelling and the equatorward horizontal motion of cold water to the north a bit too strongly.

In the second step, the long-term mean of different terms contributing to the temperature rates changes (see Eq 2.1) is evaluated. This analysis contributes to determine the potential important heat budget terms involved in the long-term changes of mixed layer temperature or SST. These important heat budget terms are the net surface heating term, the horizontal advection of heat and the vertical advection of heat. From the climatological point of view, the net surface heating term warms the coastal ocean of Angola and Northern Namibia while the horizontal advection and vertical advection cool the coastal ocean of Angola and Northern Namibia. The lateral diffusion, vertical diffusion and vertical entrainment contribution are extremely weak and do not account much for the upper-ocean heat budget climatology. Trends analysis of different parameters involved in the most important heat budget term contributing to the long-term SST change is investigated to understand the mechanism behind the warming or cooling trends in Angolan and Northern Namibia coast at seasonal scale. The results suggest that the change along the Angolan and Namibian coasts is explained by more than one mechanism acting at different time scales. For instance, in austral autumn the warming trend observed along the Angolan coast is associated with a positive trend in Q_{net} (**Figure 4.7**) and the weakening of vertical flow (**Figure 4.13**) associated with the upwelling of cooler water to the surface. However, the weakening of vertical flow is not statistically significant. In early austral summer (November-January), the warming trend observed along the Angolan and Namibian coasts is primarily associated with the intensification of the poleward flow (**Figure 4.11**) which brings more warm water from the tropics into the area of interest. It is also attributed to the weakening of the vertical flow (**Figure 4.13**), while locally, Q_{net} trend tends to cool the ocean. This result contradicts the result of Vizy and Cook (2016) who suggested that the austral SST warming trend along the Angolan and Namibian coast is associated with an increase in the net downward

atmospheric heat flux. Notably, the strong poleward flow in austral summer along the Angolan and Namibian coast is consistent with the result of Koseki et al. (2019) who attributed the poleward flow to the process of frontogenesis of the ABF. Furthermore, the poleward intensification of the Angola current is attributed to the presence and intensification of the Angola Dome. Moreover, the poleward intensification of the Angola Current suggests an intensification and poleward shift of the front as observed by Vizy et al. (2018). I also notice that the warming trend observed along the Angolan and Namibian coast reaches 100m depth in early austral summer, while it is noticeable only in the upper mixed layer for the rest of the year. At the annual scale, the subsurface water shows a cooling trend, as the cooling trend is observed for most of the year along the Angolan and Namibian coasts. This result also contradicts the conclusions of Vizy et al. (2018), who suggested that the warming of the subsurface ocean under the upper mixed layer was due partly to an increase of the Agulhas leakage (Beal et al., 2011; Lübbecke et al., 2015). The cooling trend that occurred south of the ABF, especially in austral winter and early spring, is primarily associated with the horizontal currents that advect cooler water from the east and south and intensify the upwelling of cold water from the subsurface to the surface. These changes are consistent with the changes in the wind field (not shown), which enhances the offshore ocean currents off the Namibian coast.

In the next chapter, I will study the decadal variability in the Benguela Upwelling system to see whether the 10-14 year and 23–28-year periodicity found in chapter 3 and also mentioned in the literature for South Atlantic variability for the 10-14 year are found using longer duration datasets. I also explore potential links between decadal variability and well-known climate modes or global oceanic region.

CHAPTER 5

5 DECADAL VARIABILITY IN THE BENGUELA UPWELLING SYSTEM

5.1 INTRODUCTION

Many studies of the Benguela Upwelling System have focused on SST variability at the interannual time scale and less on the Sea Surface Temperature (SST) trend. At the interannual time scale, the Benguela upwelling system is influenced in its northern part by Benguela Niño and Benguela Niña events (Shannon et al., 1986; Bachèlery et al., 2016; Rouault et al., 2018; Bachèlery et al., 2020; Illig et al., 2020). Benguela Niño is the main mode of interannual variability of SST in the Northern Benguela (Florenchie et al., 2003; Rouault et al., 2018) and is mostly due to change in the wind speed along the equator in the western tropical Atlantic, leading to the propagation of Kelvin waves along the equator and subsequent coastal trapped waves along the coast (Bachèlery et al., 2020). The Southern Benguela (SB) is influenced by the El Niño Southern Oscillation (ENSO) (Agenbag, 1996; Rouault et al., 2010; Dufois and Rouault, 2012; Blamey et al., 2015). ENSO impacts the Southern Benguela by modulating upwelling-favorable coastal winds through the latitudinal variation of South Atlantic Subtropical High (SASH) (Dufois and Rouault, 2012). Moreover, there is a dominant mode of coupled variability in the South Atlantic Ocean, the South Atlantic subtropical dipole (SASD) that connects sea level pressure (SLP) and sea surface temperature (SST) (Venegas et al., 1997; Sterl and Hazeleger, 2003; Haarsma et al., 2005; Morioka et al., 2011) which are both influenced by ENSO (Rodrigues et al., 2015).

At the long-term scale, most studies focused on trend analysis and found a poleward shift in the SASH which intensifies the upwelling in the Southern Benguela (García-Reyes et al., 2015; Rykaczewski et al., 2015; Lamont et al., 2018) leading to the cooling reported by (Hutchings et al., 2009; Rouault et al., 2010). In **Chapter 3** of this thesis, I show that the trend reported by others may be the effect of decadal variability (**Figure 3.18** and **3.19**).

To our knowledge, there are few works on the decadal variability of SST in the Benguela Upwelling System. Hutchings et al. (2009) are the first to mention decadal variability but it was not demonstrated or calculated. They assumed decadal variability using SST anomalies from a combination of ICOADS and satellite data in the Northern Benguela over the period 1950-2007. García-Reyes et al. (2018), by comparing modes of upwelling-favorable wind mode in the Benguela and California upwelling Systems, found that the summer upwelling mode in both Benguela and California Upwelling Systems has a similar quasi-decadal period of variability around 8-9 years. Furthermore, several studies have identified decadal variability in the whole Southern Atlantic. For instance, Venegas et al. (1997) in their study, found interdecadal fluctuations of an approximatively 14-16 years period in the South Atlantic Basin. Moreover, decadal variability has been identified in southern African rainfall (Dyer and Tyson, 1977; Jury, 2015; Dieppois et al., 2016). Examining southern African rainfall, Dieppois et al. (2016) have demonstrated the existence of two signals of decadal variability: quasi-decadal (8-13 years) and interdecadal (15-28 years) linked to the Pacific climate modes of variability such as ENSO, the Pacific Decadal Oscillation (PDO), and the Interdecadal Pacific Oscillation (IPO). The signals were detected in the Western Cape winter rainfall, the South Benguela upwelling region and summer rainfall for the rest of Southern Africa. Similar decadal periodicity of variability is found in **Chapter 3** of this thesis (**Figure 3.19 and 3.22**). However, the study period, 35 years, is very short to analyse decadal variability. Satellite remote sensing of SST only started in 1982 and before the satellite era, the observations are sparse in the region, especially off Angola and Namibia. To have longer and homogeneous time-series better suited to the study of decadal and multidecadal variability of the Benguela Upwelling System, I will be using the outputs of a 110 year (1900-2010) model simulation of the global ocean ice components of the Norwegian Earth System Model (NorESM) (Bentsen et al., 2013), forced by the 20th Century re-analysis. The chapter is structured as follows: Firstly, I will evaluate the skills of the NorESM model by comparing the model SST with the observation-derived SST. Secondly, the model will be used to analyse the dominant time scales of SST fluctuations using a time-space approach based on wavelet analysis. Finally, composite analysis is performed on global SST to examine teleconnections and underlying

mechanisms between climate modes and SST in the Benguela Upwelling System through each time scale of SST.

5.2 VALIDATION OF THE MODEL NORESM

5.2.1 Comparison of long-term mean SST in NorESM with Observations

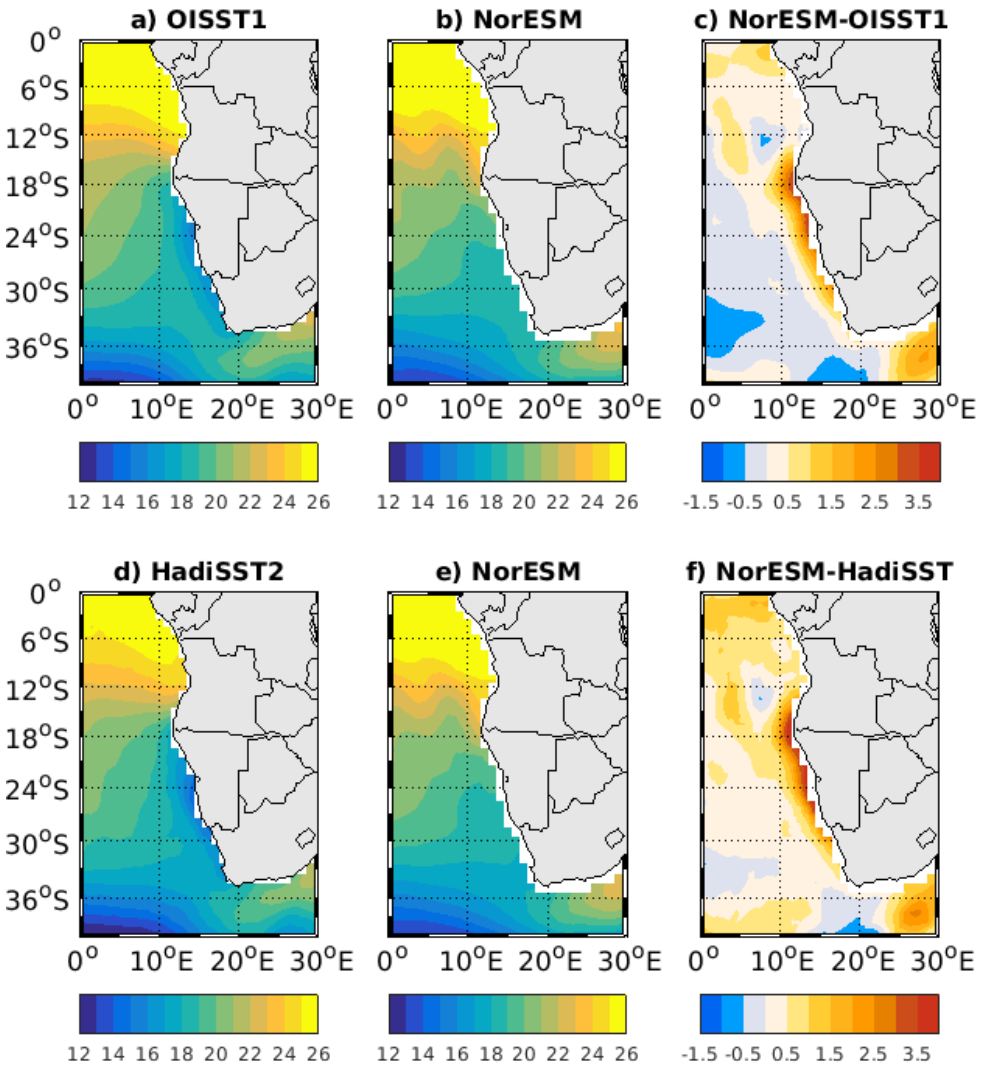

Figure 5.1: Long-term SST mean over 1982-2009 for **a)** OISST1, **b)** NorESM and **c)** the difference between NorESM and OISST1. Long-term mean over 1910-2009 for **d)** 10-ensemble mean HadISST2 **e)** NorESM and **f)** the difference between NorESM SST and 10-ensembles mean HadISST2.

In this section, I compare the SST climatology of NorESM during the satellite era with OISST1 over the period 1982-2009 (**Figure 5.1** upper panels) and then the SST climatology of NorESM is compared to HadISST2 during the entire period (1910-2009) (**Figure 5.1** lower panels). The NorESM model represents the large-scale features of the South-East Atlantic basin well, with relatively cool SST (SST <18°C) in the Benguela Upwelling system and the poleward sector. Relatively warm SST (SST> 23°C) are realistically represented off Angola and in the equatorial Atlantic basin. However, the NorESM model does not represent the upwelling close to the Namibian coast and in the ABF well. Warm bias of up to 3.5°C is observed in the model along the Namibian coast and ABF when compared with OISST1 and up to 4°C when compare with HadISST2. The warmest bias is observed in the ABF. In Southern Benguela, the difference between NorESM and OISST1 or HadISST2 remains lower than 1°C. A comparison between NorESM and NEMO over the period 1958 -2009 also shows a warm bias up to 3°C in NorESM (not shown).

5.2.2 Comparison of SST timeseries in NorESM and 10-ensemble HadISST2 in different domains

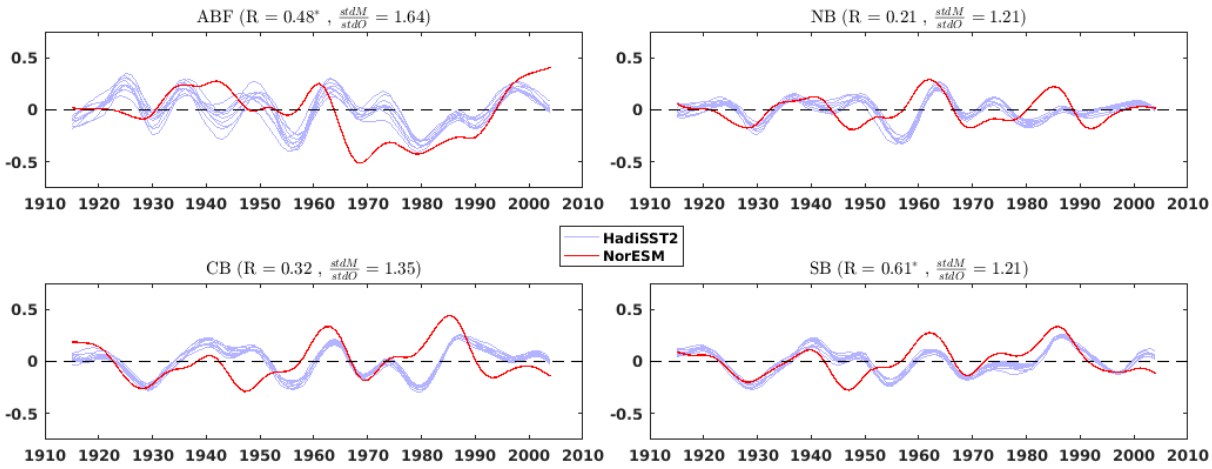

Figure 5.2: 11-Year running mean of SST anomalies from 1910 to 2009 in the four coastal domains (from top to bottom and from left to right) ABF, NB, CB, and SB. The red line is NorESM and the blue lines are the 10-ensemble members of HadISST2.

In this section, I compare the NorESM SST timeseries at lower frequencies. **Figure 5.2** shows the 11-year running mean of SST anomalies from 1910 to 2009 in the same four domains (ABF, NB, CB, and SB) as in **Chapter 3** and **Figure 3.8**, but with 4° longitudinal averages for NorESM (red line) and HadISST2 (blue line). The NorESM SST and HadISST2 show a marked low-frequency modulation in all the coastal regions. However, the low-frequency variability has more energy in the NorESM compared to HadISST2. In addition, NorESM seems to display a more consistent low-frequency SST timeseries across NB, CB, and SB, whereas the HadISST.2 data are able to capture more regional features. The ratio of the NorESM and HadiSST2 standard deviation (SD) is between 1.20 and 1.7 in all domains (**Figure 5.2**). In some domains, the period of lowest and highest values of SST are not always the same in the NorESM compared to HadISST2. In the ABF for instance (**Figure 5.2** top left panel), the NorESM model displays positive SST anomalies of up to 0.4°C in 1931-1950, 1956-1964, and 1994-2004, while negative SST anomalies of up to -0.5°C occurred in 1964-1993. The HadISST2, contrariwise, displays positive SST anomalies in 1920-1928, 1932-1940,1945-1952, 1961-1970, and 1993-2004 while negative SST anomalies occurred in 1953-1961 and 1975-1992. The correlation between NorESM SST and HadISST2 at lower frequencies, in the ABF domain, is 0.48. It is statistically significant at the 95% level (based on a Student t-test). I also note that the ABF SST in the NorESM model seems to undergo multi-decadal rather than decadal variability.

In NB and CB, the model displays positive SST anomalies up to 0.4°C in 1957-1967 and 1980-1990, while negative SST anomalies up to -0.35°C occurred in 1922-1933, 1943-1957, 1966-1975, and 1989-1988. HadISST2, on the other hand, displays positive SST anomalies with less magnitude than the model (< 0.3°C) in 1935-1954 and 1960-1967 while negative SST anomalies up to -0.35°C are observed in 1925-1935, 1953-1962, and 1975-1983. I note that positive SST anomalies occur in 1985-1998 in CB using HadISST2, while a very weak SST anomaly is observed in NB. The correlations between the NorESM model SST and HadISST2 are 0.21 and 0.32, respectively in NB and CB. These correlations are not statistically significant at the 95% level. In SB (**Figure 5.2** bottom right panel), the NorESM model SST low frequency variability matches the HadISST2 variability very well. There are positive SST anomalies in both the NorESM and 10-ensemble HadISST2 of up to 0.45°C in 1915-1923, 1959-1965, and 1982-1993, while negative SST

anomalies up to 0.4°C occur in 1925-1935, 1966-1975, and 1992-2000. However, there are discrepancies between NorESM and HadISST2 during the period 1945-1953 when NorESM has negative SST anomalies and HadISST2 has positive SST anomalies. In SB, the correlation between NorESM SST and ensemble mean HadISST2 at lower frequencies is 0.61 and is statistically significant at the 95% level. In conclusion, the NorESM and HadISST2 present evidence of decadal variability across the whole region; however, the low-frequency variability in the NorESM model is not in good agreement with the low frequency of HadISST2 in most of the domains except in SB where the NorESM and 10-ensembles HadISST2 show the same pattern of low-frequency variability. This may be because the NorESM does not represent the quasi-permanent upwelling in NB and CB well, or because there were not enough observations to build the HadISST2 dataset, especially before the 1960s. Thus, I will focus my analysis on the Southern Benguela region in the following sections.

5.3 Dominant decadal time scales of variability in the Southern Benguela (SB) Domain

5.3.1 Wavelet analysis

In this section, time scale analysis of decadal variability is carried out using the wavelet transforms as described in Section 2.2.5 of this thesis. Note that here I use the annual mean SST instead of the monthly mean. **Figure 5.3a** and **5.3b** display the local wavelet power spectrum of SST of HadiSST2 and NorESM respectively. **Figure 5.3c** displays the global wavelet spectrum of SB SST of NorESM and HadISST2 ensemble mean (red and blue line respectively). According to the global wavelet spectrum (**Figure 5.3c**), the NorESM and HadISST2 ensemble mean SST display three dominant time scales of variability significantly above the red noise background spectra: an interannual time scale of 2-8 years, a quasi-decadal time scale of 9-14 years, and an interdecadal time scale of 19-26 years. These time scales of variability have already been mentioned in **Chapter 3**. I note that the HadiSST2 ensemble mean shows a slight shift of one to two year in the period of quasi-decadal scale.

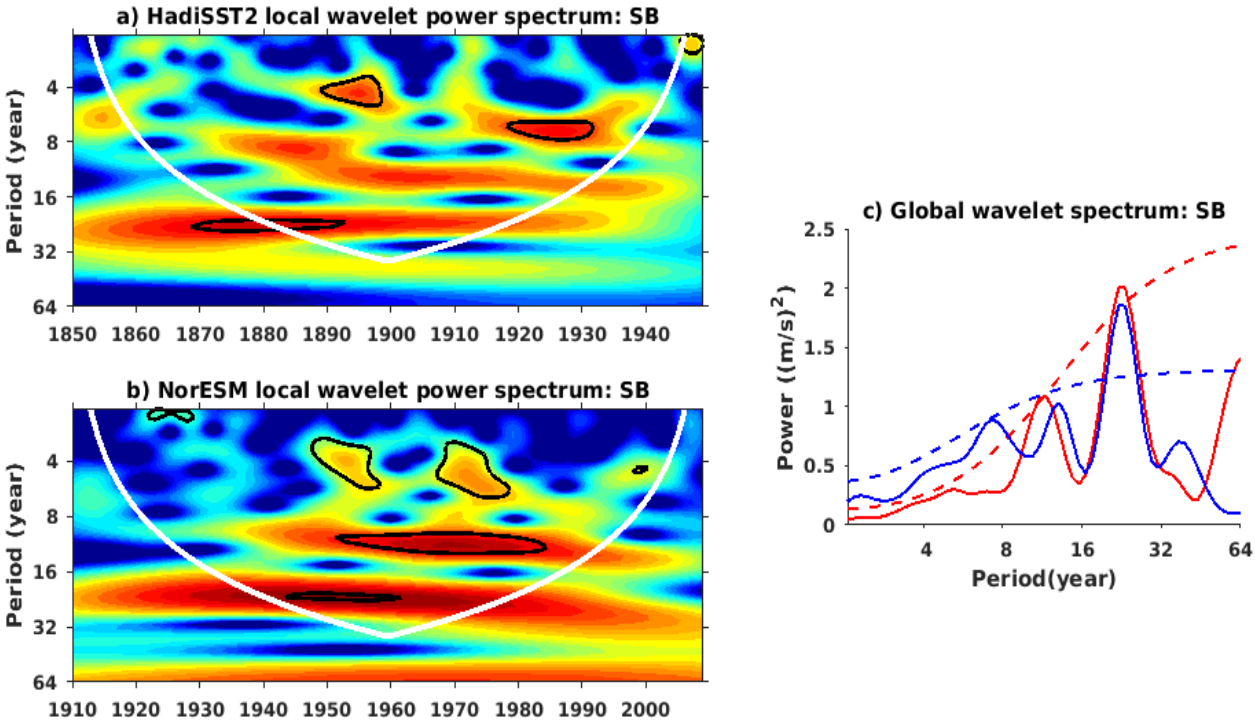

Figure 5.3: Time scale pattern of variability of the annual SB SST. (a, b) Continuous wavelet power spectrum of HadiSST2 and NorESM. The white bold line (cone of influence) delineates the area under which the coherence can be underestimated due to edge effects and zero padding. The black line contours designate the area of statistically significant coherence at 95 % level confidence limits based on 1000 Monte Carlo simulations of the red noise background spectrum. (c) Global wavelet spectrum of NorESM SB SST (red line) and the ensemble mean HadISST2 SB SST (blue line). The dashed red and blue lines indicate the spectrum of the red noise timeseries that possessed the same variance and autoregression coefficients as the annual SB SST of NorESM and ensemble mean HadISST2 respectively.

For the quasi-decadal time scale of 9-14 years, the SB SST displays significantly increased variance since the 1950s, while the SB SST displays a significant increase in variance since the 1940s at the interdecadal time scales of 19-26 years in both HadiSST2 ensemble mean (**Figure 5.3a**) and NorESM (**Figure 5.3b**). The 9-14 year time scale is close to the 14-16 year scale, a known scale of variability in the South Atlantic High-pressure System and basin-wide SST (Venegas et al., 1997). The time scale of 19-26 years has not been documented before in the Benguela upwelling,

but it has been detected in the southern African rainfall in the austral winter and summer rainfall of Western region and the rest of southern Africa, respectively (Dieppois et al., 2016) and shown to be linked to the variability in the Pacific Ocean. In the rest of the chapter, as I am interested in decadal variability, I will focus my analysis on the quasi-decadal time scale of 9-14 years and the inter-decadal time scale of 19-26 years.

5.3.2 Reconstruction of timeseries of the dominant timescale with lower frequencies

In this section, the decadal dominant scales of variability are reconstructed using the band-pass Butterworth filter. Note that the annual SB SST timeseries were detrended to reduce trend effects. **Figure 5.4** displays the reconstructed time series of the two dominant decadal scales as SB SST anomalies for the NorESM model and the HadISST2. Despite the small shift between the NorESM model and the HadISST2, they show the same variability at the quasi-decadal and Interdecadal scales. The quasi-decadal scale reconstructed SB SST timeseries (**Figure 5.4a**) displays fluctuations of about 0.11°C with a maximum amplitude of about 0.47°C and 0.42°C in NorESM model and HadISST2 respectively; larger fluctuations are observed from 1940-1990. The decadal time scale reconstructed SB SST timeseries has the same order of magnitude as the quasi-decadal time scale reconstructed SST timeseries. However, the maximum amplitude of fluctuation of the reconstructed interdecadal SB SST timeseries is about 0.1°C less than the one depicted in the quasi-decadal scale reconstructed timeseries. The maximum fluctuations are observed before 1970 in the reconstructed interdecadal SST timeseries.

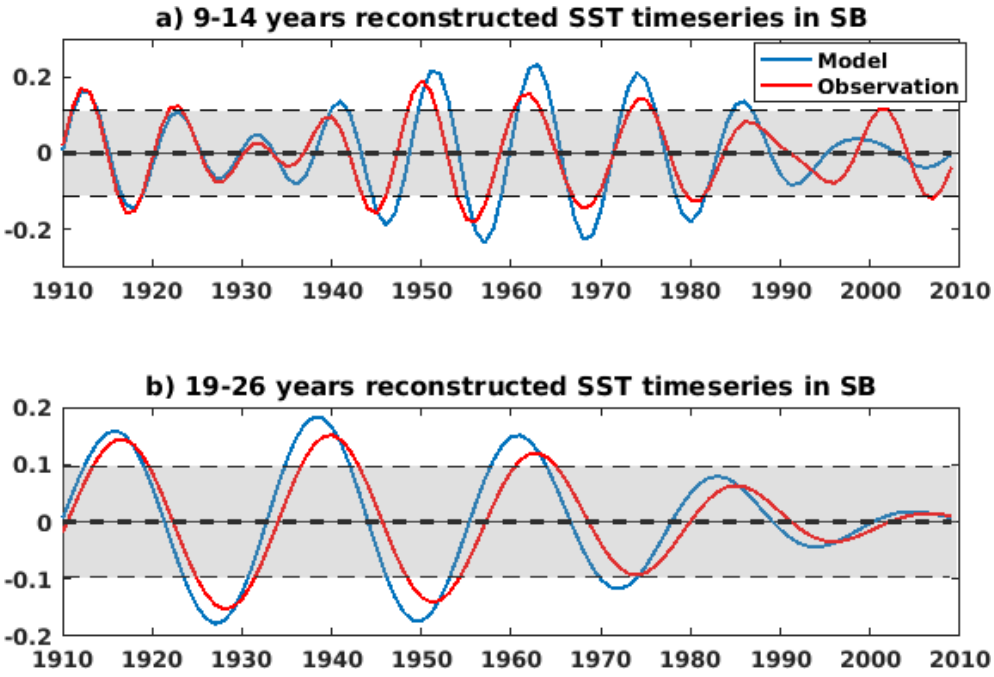

Figure 5.4: Reconstruction of decadal dominant time scale modulating SB SST of NorESM (blue line) and HadiSST2 (red line) using the band-pass Butterworth filter. a) The 9-14 years and b) the 19-26 years reconstructed SB SST timeseries. The grey shaded band delineate the area above which the SB SST anomalies greater than ±1 Standard Deviation have been selected to perform composite analysis.

5.4 CORRELATION BETWEEN SB SST AND LOCAL NET SURFACE HEAT FLUX AND MERIDIONAL WIND

In this section, I investigate the correlation between SST and meridional wind component and between SST and net surface heat fluxes (Qnet) from the model in the Southern Benguela domain using wavelet coherence (**chapter 2.2.5.2**).

5.4.1 Correlation between SB SST and local meridional wind

Figure 5.5 represents the wavelet coherence between SB SST and SB meridional wind. The Figure shows that the variability of SB SST and SB meridional wind are correlated at interannual time scale (2-8 years), quasi-decadal and interdecadal scale. At the quasi-decadal timescale (9-14 years), SB SST and SB meridional wind show coherency values larger than 0.7; they are in opposite phase during the period 1970-1995. The anti-correlation between SST and wind speed is due to the fact that at that scale, higher than normal wind speed would decrease

the surface temperature by upwelling bringing colder subsurface water to the surface. This process is stronger at the coast where the wind stress curl is higher due to the effect of the coastline in reducing wind stress abruptly. The anti-correlation between SB SST and SB meridional wind at the 9-14 year time scale is also observed during the period 1910-1920. However, this latter period is outside of the cone of influence (white bold line), where the ability to interpret the result is limited by the edge effects. In addition, the comparison between SB SST and SB meridional wind reconstructed timeseries at the quasi-decadal time scale (19-26 years) (**Figure 5.5b**) shows a good opposite phase correlation between these two timeseries especially over the period 1910-1920 and 1960-1985. As the quasi-decadal scale of variability, the SB SST and SB meridional wind show a higher anti-phase coherency (greater than 0.7) since 1930s at the interdecadal scale of variability. This result is also confirmed in **Figure 5.5c** where the comparison between the reconstructed SB SST and SB meridional wind timeseries at the interdecadal time scale shows a negative correlation. Overall, the wavelet coherence illustrates the phase opposition between SB SST and SB wind at all the significant time scales, highlighting once again the wind impact on SST in the Benguela region.

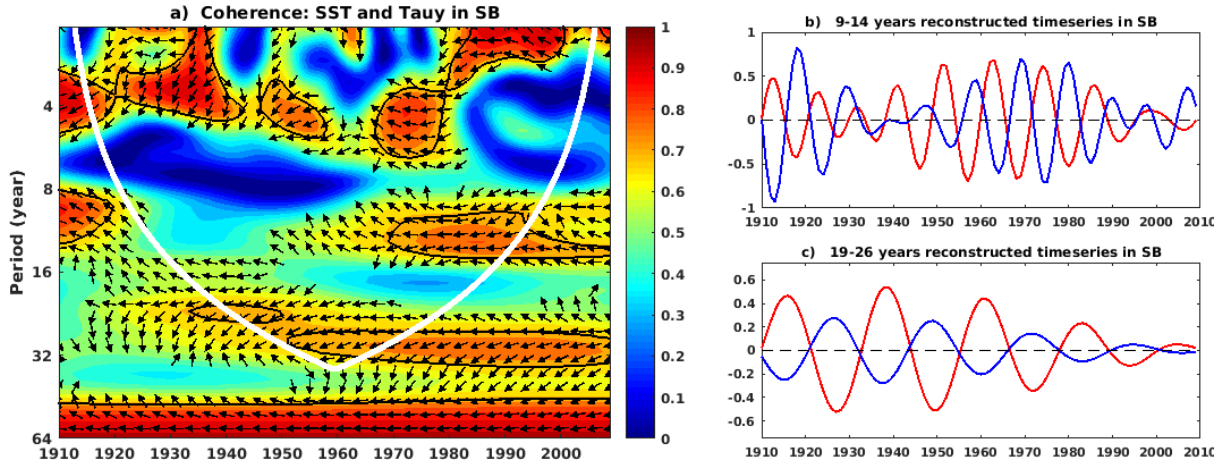

Figure 5.5: Wavelet-based SB SST- SB meridional wind component coherence analysis. a) squared cross wavelet coherence. The Y-axis represent the time scales and the colour scale represents the magnitude of the squared cross-wavelet coherence. The white bold line (cone of influence) delineates the area under which the coherence can be underestimated due to edge effects and zero padding. The black line contours designate the area of statistically significant coherence at 95 % level confidences limits based on 1000 Monte Carlo simulations of the red noise background

spectrum sharing the same autoregressive coefficients as the original data. The arrows represent the relative phase between SB SST and SB meridional wind: a rightward-pointing arrow indicates in-phase coherence between the two signals, a leftward pointing arrow indicate anti-phase coherence. b) Comparison of the quasi-decadal time scale (9-14 years) reconstructed signal between the SB SST (red line) and SB meridional wind (blue line) signal. c) Comparison of the interdecadal time scale (19-26 years) reconstructed signal between the SB SST and SB meridional wind signal.

5.4.2 Correlation between SB SST and SB Qnet

Net surface heat flux (Qnet) influences the South Atlantic Ocean. The temperatures change in the subtropical Atlantic have been found to be driven by Qnet (Colberg and Reason, 2006; Vizy and Cook, 2016). **Figure 5.6** represents the wavelet coherence between SB SST and SB surface heat net fluxes (Qnet). As in the previous section, the Figure shows a good coherence between SB SST and SB Qnet at the SB SST dominant time scales: interannual time scale (2-8 years), quasi-decadal (9-14 years), and interdecadal time scale (19-26 years). At the quasi-decadal time scale, **Figure 5.6a** shows an anti-phase coherence at the beginning of the period 1910-1925 and in-phase coherence at the end of the period from 1965-2010. Between these two periods, a significant transient leading phase of 90 degrees (SB Qnet leading) is observed between SB SST and SB Qnet. The coherence is statistically significant and greater than 0.8 from 1910 to 1960. These results are confirmed in **Figure 5.6b** where the quasi-decadal reconstructed SB SST and SB Qnet show a negative correlation from 1910 to 2025, positive lag correlation of ∼2-3 years from 1930 to 1906 and positive correlation from 1970 to 2009. To be explicit, Qnet warms the ocean at those latitudes, especially in upwelling regions, where latent and sensible heat flux are quite low and solar radiation quite high. However, in upwelling regions, the wind is the main driver of SST variability. So strong wind decreases the SST while Qnet increases the SST. When upwelling favorable stop or decrease substantially the ocean warms up quickly, especially in summer. In Angola where there is no strong wind-driven upwelling. Qnet has a more important role in warming the ocean but advection and deepening of the thermocline and mixed layer during Benguela Nino or at certain times of the year have also a key role (Rouault et al., 2012). At the

interdecadal scale, higher anti-phase coherences greater than 0.8 are found throughout the study period (**Figure 5.6a** and **c**).

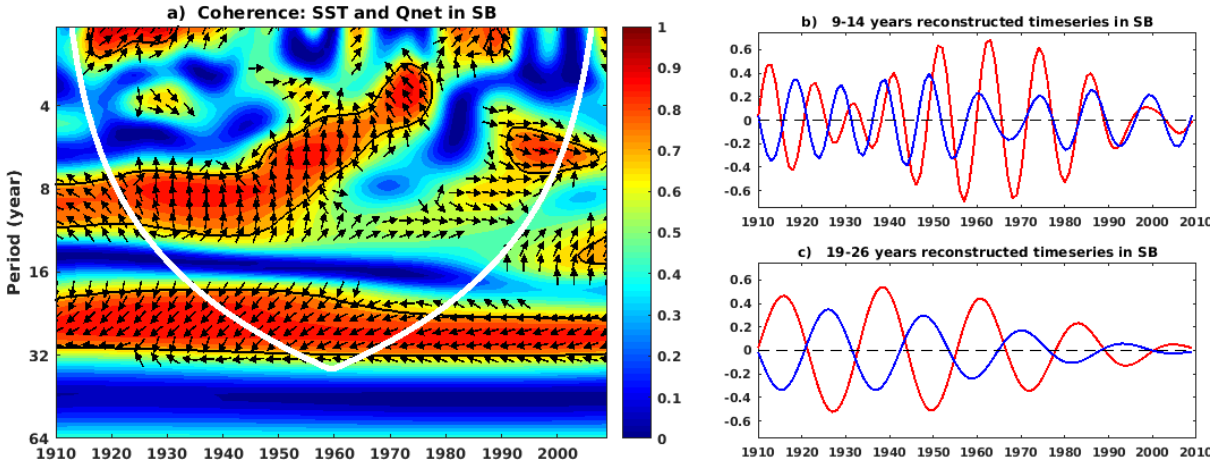

Figure 5.6: Same as Figure 5.5 but SB Qnet (blue line) instead of SB meridional wind.

5.5 SB SST MULTISCALE RELATIONSHIP WITH GLOBAL SSTS

5.5.1 SB SST and global SST anomalies

The fluctuations of the SST in the Benguela upwelling are influenced by the coupled modes of atmosphere-ocean interactions. Benguela SST is influenced by ENSO (Rouault et al., 2010; Dufois and Rouault, 2012) and by Benguela Niño/Niña (Bachèlery et al., 2020; Illig et al., 2020). In this section, I investigate the teleconnection of SB SST with the global SST for the low-frequency modulation at time scales of 9-14 years and 19-26 years. The analysis is based on composite anomalies of warm and cold periods (see **chapter 2.2.6**).

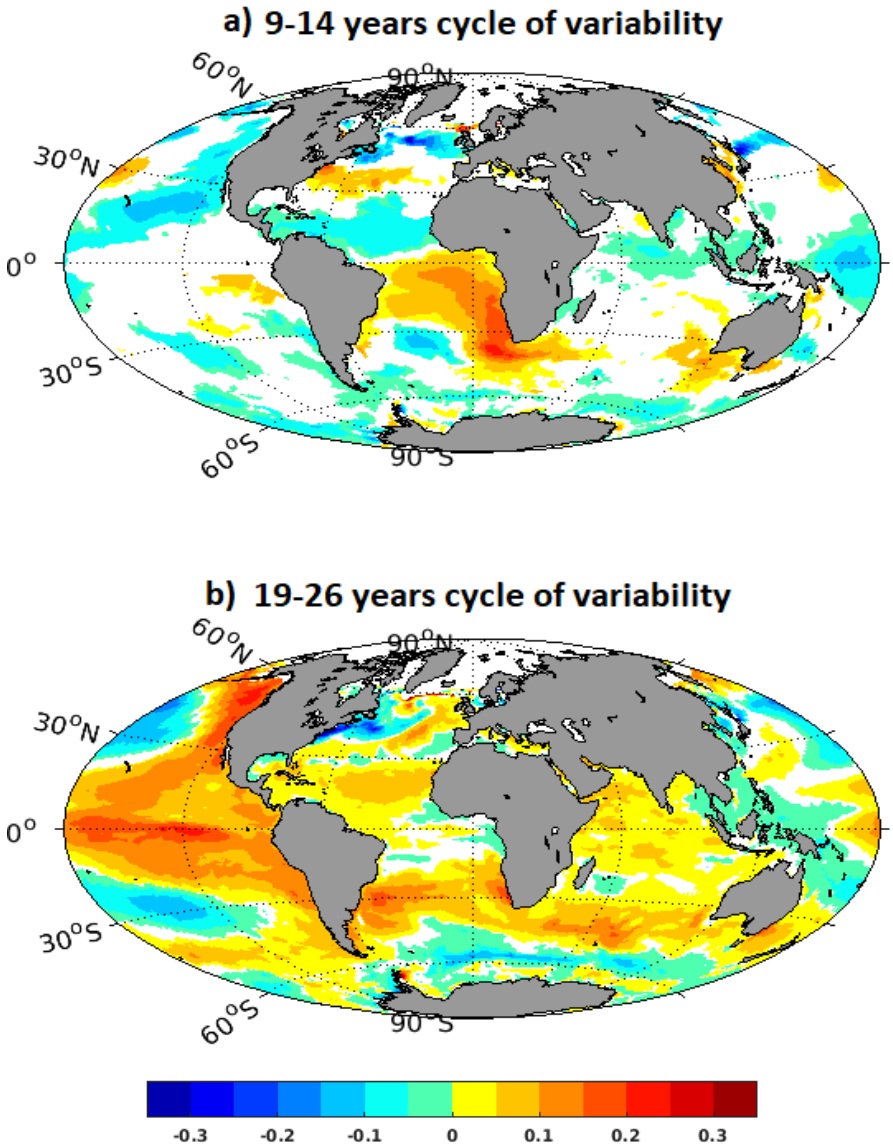

Figure 5.7: Composite SST anomalies associated with periods of high amplitude for the quasi-decadal (9-14 year) and interdecadal (19-26 year) cycles of SST variability in SB. (a) extreme warm period of 9-14 year cycle of SST variability (9-14 year reconstructed SB SST timeseries (**Figure 5.4**) ≥ 1 Standard Deviation (SD)). (b) same as (a) but for the interdecadal SST variability (19-26 year reconstructed SB SST timeseries (**Figure 5.4**) ≥ 1 SD). Shaded areas represent the 95% statistically significant values estimated based on a bootstrap method using 10,000 samples.

Figure 5.7 shows the global SST composite anomalies based on warm periods of the reconstructed SB SST timeseries at quasi-decadal (**Figure 5.7 a**) and interdecadal (**Figure 5.7 b**) time scales.

At the quasi-decadal scale, except the southwestern part of the domain where cold anomalies are detected, positive SB SST anomalies are related to warm anomalies in most parts of the South Atlantic including the Agulhas region. This pattern is consistent with the dominant mode in the South Atlantic which consists of a northeast-southwest-oriented dipole suggested by Sterl and Hazeleger (2003). Positive SB SST anomalies are also related to cold anomalies in the tropical North Atlantic (0-30°N) and SST in the California Upwelling System. The latter relationship between SB SST and the California upwelling system is consistent with the results of García-Reyes et al. (2018). The positive anomalies in the south tropical Atlantic and negative anomalies in the north tropical Atlantic are consistent with the Atlantic Meridional Mode (AMM) (Xie and Carton, 2004). There is no significant relation between SB SST and Equatorial Pacific or Indian Ocean SST at the quasi-decadal scale of variability. Contrary to the quasi-decadal scale of variability, at the interdecadal scale, positive SB SST anomalies are related to warm SST anomalies (> 0.2°C) in the Tropical Pacific flanked by a horseshoe pattern of opposite sign. The positive SB SST anomalies are also related to warm SST anomalies in the subtropical Atlantic and the Indian Ocean. I note the pattern of warm anomalies is significant over the whole Indian Ocean and no statistically significant relationship is observed between SB SST and equatorial Atlantic. However, the warm anomalies in the Indian Ocean and north subtropical Atlantic are smaller than the warm SST anomalies observed in Tropical Pacific. The SB warm period global signal is reminiscent of El Niño and the SB cold period of La Niña. The impact of ENSO at the interannual scale on the Benguela Upwelling System and southern African climate is well known and the mechanisms are well identified (Dufois and Rouault, 2012; Blamey et al., 2015; Dieppois et al., 2016). The mechanisms are a modification of the global Hadley and Walker circulation and the low-pressure system of the temperate region of the Southern Hemisphere. This study indicates that the mechanisms may also work at the decadal scale as proposed and demonstrated by Dieppois et al. (2016) for southern African rainfall.

5.5.2 Correlation between Southern Benguela SST with climate modes

To further identify the connection between climate modes and the SB SST, the correlations of the SST with El Niño-Southern Oscillation (ENSO), Interdecadal Pacific Oscillation (IPO), Pacific Decadal Oscillation (PDO) and Atlantic Meridional Oscillation (AMO) are also calculated for the quasi-decadal and Interdecadal scale and recapitulated in **Table 5.1**. These modes are the main modes of decadal to multidecadal variability. The indices are calculated using model data. The indices from other sources of data are also used (**see chapter 2.1.2**). First, the climate mode index is subjected to wavelet analysis to see if the index presents at least one similar decadal dominant scale found in SST before being correlated with SST. Wavelet coherence is then used and the correlation between the reconstructed timeseries of the climate mode index and SB SST at each decadal dominant scale is calculated.

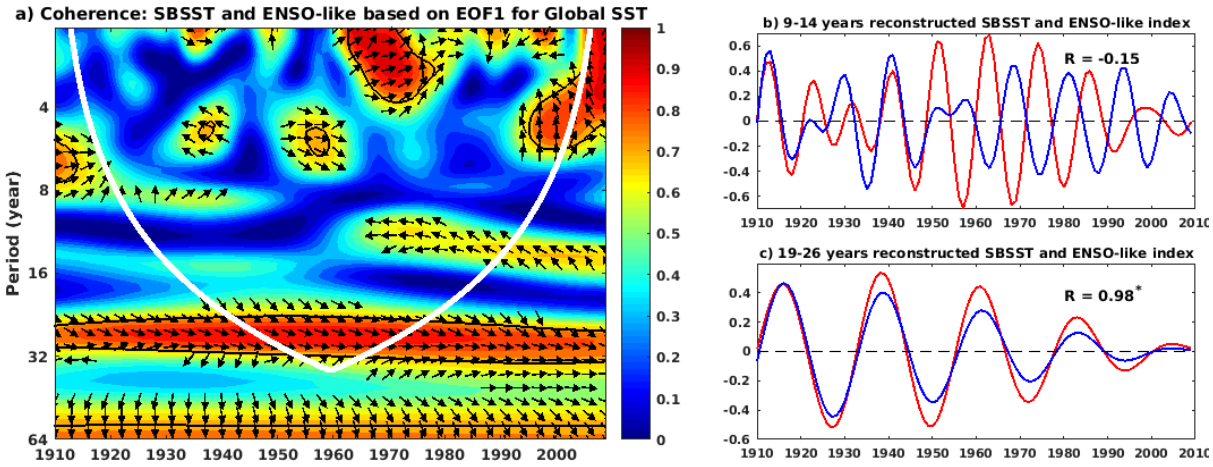

Figure 5.8: Same as Figure 5.5 but with SB SST (red line) and ENSO-like index (blue line) estimated as the Principal Component (PC1) of the first EOF of the annual mean SST anomalies for global SST. The SST anomalies are estimated by subtracting the global annual mean SST anomalies from SST anomalies in each point for the global ocean (see Zhang et al., 1996).

Figure 5.8 presents the wavelet coherence between SST anomalies and an ENSO-like index estimated from the principal component of the first Empirical Orthogonal Function EOF1 of annual SST anomalies over the global ocean calculated as in Zhang et al. (1997). The figure shows higher coherence between the SB SST and the ENSO-like index at the interannual time scale (2-8 years), and the interdecadal time scale. No statistically significant coherency is

observed at the quasi-decadal time scale (R2< 0.3). The correlation between the quasi-decadal reconstructed SST and ENSO-like index timeseries is about R = -0.15 (**Figure 5.8b** and **Table 5.1**). Contrary to the quasi-decadal scale, at the interdecadal time scale, I observe higher statistically significant phase coherence larger than 0.8 since the 1920s. The maximum value of squared coherence is found after 1960. A comparison between the interdecadal reconstructed SB SST and IPO index timeseries (**Figure 5.8c**) shows a high statistically significant correlation of about R = 0.98.

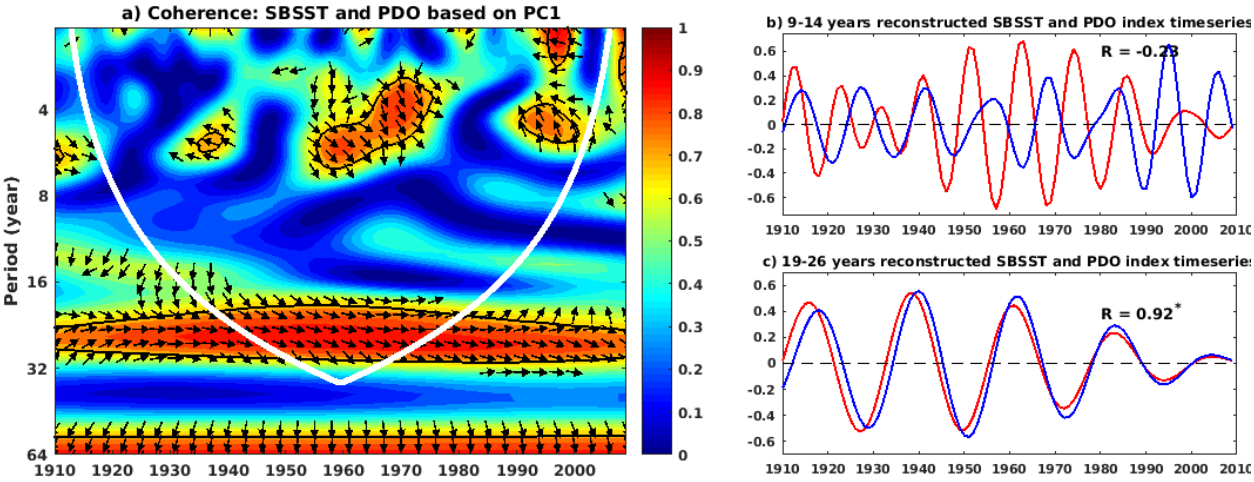

Figure 5.9: Same as Figure 5.5 but with SB SST (red line) and PDO index (blue line) defined as the Principal Component (PC1) of the first EOF of the annual mean SST anomalies in the North Pacific Ocean, poleward of 20°N. The SST anomalies are estimated by subtracting the global annual mean SST anomalies from SST anomalies in each point of the North Pacific Ocean.

The wavelet coherence between PDO index based on the leading Pattern (EOF) of SST anomalies in the North Pacific basin (typically poleward of 20°N) as described by Mantua et al. (1997) and SB SST **(Figure 5.9**) shows the same pattern of coherence as ENSO-like with SB SST. The PDO and SB SST show a higher statistically significant phase coherence since 1920s at interdecadal time scale. The maximum value squared coherence is observed around 1950s. The correlation between the reconstructed PDO index and SB SST at the interdecadal scale is about R = 0.92 (**Figure 5.9c** and **table 5.1**). No statistically significant coherency is observed at the quasi-

decadal time scale (R^2< 0.4) (**Figure 5.9a**). The correlation between the reconstructed PDO index and SB SST is about R = -0.23 (**Figure 5.9c**) at the quasi-decadal time scale.

The wavelet coherence between IPO index based on TPI computed on annual mean SST without any filtering (Henley et al., 2015) and SB SST is shown in **Figure 5.10**. The Figure shows the same pattern of coherency as in **Figures 5.8** and **5.9**. Higher coherence between the SB SST and the IPO index is observed at the interannual time scale (2-8 years) and the interdecadal time scale. No statistically significant coherency is observed at the quasi-decadal time scale. The correlation between the reconstructed IPO and SB SST is about R = -0.05 at quasi decadal scale (**Figure 5.10b** and **table 5.1**) while it is about R = 0.95 at interdecadal scale (**Figure 5.10c** and **table 5.1**).

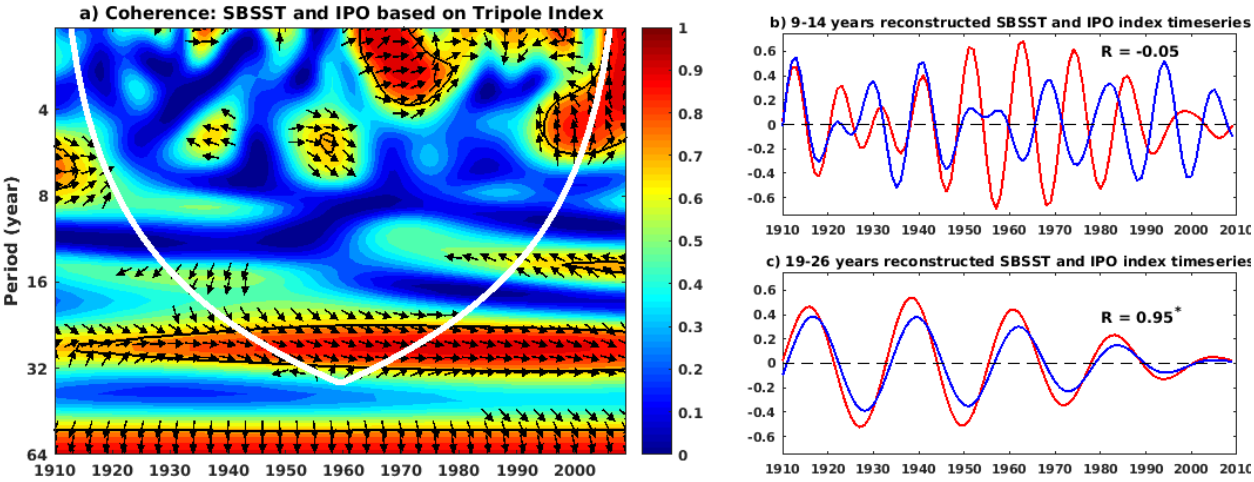

Figure 5.10: Same as Figure 5.5 but with SB SST (red line) and IPO index (blue line) based on Tripole Index.

In contrast, the wavelet coherence between AMO and SB SST (**Figure 5.11**) does not show any statistical coherence at the two dominant decadal scales of variability of SB SST. However higher anti-phase coherence is observed between 45- and 60-years cycles which is a dominant time scale of variability of the AMO (Kerr, 2000). The correlations between the reconstructed AMO and SB SST at quasi-decadal and interdecadal time scales are not statistically significant and are about R = -0.20 and R = -0.21, respectively (**Table 5.1**).

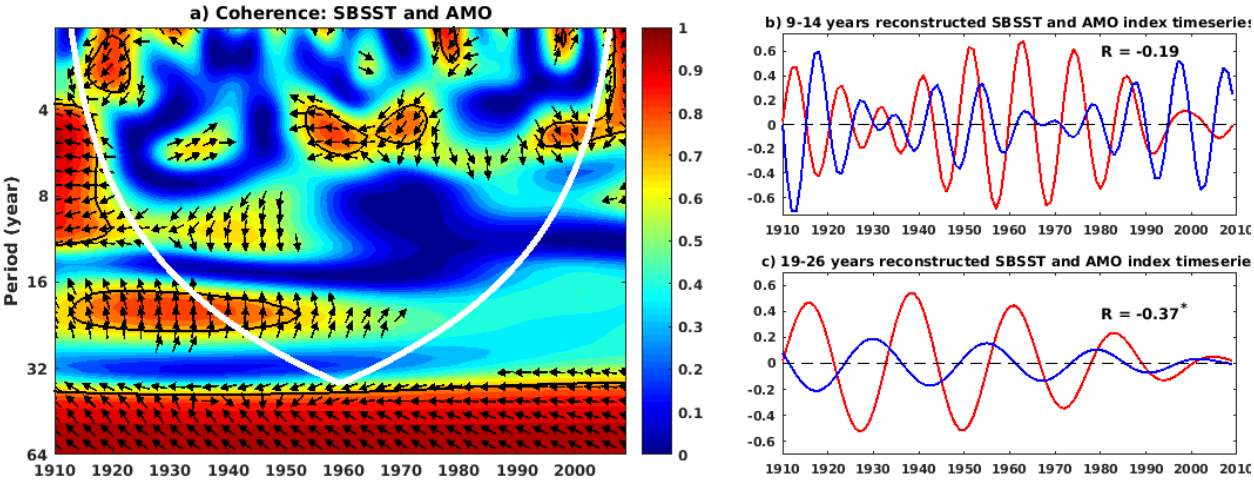

Figure 5.11: Same as Figure 5.5 but with SB SST (red line) and AMO index (blue line) estimated as the average anomalies SST in north Atlantic (0-80°N).

Table 5.1: Correlation coefficients at quasi-decadal and interdecadal scales of the SB SST from the NorESM model with ENSO-like, IPO, PDO and AMO from different sources of data. Significant correlations are highlighted by *. The table also shows if the climate mode has a significant peak of energy at the decadal/interdecadal period.

		Decadal scale (9-14 years)		Interdecadal scale (19-26) years	
Climate mode	Source data of climate mode index	signal	Correlation with model SB SST	signal	Correlation with model SB SST
ENSO-like	NorESM based on leading PC of monthly SST anomalies over the global ocean (ENSO-like)	yes	-0.15	no	0.98*
IPO	NorESM (based on tripole index)	yes	-0.05	no	0.95*
	ERSST5 unfiltered data (based on tripole index)	yes	-0.03	yes	0.99*
PDO	NorESM (based on leading PC of monthly SST)	yes	-0.23	yes	0.92*
	UKMO historical SST, and OISST (based on leading PC of monthly SST)	yes	-0.17	yes	0.91*
AMO	NorESM	No	-0.19	Yes but not significant	-0.37
	HadISST1	Yes but not significant	-0.20	Yes but not significant	-0.21

5.6 DISCUSSION AND CONCLUSION

In this chapter, the decadal fluctuations in the Benguela Upwelling System are investigated and their teleconnections with large scale climate modes through the decadal dominant time scales of variability are explored. NorESM represents the large-scale features of the South-East Atlantic basin well but does not represent the upwelling close to the Namibian coast and ABF well. Warm biases, up to 4°C, are observed along the Namibian coast and in the ABF. This area is known as an area with large SST biases in ocean models (Richter and Xie, 2008; Richter, 2015). The causes are diverse and have been attributed to the spurious weakening of the north-flowing Benguela Current as well as to the misrepresentation of wind data used to force the model (Small et al., 2015; Bonino et al., 2019). Excessive negative wind stress curl in the nearshore can modify the simulated south-flowing Angola Current which tends to be stronger than in the observations, bringing more warm tropical water to the ABF than normal (Small et al., 2015; Koseki et al., 2018). The SST biases in the NorESM model are also associated with remote forcing. For instance, misrepresentation of equatorial westerly wind in the model contributes strongly to incorrect thermocline depth representation and its influence on SST in Northern Benguela (Patricola et al., 2012; Goubanova et al., 2019). A comparison of the NorESM model and observations at low-frequency shows good agreement between NorESM and the HadISST2 SST fluctuations in the Southern Benguela. However, in the Northern Benguela, disagreement is observed between NorESM model and HadISST2. Weak agreement is also observed between HadISST2, HadISST1, and ERSST5 (not shown), indicating a critical problem even in observational data in the Northern Benguela domain. Lack of consensus between observations can be explained by poor spatial and temporal coverage of observational data in some regions prior to the satellite era (Deser et al., 2010), and to the different techniques used to fill the gaps of missing value. As there is no agreement between models and observations in the other regions, I focused my analyses on the Southern Benguela domain and found that there are three significant time scales of variability: interannual (2-8 years), quasi-decadal (9-14 years) and interdecadal (19-26 years). The teleconnections between SB SST and SST over the global ocean are different at both quasi-decadal and interdecadal time scales. At the interdecadal scale, the tropical and subtropical oceans, especially in the Pacific Ocean appear to be strongly linked

to SB SST fluctuations. The teleconnection of the tropical Pacific (ENSO-like) and PDO with SB SST are statistically significant. At the quasi-decadal time scale, there is no relationship between SB SST and the climate modes used in my study. However, the composite anomalies show a link between the SB SST and the whole South Atlantic Ocean. The pattern of SB SST composite anomalies in the South Atlantic is reminiscent of the South Atlantic Subtropical Dipole mode (SASD), the dominant mode of variability in the South Atlantic Basin (Venegas et al., 1997; Sterl and Hazeleger, 2003; Morioka et al., 2011). At the interannual time scale, ENSO variability affects SB SST by modulating the latitudinal variation of the South Atlantic Subtropical High (SASH) (Dufois and Rouault, 2012; Sun et al., 2017). This could be the same mechanism that occurs at the interdecadal scale. This study, for the first time, establishes a connection between PDO and ENSO-like oscillations of SB SST. The IPO and ENSO-like, whose physical independence remains controversial (Folland et al., 1999; Tourre et al., 2005), also drives the SB SST anomalies at the Interdecadal time scale.

6 CONCLUSIONS AND PERSPECTIVES

The Benguela Upwelling System, one of the four major coastal upwelling regions in the world ocean, is of great importance. It is a source of economic for the adjacent countries and plays an important role in the climate of the neighboring countries in the southern Africa. The focus of this thesis is to understand the long-term change and decadal variability in the Benguela Upwelling System and how this decadal variability is linked to climate modes. A first assessment was to investigate the long-term change in the Benguela upwelling since the 80's. To study long-term trends and because of the possibility of decadal or multidecadal variability in the Benguela Upwelling System, I used all the longest datasets possible of the satellite era 1982 to find out if trends were the same using different products. Most high-resolution datasets except for Pathfinder do not exceed 20 years. Only HadiSST1, OISST1, OISST0.25 and Pathfinder data were available from 1982 for that study. I also used five reanalysed climate atmospheric datasets to make a comparative analysis of the trends and to check if it was corresponding to the SST trends. This study, to my knowledge, is the first study in the region using several SST datasets and most reanalysis wind datasets to analyse and compare trends. Most studies in the region use either a model or one SST dataset and one reanalysis product to study long-term trends. The trend analysis is conducted at the annual and monthly scales. The use of different datasets revealed serious discrepancies in trends in SST, which is a concern. Notably, most discrepancies between SST datasets occur from 1982 to 1985. However, after a thorough examination, I report some agreement between datasets. The trend analyses of SST and surface winds show that the Angola-Benguela Upwelling has changed significantly over the period 1982-2017. The trends vary in space and most important depends on the season. Cooling trends up to -0.4°C per decade are observed in the southern part of the Benguela Upwelling System and are present throughout the austral summer and autumn while warming trends up to 0.8°C occur in austral summer in the northern part of the upwelling system. A comparison of wind trends with SST trends confirms the reason for the SST cooling trend in Southern Benguela with a colocalized intensification of equatorward (upwelling-favorable) coastal winds in the Southern Benguela due to the poleward

expansion and intensification of the South Atlantic Subtropical High atmospheric system. This result is consistent with the studies of Narayan et al. (2010), Rouault et al. (2010), Blamey et al. (2012), and Tim et al. (2015). However, the reanalysed data near the coast does not show much significant trend while offshore the wind seems to have increased for most products which could a reanalysis shortcoming. At first sight, in Northern Benguela, looking at the annual trend, the decrease in upwelling-favorable coastal winds seems to agree with the SST warming trend observed. However, the examination of the seasonal trends in the Northern Benguela and ABF reveals that the SST warming happens only in austral spring and summer while no trend in coastal winds is observed during these seasons. Moreover, the wind has increased offshore Northern Namibia. Vizy and Cook (2016) in their study, explain the SST warming in the Northern Benguela and ABF by a decrease in the surface winds due to the poleward shift of the SASH. The disagreement between the Vizy and Cook (2016) conclusion and my findings may arise from the fact that they did not examine the seasonal trends. The Ocean General Circulation Model (OGCM-NEMO) is thus used to further understand the main process of the warming in Southern Angola, ABF, and Northern Benguela in **Chapter 4**. Results of **chapter 4** suggest advection of warm water for the warming in the Northern Benguela.

To investigate the main processes leading to the warming trends in Southern Angola, ABF, and Northern Benguela, the OGCM-NEMO model SST trends are compared to the observed SST trends over the period 1986-2015 (**Chapter 4**). The model produces a strong cooling trend in the Northern Benguela compared with observations due to a positive trend in upwelling-favorable coastal winds used to force the ocean model. However, in Angola, the modelled warming trend is realistically simulated. Furthermore, the annual cycle of the SST trend is realistically simulated with the model despite a slight overestimation of the winter cooling trend in Northern Namibia. The realistic simulation of the annual cycle of SST trend allows me to use the model to study the mechanisms causing the summer warming and the winter cooling trend. The analysis of each of the model's heat budget components and their contributions to the overall SST trend suggests that the austral summer warming trend observed along the Angolan and Namibian coasts is primarily associated with an intensification of the poleward flow, bringing more warm water from the tropics to the coastal region and with a weakening of the vertical flow of cold upwelled water

to the surface. Locally, the net surface heat flux tends to create a negative trend. This result remains in contrast with the result of (Vizy et al., 2018) who suggest that the SST warming trend along the Angola-Namibia coast is associated with an increase in the net downward atmospheric heat fluxes. This contradictory result may arise from the fact that I used in my study the ocean general circulation model while Vizy et al. (2018) study used a coupled regional climate model which have notorious problems in the region such as the so-called warm bias. Caution is required when extracting trends from a coupled climate model, particularly in regions like the tropical Atlantic, where these models are known to produce a mean warm bias (Richter et al., 2012; Toniazzo and Woolnough, 2014; Exarchou et al., 2018; Koseki et al., 2018). Furthermore, in my study, the warming trend observed along the Angolan and Namibian coasts reaches 100m depth in early summer. Another finding of this study is that the poleward intensification of the Angola Current, at the origin of the warming, is attributed to the intensification of the cyclonic circulation around the Angola thermal Dome.

Finally, in **Chapter 5** the decadal variability in the Benguela upwelling system, identified in **Chapter 3**, and the teleconnections with climate modes are investigated using a long-term ocean model simulation of 110 years (1900 - 2010) of the global ocean-ice components of the Norwegian Earth System Model (NorESM). The model gives a good representation of the low-frequency variability of the Southern Benguela upwelling. Focusing on the Southern Benguela, where the observational and model variability agrees well, spectral analyses reveal the presence of three dominant scales of variability: the interannual (2-8 years), the quasi-decadal (9-14 years), and the Interdecadal (19-26 years) variability. A novel finding at the interdecadal time scale is that there is a teleconnection between the Southern Benguela SST and the global SST. In the Southern Benguela, low-frequency SST modulation is linked to the variability in the tropical Pacific (ENSO-like) and the Pacific Decadal Oscillation (PDO) in the Northern Pacific. At the quasi-decadal scale, there is no relationship between Southern Benguela SST and the tropical or North Pacific fluctuations. However, at this time scale, the composite anomalies show a link between the Southern Benguela SST and the whole South Atlantic Ocean SST. The pattern of the Southern Benguela SST composite anomalies in the South Atlantic resembles closely the South Atlantic Subtropical Dipole mode reported in the literature.

To understand the long-term change in the Benguela Upwelling System over the last 37 years, I used a comparative method based on monthly means. As upwelling is not observed every day and upwelling events can be triggered in less than a day, using monthly mean data, further work will involve a study of long-term trends based on upwelling events at the daily scale, their intensification, duration, and frequency to better quantify the real change in the Benguela Upwelling System. For instance, is the cooling trends due to more upwelling events, more intense events, or stronger wind at the seasonal scale. In addition, this thesis throws some light on how the Benguela Upwelling System has changed over the past 10 decades. In addition to the linear trend, this study shows that the Benguela Upwelling SST undergoes some decadal variability. The interdecadal time scale variability in Southern Benguela is influenced by the tropical and Northern Pacific variability, but how? Further studies will focus in more detail on the mechanisms of teleconnections between the tropical and northern Pacific and the Southern Benguela at the interdecadal scale, to understand which mechanism(s) links ENSO and PDO climate modes with the Southern Benguela Upwelling. The analysis could be extended to the Northern and Central Benguela by using better simulations. Furthermore, in my study, the Atlantic Multidecadal Oscillation (AMO) seems to have an impact on Southern Benguela SST. However, the period of study for the relationship between AMO and the Benguela decadal variability is limited to only 100 years which is too short to highlight the impact of the AMO which has a scale variability of 50 to 60 years. Longer model simulations, at least 200 years are therefore needed for further investigation of the AMO impact on the Benguela Upwelling System. It is also important to examine climate projection outputs to investigate the future decadal variability and if it is possible to distinguish the impact of climate change from the impact of natural decadal and multidecadal climate variability in the Benguela Upwelling System. The coupled model CMIP6 used by IPCC will need to be checked to see if they do reproduce the decadal and multidecadal variability presented here. This will be useful to contextualise what part of the last four decades changes in Benguela Upwelling can be attributed to anthropogenic climate change or natural climate variability? At last, the comparative method systematically used in that thesis with all datasets possible should be used in the other EBUS and should be done also at the seasonal scale and the impact of the change in the marine ecosystem should be ascertained.

Bibliography

Abrahams, A., R. W. Schlegel, and A. J. Smit (2021), Variation and change of upwelling dynamics detected in the world's eastern boundary upwelling systems.

Agenbag, J. (1996), Pacific ENSO events reflected in meteorological and oceanographic perturbations in the southern Benguela system, *South African journal of science*, *92*(5), 243-247.

Albert, A., V. Echevin, M. Lévy, and O. Aumont (2010), Impact of nearshore wind stress curl on coastal circulation and primary productivity in the Peru upwelling system, *Journal of Geophysical Research: Oceans*, *115*(C12).

Antonov, J., S. Levitus, T. P. Boyer, M. E. Conkright, T. D. O'Brien, and C. Stephens (1998), *World ocean atlas 1998: temperature of the Atlantic Ocean*, US Department of Commerce, National Oceanic and Atmospheric Administration National Environmental Satellite, Data, and Information Service.

Bachèlery, M.-L., S. Illig, and M. Rouault (2020), Interannual coastal trapped waves in the Angola-Benguela upwelling system and Benguela Niño and Niña events, *Journal of Marine Systems*, *203*, 103262.

Bachèlery, M. L., S. Illig, and I. Dadou (2016), Interannual variability in the South-East Atlantic Ocean, focusing on the Benguela Upwelling System: Remote versus local forcing, *Journal of Geophysical Research: Oceans*, *121*(1), 284-310.

Bakun, A. (1990), Global climate change and intensification of coastal ocean upwelling, *Science*, *247*(4939), 198-201.

Bakun, A., B. A. Black, S. J. Bograd, M. Garcia-Reyes, A. J. Miller, R. R. Rykaczewski, and W. J. Sydeman (2015), Anticipated effects of climate change on coastal upwelling ecosystems, *Current Climate Change Reports*, *1*(2), 85-93.

Bakun, A., D. B. Field, A. Redondo-Rodriguez, and S. J. Weeks (2010), Greenhouse gas, upwelling-favorable winds, and the future of coastal ocean upwelling ecosystems, *Global Change Biology*, *16*(4), 1213-1228.

Beal, L. M., W. P. De Ruijter, A. Biastoch, and R. Zahn (2011), On the role of the Agulhas system in ocean circulation and climate, *Nature*, *472*(7344), 429-436.

Bentsen, M., I. Bethke, J. B. Debernard, T. Iversen, A. Kirkevåg, Ø. Seland, H. Drange, C. Roelandt, I. A. Seierstad, and C. Hoose (2013), The Norwegian Earth System Model, NorESM1-M–Part 1: description and basic evaluation of the physical climate, *Geoscientific Model Development*, *6*(3), 687-720.

Blamey, L. K., J. A. Howard, J. Agenbag, and A. Jarre (2012), Regime-shifts in the southern Benguela shelf and inshore region, *Progress in Oceanography*, *106*, 80-95.

Blamey, L. K., L. J. Shannon, J. J. Bolton, R. J. Crawford, F. Dufois, H. Evers-King, C. L. Griffiths, L. Hutchings, A. Jarre, and M. Rouault (2015), Ecosystem change in the southern Benguela and the underlying processes, *Journal of Marine Systems*, *144*, 9-29.

Blanke, B., S. Speich, A. Bentamy, C. Roy, and B. Sow (2005), Modeling the structure and variability of the southern Benguela upwelling using QuikSCAT wind forcing, *Journal of Geophysical Research: Oceans*, *110*(C7).

Bleck, R., C. Rooth, D. Hu, and L. T. Smith (1992), Salinity-driven thermocline transients in a wind-and thermohaline-forced isopycnic coordinate model of the North Atlantic, *Journal of Physical Oceanography*, *22*(12), 1486-1505.

Bleck, R., and L. T. Smith (1990), A wind-driven isopycnic coordinate model of the north and equatorial Atlantic Ocean: 1. Model development and supporting experiments, *Journal of Geophysical Research: Oceans*, *95*(C3), 3273-3285.

Bonino, G., S. Masina, D. Iovino, A. Storto, and H. Tsujino (2019), Eastern Boundary Upwelling Systems response to different atmospheric forcing in a global eddy-permitting ocean model, *Journal of Marine Systems*, *197*, 103178.

Boyd, A., and J. Agenbag (1985), Seasonal trends in the longshore distribution of surface temperatures off Southwestern Africa 18-34 S, and their relation to subsurface conditions and currents in the area 21-24 S, paper presented at International Symposium on the Most Important Upwelling Areas off Western Africa(Cape Blanco and Benguela).

Boyer, T. P. (1998), World ocean atlas 1998, *Salinity of the Atlantic Ocean. NOAA Atlas, NESDIS 30*, *4*, 166, https://ci.nii.ac.jp/naid/10029524444/en/.

Carr, M.-E. (2001), Estimation of potential productivity in Eastern Boundary Currents using remote sensing, *Deep Sea Research Part II: Topical Studies in Oceanography*, *49*(1-3), 59-80.

Carr, M.-E., and E. J. Kearns (2003), Production regimes in four Eastern Boundary Current systems, *Deep Sea Research Part II: Topical Studies in Oceanography*, *50*(22-26), 3199-3221.

Chavez, F. P., and M. Messié (2009), A comparison of eastern boundary upwelling ecosystems, *Progress in Oceanography*, *83*(1-4), 80-96.

Colas, F., J. C. McWilliams, X. Capet, and J. Kurian (2012), Heat balance and eddies in the Peru-Chile current system, *Climate dynamics*, *39*(1), 509-529.

Colberg, F., and C. Reason (2006), A model study of the Angola Benguela Frontal Zone: Sensitivity to atmospheric forcing, *Geophysical research letters*, *33*(19).

Dai, A., T. Qian, K. E. Trenberth, and J. D. Milliman (2009), Changes in continental freshwater discharge from 1948 to 2004, *Journal of climate*, *22*(10), 2773-2792.

Dai, A., and K. E. Trenberth (2002), Estimates of freshwater discharge from continents: Latitudinal and seasonal variations, *Journal of hydrometeorology*, *3*(6), 660-687.

Dee, D. P., et al. (2011), The ERA-Interim reanalysis: configuration and performance of the data assimilation system, *Quarterly Journal of the Royal Meteorological Society*, *137*(656), 553-597, doi:10.1002/qj.828.

Demarcq, H., R. Barlow, and F. Shillington (2003), Climatology and variability of sea surface temperature and surface chlorophyll in the Benguela and Agulhas ecosystems as observed by satellite imagery, *African Journal of Marine Science*, *25*(1), 363-372.

Demarcq, H., and V. Faure (2000), Coastal upwelling and associated retention indices derived from satellite SST. Application to Octopus vulgaris recruitment, *Oceanologica Acta*, *23*(4), 391-408.

Desbiolles, F., B. Blanke, A. Bentamy, and N. Grima (2014), Origin of fine-scale wind stress curl structures in the Benguela and Canary upwelling systems, *Journal of Geophysical Research: Oceans*, *119*(11), 7931-7948.

Deser, C., M. A. Alexander, S.-P. Xie, and A. S. Phillips (2010), Sea surface temperature variability: Patterns and mechanisms, *Annual review of marine science*, *2*, 115-143.

Dieppois, B., B. Pohl, M. Rouault, M. New, D. Lawler, and N. Keenlyside (2016), Interannual to interdecadal variability of winter and summer southern African rainfall, and their teleconnections, *Journal of Geophysical Research: Atmospheres*, *121*(11), 6215-6239.

Doi, T., T. Tozuka, H. Sasaki, Y. Masumoto, and T. Yamagata (2007), Seasonal and interannual variations of oceanic conditions in the Angola Dome, *Journal of Physical Oceanography*, *37*(11), 2698-2713.

Dufois, F., and M. Rouault (2012), Sea surface temperature in False Bay (South Africa): Towards a better understanding of its seasonal and inter-annual variability, *Continental Shelf Research*, *43*, 24-35.

Dussin, R., B. Barnier, L. Brodeau, and J. M. Molines (2016), Drakkar forcing set dfs5, edited, Repport.

Dyer, T., and P. Tyson (1977), Estimating above and below normal rainfall periods over South Africa, 1972–2000, *Journal of Applied Meteorology*, *16*(2), 145-147.

Echevin, V., K. Goubanova, A. Belmadani, and B. Dewitte (2012), Sensitivity of the Humboldt Current system to global warming: a downscaling experiment of the IPSL-CM4 model, *Climate Dynamics*, *38*(3), 761-774.

Efron, B., and R. Tibshirani (1991), Statistical data analysis in the computer age, *Science*, *253*(5018), 390-395.

Exarchou, E., C. Prodhomme, L. Brodeau, V. Guemas, and F. Doblas-Reyes (2018), Origin of the warm eastern tropical Atlantic SST bias in a climate model, *Climate Dynamics*, *51*(5), 1819-1840.

Farge, M. (1992), Wavelet transforms and their applications to turbulence, *Annual review of fluid mechanics*, *24*(1), 395-458.

Fennel, W., T. Junker, M. Schmidt, and V. Mohrholz (2012), Response of the Benguela upwelling systems to spatial variations in the wind stress, *Continental Shelf Research*, *45*, 65-77.

Field, J., and F. Shillington (2006), Variability of the Benguela Current system, *The sea*, *14*, 833-861.

Florenchie, P., J. R. Lutjeharms, C. Reason, S. Masson, and M. Rouault (2003), The source of Benguela Niños in the south Atlantic Ocean, *Geophysical Research Letters*, *30*(10).

Florenchie, P., C. Reason, J. Lutjeharms, M. Rouault, C. Roy, and S. Masson (2004), Evolution of interannual warm and cold events in the southeast Atlantic Ocean, *Journal of Climate*, *17*(12), 2318-2334.

Folland, C., D. Parker, A. Colman, and R. Washington (1999), Large scale modes of ocean surface temperature since the late nineteenth century, in *Beyond El Niño*, edited, pp. 73-102, Springer.

Fréon, P., M. Barange, and J. Aristegui (2009), Eastern boundary upwelling ecosystems: integrative and comparative approaches preface, *Progress in Oceanography*, *83*, Jan-14.

García-Reyes, M., T. Lamont, W. J. Sydeman, B. A. Black, R. R. Rykaczewski, S. A. Thompson, and S. J. Bograd (2018), A comparison of modes of upwelling-favorable wind variability in the Benguela and California current ecosystems, *Journal of Marine Systems*, *188*, 17-26.

García-Reyes, M., W. J. Sydeman, D. S. Schoeman, R. R. Rykaczewski, B. A. Black, A. J. Smit, and S. J. Bograd (2015), Under pressure: Climate change, upwelling, and eastern boundary upwelling ecosystems, *Frontiers in Marine Science*, *2*, 109.

Garzoli, S., and A. Gordon (1996), Origins and variability of the Benguela Current, *Journal of Geophysical Research: Oceans*, *101*(C1), 897-906.

Giraud, X., and A. Paul (2010), Interpretation of the paleo–primary production record in the NW African coastal upwelling system as potentially biased by sea level change, *Paleoceanography*, *25*(4).

Goubanova, K., E. Sanchez-Gomez, C. Frauen, and A. Voldoire (2019), Respective roles of remote and local wind stress forcings in the development of warm SST errors in the South-Eastern Tropical Atlantic in a coupled high-resolution model, *Climate Dynamics*, *52*(3-4), 1359-1382.

Grinsted, A., J. C. Moore, and S. Jevrejeva (2004), Application of the cross wavelet transform and wavelet coherence to geophysical time series, *Nonlinear processes in geophysics*, *11*(5/6), 561-566.

Haarsma, R. J., E. J. Campos, W. Hazeleger, C. Severijns, A. R. Piola, and F. Molteni (2005), Dominant modes of variability in the South Atlantic: A study with a hierarchy of ocean–atmosphere models, *Journal of climate*, *18*(11), 1719-1735.

Hagen, E., R. Feistel, J. J. Agenbag, and T. Ohde (2001), Seasonal and interannual changes in intense Benguela upwelling (1982–1999), *Oceanologica Acta*, *24*(6), 557-568.

He, Y.-C., H. Drange, Y. Gao, and M. Bentsen (2016), Simulated Atlantic Meridional Overturning Circulation in the 20th century with an ocean model forced by reanalysis-based atmospheric data sets, *Ocean Modelling*, *100*, 31-48.

Henley, B. J., J. Gergis, D. J. Karoly, S. Power, J. Kennedy, and C. K. Folland (2015), A tripole index for the interdecadal Pacific oscillation, *Climate Dynamics*, *45*(11-12), 3077-3090.

Hernandez, O., J. Jouanno, V. Echevin, and O. Aumont (2017), Modification of sea surface temperature by chlorophyll concentration in the Atlantic upwelling systems, *Journal of Geophysical Research: Oceans*, *122*(7), 5367-5389.

Hersbach, H., B. Bell, P. Berrisford, S. Hirahara, A. Horányi, J. Muñoz-Sabater, J. Nicolas, C. Peubey, R. Radu, and D. Schepers (2020), The ERA5 global reanalysis, *Quarterly Journal of the Royal Meteorological Society*, *146*(730), 1999-2049.

Huang, B., P. W. Thorne, V. F. Banzon, T. Boyer, G. Chepurin, J. H. Lawrimore, M. J. Menne, T. M. Smith, R. S. Vose, and H.-M. Zhang (2017), Extended reconstructed sea surface temperature, version 5 (ERSSTv5): upgrades, validations, and intercomparisons, *Journal of Climate*, *30*(20), 8179-8205.

Huenerlage, K., and F. Buchholz (2013), Krill of the northern Benguela Current and the Angola-Benguela frontal zone compared: physiological performance and short-term starvation in Euphausia hanseni, *Journal of plankton research*, *35*(2), 337-351.

Hutchings, L., C. Van der Lingen, L. Shannon, R. Crawford, H. Verheye, C. Bartholomae, A. Van der Plas, D. Louw, A. Kreiner, and M. Ostrowski (2009), The Benguela Current: An ecosystem of four components, *Progress in Oceanography*, *83*(1-4), 15-32.

Illig, S., M. L. Bachèlery, and J. F. Lübbecke (2020), Why Do Benguela Niños Lead Atlantic Niños?, *Journal of Geophysical Research: Oceans*, *125*(9), e2019JC016003.

Imbol Koungue, R. A., S. Illig, and M. Rouault (2017), Role of interannual K elvin wave propagations in the equatorial A tlantic on the A ngola B enguela C urrent system, *Journal of Geophysical Research: Oceans*, *122*(6), 4685-4703.

Imbol Koungue, R. A., M. Rouault, S. Illig, P. Brandt, and J. Jouanno (2019), Benguela Niños and Benguela Niñas in forced ocean simulation from 1958 to 2015, *Journal of Geophysical Research: Oceans*, *124*(8), 5923-5951.

Imbol Nkwinkwa Njouodo, A. S., M. Rouault, N. Keenlyside, and S. Koseki (2021), Impact of the Agulhas Current on southern Africa precipitation: a modelling study, *Journal of Climate*, 1-50.

Jarre, A., L. Hutchings, S. P. Kirkman, A. Kreiner, P. C. Tchipalanga, P. Kainge, U. Uanivi, A. K. van der Plas, L. K. Blamey, and J. C. Coetzee (2015), Synthesis: climate effects on biodiversity, abundance and distribution of marine organisms in the B enguela, *Fisheries Oceanography*, *24*, 122-149.

Jury, M. R. (2015), Factors contributing to a decadal oscillation in South African rainfall, *Theoretical and Applied Climatology*, *120*(1), 227-237.

Kanamitsu, M., W. Ebisuzaki, J. Woollen, S.-K. Yang, J. J. Hnilo, M. Fiorino, and G. L. Potter (2002), NCEP–DOE AMIP-II Reanalysis (R-2), *Bulletin of the American Meteorological Society*, *83*(11), 1631-1644, doi:10.1175/bams-83-11-1631.

Kennedy, J., N. Reyner, S. Millington, and M. Saunby (2020), The Met Office Hadley Centre sea ice and sea-surface temperature data set, version 2, part 2: Sea surface temperature analysis, edited, in preparation.

Kerr, R. A. (2000), A North Atlantic climate pacemaker for the centuries, *Science*, *288*(5473), 1984-1985.

Kilpatrick, K., G. Podesta, and R. Evans (2001), Overview of the NOAA/NASA advanced very high resolution radiometer Pathfinder algorithm for sea surface temperature and associated matchup database, *Journal of Geophysical Research: Oceans*, *106*(C5), 9179-9197.

Kobayashi, S., Y. Ota, Y. Harada, A. Ebita, M. Moriya, H. Onoda, K. Onogi, H. Kamahori, C. Kobayashi, and H. Endo (2015), The JRA-55 reanalysis: General specifications and basic characteristics, *Journal of the Meteorological Society of Japan. Ser. II*, *93*(1), 5-48.

Kopte, R., P. Brandt, M. Dengler, P. Tchipalanga, M. Macuéria, and M. Ostrowski (2017), The Angola Current: Flow and hydrographic characteristics as observed at 11 S, *Journal of Geophysical Research: Oceans*, *122*(2), 1177-1189.

Koseki, S., H. Giordani, and K. Goubanova (2019), Frontogenesis of the Angola-Benguela frontal zone.

Koseki, S., N. Keenlyside, T. Demissie, T. Toniazzo, F. Counillon, I. Bethke, M. Ilicak, and M.-L. Shen (2018), Causes of the large warm bias in the Angola–Benguela Frontal Zone in the Norwegian Earth System Model, *Climate Dynamics*, *50*(11-12), 4651-4670.

Lamont, T., M. García-Reyes, S. Bograd, C. Van Der Lingen, and W. Sydeman (2018), Upwelling indices for comparative ecosystem studies: Variability in the Benguela Upwelling System, *Journal of Marine Systems*, *188*, 3-16.

Large, W., and S. Yeager (2009), The global climatology of an interannually varying air–sea flux data set, *Climate dynamics*, *33*(2-3), 341-364.

Li, G., and S. P. Xie (2012), Origins of tropical-wide SST biases in CMIP multi-model ensembles, *Geophysical research letters*, *39*(22).

Liu, W. T., W. Tang, and P. S. Polito (1998), NASA scatterometer provides global ocean-surface wind fields with more structures than numerical weather prediction, *Geophysical Research Letters*, *25*(6), 761-764.

Lübbecke, J. F., C. W. Böning, N. S. Keenlyside, and S. P. Xie (2010), On the connection between Benguela and equatorial Atlantic Niños and the role of the South Atlantic Anticyclone, *Journal of Geophysical Research: Oceans*, *115*(C9).

Lübbecke, J. F., J. V. Durgadoo, and A. Biastoch (2015), Contribution of increased Agulhas leakage to tropical Atlantic warming, *Journal of Climate*, *28*(24), 9697-9706.

Lutjeharms, J., and J. Meeuwis (1987), The extent and variability of South-East Atlantic upwelling, *South African Journal of Marine Science*, *5*(1), 51-62.

Mackas, D. L., P. T. Strub, A. Thomas, and V. Montecino (2006), Eastern ocean boundaries pan-regional overview.

Madec, G., R. Bourdallé-Badie, P.-A. Bouttier, C. Bricaud, D. Bruciaferri, D. Calvert, J. Chanut, E. Clementi, A. Coward, and D. Delrosso (2017), NEMO ocean engine.

Mantua, N. J., S. R. Hare, Y. Zhang, J. M. Wallace, and R. C. Francis (1997), A Pacific interdecadal climate oscillation with impacts on salmon production, *Bulletin of the american Meteorological Society*, *78*(6), 1069-1080.

Mazeika, P. (1967), Thermal domes in the eastern tropical atlantic ocean 1, *Limnology and Oceanography*, *12*(3), 537-539.

Mercier, H., M. Arhan, and J. R. Lutjeharms (2003), Upper-layer circulation in the eastern Equatorial and South Atlantic Ocean in January–March 1995, *Deep Sea Research Part I: Oceanographic Research Papers*, *50*(7), 863-887.

Mohrholz, V., C. Bartholomae, A. Van der Plas, and H. Lass (2008), The seasonal variability of the northern Benguela undercurrent and its relation to the oxygen budget on the shelf, *Continental Shelf Research*, *28*(3), 424-441.

Mohrholz, V., M. Schmidt, and J. Lutjeharms (2001), The hydrography and dynamics of the Angola-Benguela Frontal Zone and environment in April 1999: BENEFIT Marine Science, *South African Journal of Science*, *97*(5-6), 199-208.

Molod, A., L. Takacs, M. Suarez, and J. Bacmeister (2015), Development of the GEOS-5 atmospheric general circulation model: evolution from MERRA to MERRA2, *Geoscientific Model Development*, *8*(5), 1339-1356, doi:10.5194/gmd-8-1339-2015.

Monteiro, P., A. Van Der Plas, J.-L. Melice, and P. Florenchie (2008), Interannual hypoxia variability in a coastal upwelling system: Ocean–shelf exchange, climate and ecosystem-state implications, *Deep Sea Research Part I: Oceanographic Research Papers*, *55*(4), 435-450.

Morioka, Y., T. Tozuka, and T. Yamagata (2011), On the growth and decay of the subtropical dipole mode in the South Atlantic, *Journal of Climate*, *24*(21), 5538-5554.

Narayan, N., A. Paul, S. Mulitza, and M. Schulz (2010), Trends in coastal upwelling intensity during the late 20th century, *Ocean Science*, *6*(3), 815-823.

Nelson, G., and L. Hutchings (1983), The Benguela upwelling area, *Progress in Oceanography*, *12*(3), 333-356.

Patricola, C. M., and P. Chang (2017), Structure and dynamics of the Benguela low-level coastal jet, *Climate Dynamics*, *49*(7), 2765-2788.

Patricola, C. M., M. Li, Z. Xu, P. Chang, R. Saravanan, and J.-S. Hsieh (2012), An investigation of tropical Atlantic bias in a high-resolution coupled regional climate model, *Climate dynamics*, *39*(9), 2443-2463.

Penven, P., V. Echevin, J. Pasapera, F. Colas, and J. Tam (2005), Average circulation, seasonal cycle, and mesoscale dynamics of the Peru Current System: A modeling approach, *Journal of Geophysical Research: Oceans*, *110*(C10).

Penven, P., J. Pasapera, J. Tam, and C. Roy (2003), Modeling the Peru upwelling system seasonal dynamics, *GLOBEC International Newsletter*, *9*(2), 23-25.

Penven, P., C. Roy, G. Brundrit, A. C. De Verdière, P. Fréon, A. Johnson, J. Lutjeharms, and F. Shillington (2001), A regional hydrodynamic model of upwelling in the Southern Benguela, *South African Journal of Science*, *97*(11-12), 472-475.

Peterson, R. G., and L. Stramma (1991), Upper-level circulation in the South Atlantic Ocean, *Progress in oceanography*, *26*(1), 1-73.

Pfaff, M. C., R. C. Logston, S. J. Raemaekers, J. C. Hermes, L. K. Blamey, H. C. Cawthra, D. R. Colenbrander, R. J. Crawford, E. Day, and N. Du Plessis (2019), A synthesis of three decades of socio-ecological change in False Bay, South Africa: setting the scene for multidisciplinary research and management, *Elementa: Science of the Anthropocene*, *7*.

Preston-Whyte, R. A., and P. D. Tyson (1988), *Atmosphere and weather of southern Africa*, Oxford University Press.

Rayner, N., J. Kennedy, R. Smith, and H. Titchner (2020), The Met Office Hadley Centre sea ice and sea surface temperature data set, version 2, part 3: the combined analysis, *J Geophys Res Atmos*, *119*(in preparation), 2864.

Rayner, N., D. E. Parker, E. Horton, C. Folland, L. Alexander, D. Rowell, E. Kent, and A. Kaplan (2003), Global analyses of sea surface temperature, sea ice, and night marine air temperature since the late nineteenth century, *Journal of Geophysical Research: Atmospheres*, *108*(D14), 4407.

Reynolds, R. W., N. A. Rayner, T. M. Smith, D. C. Stokes, and W. Wang (2002), An improved in situ and satellite SST analysis for climate, *Journal of climate*, *15*(13), 1609-1625.

Reynolds, R. W., T. M. Smith, C. Liu, D. B. Chelton, K. S. Casey, and M. G. Schlax (2007), Daily high-resolution-blended analyses for sea surface temperature, *Journal of Climate*, *20*(22), 5473-5496.

Richter, I. (2015), Climate model biases in the eastern tropical oceans: Causes, impacts and ways forward, *Wiley Interdisciplinary Reviews: Climate Change*, *6*(3), 345-358.

Richter, I., and S.-P. Xie (2008), On the origin of equatorial Atlantic biases in coupled general circulation models, *Climate Dynamics*, *31*(5), 587-598.

Richter, I., S.-P. Xie, A. T. Wittenberg, and Y. Masumoto (2012), Tropical Atlantic biases and their relation to surface wind stress and terrestrial precipitation, *Climate dynamics*, *38*(5-6), 985-1001.

Rodrigues, R. R., E. J. Campos, and R. Haarsma (2015), The impact of ENSO on the South Atlantic subtropical dipole mode, *Journal of Climate*, *28*(7), 2691-2705.

Rouault, M. (2012), Bi-annual intrusion of tropical water in the northern Benguela upwelling, *Geophysical research letters*, *39*(12).

Rouault, M., P. Florenchie, N. Fauchereau, and C. J. Reason (2003), South East tropical Atlantic warm events and southern African rainfall, *Geophysical Research Letters*, *30*(5).

Rouault, M., S. Illig, C. Bartholomae, C. Reason, and A. Bentamy (2007), Propagation and origin of warm anomalies in the Angola Benguela upwelling system in 2001, *Journal of Marine Systems*, *68*(3-4), 473-488.

Rouault, M., S. Illig, J. Lübbecke, and R. A. I. Koungue (2018), Origin, development and demise of the 2010–2011 Benguela Niño, *Journal of Marine Systems*, *188*, 39-48.

Rouault, M., P. Penven, and B. Pohl (2009), Warming in the Agulhas Current system since the 1980's, *Geophysical Research Letters*, *36*(12).

Rouault, M., B. Pohl, and P. Penven (2010), Coastal oceanic climate change and variability from 1982 to 2009 around South Africa, *African Journal of Marine Science*, *32*(2), 237-246.

Rouault, M., and Y. Richard (2003), Intensity and spatial extension of drought in South Africa at different time scales, *Water Sa*, *29*(4), 489-500.

Roy, C., S. Weeks, M. Rouault, G. Nelson, R. Barlow, and C. Van der Lingen (2001), Extreme oceanographic events recorded in the Southern Benguela during the 1999-2000 summer season, *South African Journal of Science*, *97*(11-12), 465-471.

Rykaczewski, R. R., J. P. Dunne, W. J. Sydeman, M. García-Reyes, B. A. Black, and S. J. Bograd (2015), Poleward displacement of coastal upwelling-favorable winds in the ocean's eastern boundary currents through the 21st century, *Geophysical Research Letters*, *42*(15), 6424-6431.

Santos, F., M. Gomez-Gesteira, and I. Alvarez (2012), Differences in coastal and oceanic SST trends due to the strengthening of coastal upwelling along the Benguela current system, *Continental Shelf Research*, *34*, 79-86.

Shannon, L., J. Agenbag, and M. Buys (1987), Large-and mesoscale features of the Angola-Benguela front, *South African Journal of Marine Science*, *5*(1), 11-34.

Shannon, L., A. Boyd, G. Brundrit, and J. Taunton-Clark (1986), On the existence of an El Niño-type phenomenon in the Benguela system, *Journal of marine Research*, *44*(3), 495-520.

Shannon, L., and G. Nelson (1996), The Benguela: large scale features and processes and system variability, in *The south atlantic*, edited, pp. 163-210, Springer.

Shannon, L. V. (1985), The Benguela ecosystem. I: Evolution of the Benguela physical features and processes, *Oceanography and Marine Biology*, *23*, 105-182.

Shannon, V. (2006), 1 A plan comes together, in *Large Marine Ecosystems*, edited, pp. 3-10, Elsevier.

Small, R. J., E. Curchitser, K. Hedstrom, B. Kauffman, and W. G. Large (2015), The Benguela upwelling system: Quantifying the sensitivity to resolution and coastal wind representation in a global climate model, *Journal of Climate*, *28*(23), 9409-9432.

Smit, A. J., M. Roberts, R. J. Anderson, F. Dufois, S. F. Dudley, T. G. Bornman, J. Olbers, and J. J. Bolton (2013), A coastal seawater temperature dataset for biogeographical studies: large biases between in situ and remotely-sensed data sets around the coast of South Africa, *PLoS One*, *8*(12), e81944.

Sterl, A., and W. Hazeleger (2003), Coupled variability and air-sea interaction in the South Atlantic Ocean, *Climate Dynamics*, *21*(7-8), 559-571.

Stramma, L., and M. England (1999), On the water masses and mean circulation of the South Atlantic Ocean, *Journal of Geophysical Research: Oceans*, *104*(C9), 20863-20883.

Sun, X., K. H. Cook, and E. K. Vizy (2017), The South Atlantic subtropical high: climatology and interannual variability, *Journal of Climate*, *30*(9), 3279-3296, https://journals.ametsoc.org/doi/abs/10.1175/JCLI-D-16-0705.1.

Sydeman, W., M. García-Reyes, D. S. Schoeman, R. Rykaczewski, S. Thompson, B. Black, and S. Bograd (2014), Climate change and wind intensification in coastal upwelling ecosystems, *Science*, *345*(6192), 77-80, https://science.sciencemag.org/content/345/6192/77.long.

Tchipalanga, P., M. Dengler, P. Brandt, R. Kopte, M. Macuéria, P. Coelho, M. Ostrowski, and N. S. Keenlyside (2018), Eastern boundary circulation and hydrography off angola: building angolan oceanographic capacities, *Bulletin of the American Meteorological Society*, *99*(8), 1589-1605.

Tim, N., E. Zorita, K.-C. Emeis, F. U. Schwarzkopf, A. Biastoch, and B. Hünicke (2019), Analysis of the position and strength of westerlies and trades with implications for Agulhas leakage and South Benguela upwelling, *Earth System Dynamics*, *10*(4), 847-858.

Tim, N., E. Zorita, and B. Hünicke (2015), Decadal variability and trends of the Benguela upwelling system as simulated in a high-resolution ocean simulation, *Ocean Sci*, *11*(3), 483-502.

Tim, N., E. Zorita, F. U. Schwarzkopf, S. Rühs, K. C. Emeis, and A. Biastoch (2018), The impact of Agulhas leakage on the central water masses in the Benguela upwelling system from a high-resolution ocean simulation, *Journal of Geophysical Research: Oceans*, *123*(12), 9416-9428.

Titchner, H. A., and N. A. Rayner (2014), The Met Office Hadley Centre sea ice and sea surface temperature data set, version 2: 1. Sea ice concentrations, *Journal of Geophysical Research: Atmospheres*, *119*(6), 2864-2889.

Toniazzo, T., and S. Woolnough (2014), Development of warm SST errors in the southern tropical Atlantic in CMIP5 decadal hindcasts, *Climate dynamics*, *43*(11), 2889-2913.

Torrence, C., and G. P. Compo (1998), A practical guide to wavelet analysis, *Bulletin of the American Meteorological society*, *79*(1), 61-78.

Torrence, C., and P. J. Webster (1999), Interdecadal changes in the ENSO–monsoon system, *Journal of climate*, *12*(8), 2679-2690.

Tourre, Y. M., C. Cibot, L. Terray, W. B. White, and B. Dewitte (2005), Quasi-decadal and inter-decadal climate fluctuations in the Pacific Ocean from a CGCM, *Geophysical Research Letters*, *32*(7).

Trenberth, K. E., and D. J. Shea (2006), Atlantic hurricanes and natural variability in 2005, *Geophysical research letters*, *33*(12).

Veitch, J., P. Florenchie, and F. Shillington (2006), Seasonal and interannual fluctuations of the Angola–Benguela Frontal Zone (ABFZ) using 4.5 km resolution satellite imagery from 1982 to 1999, *International Journal of Remote Sensing*, *27*(05), 987-998.

Veitch, J., P. Penven, and F. Shillington (2009), The Benguela: A laboratory for comparative modeling studies, *Progress in Oceanography*, *83*(1-4), 296-302.

Veitch, J., P. Penven, and F. Shillington (2010), Modeling equilibrium dynamics of the Benguela Current System, *Journal of Physical Oceanography*, *40*(9), 1942-1964.

Venegas, S., L. Mysak, and D. Straub (1997), Atmosphere–ocean coupled variability in the South Atlantic, *Journal of Climate*, *10*(11), 2904-2920.

Verheye, H., and W. Ekau (2005), Maintenance mechanisms of plankton populations in frontal zones in the Benguela and Angola Current systems: a preface, *African Journal of Marine Science*, *27*(3), 611-615.

Vizy, E. K., and K. H. Cook (2016), Understanding long-term (1982–2013) multi-decadal change in the equatorial and subtropical South Atlantic climate, *Climate Dynamics*, *46*(7-8), 2087-2113.

Vizy, E. K., K. H. Cook, and X. Sun (2018), Decadal change of the south Atlantic ocean Angola–Benguela frontal zone since 1980, *Climate Dynamics*, 1-23.

Volbers, A., H.-S. Niebler, J. Giraudeau, H. Schmidt, and R. Henrich (2003), Palaeoceanographic Changes in the Northern Benguela Upwelling System over the last 245.000 Years as

Derived from Planktic Foraminifera Assemblages, in *The South Atlantic in the Late Quaternary*, edited, pp. 601-622, Springer.

Wacongne, S., and B. Piton (1992), The near-surface circulation in the northeastern corner of the South Atlantic Ocean, *Deep Sea Research Part A. Oceanographic Research Papers*, *39*(7-8), 1273-1298.

Wang, D., T. C. Gouhier, B. A. Menge, and A. R. Ganguly (2015), Intensification and spatial homogenization of coastal upwelling under climate change, *Nature*, *518*(7539), 390-394.

Wolski, P., S. Conradie, C. Jack, and M. Tadross (2021), Spatio-temporal patterns of rainfall trends and the 2015–2017 drought over the winter rainfall region of South Africa, *International Journal of Climatology*, *41*, E1303-E1319.

Woodruff, S. D., S. J. Worley, S. J. Lubker, Z. Ji, J. Eric Freeman, D. I. Berry, P. Brohan, E. C. Kent, R. W. Reynolds, and S. R. Smith (2011), ICOADS Release 2.5: extensions and enhancements to the surface marine meteorological archive, *International journal of climatology*, *31*(7), 951-967.

Xie, S.-P., and J. A. Carton (2004), Tropical Atlantic variability: Patterns, mechanisms, and impacts, *Earth's Climate: The Ocean-Atmosphere Interaction, Geophys. Monogr*, *147*, 121-142.

Yu, L., X. Jin, and R. A. Weller (2006), Role of net surface heat flux in seasonal variations of sea surface temperature in the tropical Atlantic Ocean, *Journal of climate*, *19*(23), 6153-6169.

Zhang, Y., J. M. Wallace, and D. S. Battisti (1997), ENSO-like interdecadal variability: 1900–93, *Journal of climate*, *10*(5), 1004-1020.

Zhang, Y., J. M. Wallace, and N. Iwasaka (1996), Is climate variability over the North Pacific a linear response to ENSO?, *Journal of Climate*, *9*(7), 1468-1478.